PULSED LASER PHOTOLYSIS KINETICS STUDY OF REACTIONS BETWEEN SMALL RADICAL SPECIES

BY
JOHN MICHAEL NICOVICH

A DISSERTATION PRESENTED TO THE GRADUATE SCHOOL
OF THE UNIVERSITY OF FLORIDA IN PARTIAL FULFILLMENT
OF THE REQUIREMENTS FOR THE DEGREE OF
DOCTOR OF PHILOSOPHY

UNIVERSITY OF FLORIDA

1993

ACKNOWLEDGMENTS

To begin with, I must recognize the assistance, encouragement and patience of my research advisor, Dr. R. J. Hanrahan, and my coworkers at the Georgia Tech Research Institute (GTRI), in particular, Drs. P. H. Wine and A. R. Ravishankara. The research reported here was supported financially by the National Aeronautics and Space Administration (NASA) by subcontracts through the Jet Propulsion Laboratory (JPL). Additional support for the $O(^3P) + ClO$ study was provided by the Chemical Manufacturers Association (CMA). Partial financial support for the author was received from GTRI through a tuition reimbursement program and other funds. The efficient and friendly typing service provided by Gail Tucker is gratefully acknowledged. Finally, I thank my family for putting up with me for all this time.

TABLE OF CONTENTS

Page

ACKNOWLEDGMENTS ii

ABSTRACT v

CHAPTERS

I. INTRODUCTION 1

II. PULSED LASER PHOTOLYSIS STUDY OF THE REACTION BETWEEN $O(^3P)$ AND HO_2 11

Introduction 11
Experimental Section 15
Actinometry 18
Kinetic Measurements 24
Results and Discussion 28

Secondary Reactions that Effect [HO_2] 33
Comparison with Other Studies 44
Comments on the Pressure Independence of k_1 46

III. TEMPERATURE DEPENDENCE OF THE $O(^3P)$ + HO_2 RATE COEFFICIENT 49

Introduction 49
Experimental Section 50
Results and Discussion 57

Secondary Chemistry 59
Summary of Results 68
Comparison with Previous Work 71
Implications for Atmospheric Chemistry 74

IV. PULSED LASER PHOTOLYSIS KINETICS STUDY OF THE O(^{3}P) + ClO REACTION 76

Introduction 76
Experimental 78
Results 83
Discussion 105
Summary 111

V. CONCLUSIONS 113

APPENDICES

A. FURTHER DETAILS OF THE EXPERIMENTAL METHODS 118

Introduction 118
Flow Systems 119
Resonance Lamps 122
Fluorescence Detection 124
Signal Acquisition 125
UV Photometry 127
Numerical Simulations 131

B. LIST OF REACTIONS 133

REFERENCES 135

BIOGRAPHICAL SKETCH 140

Abstract of Dissertation Presented to the Graduate School
of the University of Florida in Partial Fulfillment of the
Requirements for the Degree of Doctor of Philosophy

PULSED LASER PHOTOLYSIS KINETICS STUDY OF REACTIONS BETWEEN SMALL RADICAL SPECIES

By

John Michael Nicovich

May 1993

Chairman: Robert J. Hanrahan
Major Department: Chemistry

The kinetics of the important stratospheric reaction $O(^3P) + HO_2 \rightarrow OH + O_2$ (1) has been studied at 298 K as a function of N_2 diluent gas pressure from 10 to 500 Torr and also as a function of temperature from 266 to 391 K in 80 Torr of N_2. Pulsed 248.5 nm KrF laser photolysis of $O_3/H_2O_2/N_2$ mixtures produced $O(^1D)$ and OH. The $O(^1D)$ was rapidly quenched to $O(^3P)$ by N_2 and HO_2 was produced by reaction of OH with H_2O_2. $O(^3P)$ was monitored by time-resolved resonance fluorescence. The concentration of the excess species, HO_2, was calculated from experimentally measured parameters. This is the first study of this reaction under pseudo-first order conditions at pressures greater than a few Torr and the first time the described techniques have been employed for studying radical-radical reactions.

The temperature and pressure dependence of another important stratospheric reaction, $O(^3P) + ClO \rightarrow Cl + O_2$ (2), has been studied over the ranges 231 to 367 K and 25 to 500 Torr. Pulsed 351 nm XeF laser photolysis of $Cl_2/O_3/N_2$ mixtures produced Cl in excess over O_3. After a delay sufficient for the reaction $Cl + O_3 \rightarrow ClO + O_2$ to go to completion, a small fraction of the ClO was photolyzed by a 266 nm Nd:YAG laser pulse. The decay of $O(^3P)$ in an excess of a known concentration of ClO was followed by resonance fluorescence spectroscopy. A few measurements of the rate coefficient for the reaction $ClO + ClO \rightarrow$ products were also performed.

The rate coefficients for both reactions (1) and (2) were found to be independent of pressure. Our results are described by the following Arrhenius expressions in units of 10^{-11} cm^3 $molecule^{-1}$ s^{-1}: $k_1(T) = (2.91 \pm 0.70)\exp[(228 \pm 75)/T]$ and $k_2(T) = (1.55 \pm 0.33)\exp[(263 \pm 60)/T]$. The errors are 2σ and represent precision only. The results are compared with previous measurements and the implications of these findings to atmospheric chemistry are discussed.

CHAPTER I

INTRODUCTION

The kinetics of gas phase reactions between free radicals, species containing one or more unpaired electrons, are of importance from both basic and practical standpoints. Radical-radical reactions often proceed on an attractive potential energy surface with no barrier to the formation of a bound intermediate. These reactions therefore offer relatively simple systems that have, over the past two decades, become amenable to theoretical studies. An in-depth discussion of the theoretical basis for the observed kinetics of radical-radical reactions is beyond the scope of this work but can be found elsewhere.[1] From a more applied point of view, radical-radical reactions play critical roles in complex chemical systems such as in combustion and in the chemistry of the Earth's atmosphere.

Experimentally, the kinetics of radical-radical reactions are difficult to study. Radical-radical reactions are usually fast and in order to study the kinetics it is necessary to generate and quantify two reactive intermediates. Note that under the definition given here for free radicals there are a few species, such as NO_2, NO and O_2, that do not have to be generated *in situ*. It is often the case that the self-reactions of the radicals, as well as the reactions of the radicals with reaction products, are rapid, making it more difficult to quantify radical concentrations. The most commonly employed techniques for directly studying the kinetics of radical-radical reactions are variations of flow-tube experiments. In flow-tube studies, the concentration of one species is monitored at a known distance downstream from where it is mixed with an excess of a second species. Knowledge of the flow velocity allows the distance to be converted to a reaction time and variation of the distance and the concentrations leads to the kinetic information. A major advantage of flow-tube experiments is adaptability. Many different detectors can be used to obtain reactant concentrations and a wide variety of radicals can be generated, often in an electrical discharge or by thermal decomposition. Standard discharge-flow methods are restricted to pressures in the 1 to 10 Torr range, although some recent studies have reported experiments performed at higher pressures.[2,3] A major disadvantage is the possibility of undetected heterogeneous effects. A more detailed description of flow-tube experiments can be found elsewhere.[4] In part, the present studies were undertaken to develop an alternate experimental method for the study of radical-radical reactions. Previous results on the two reactions studied in the present work are derived mainly from flow-tube experiments. Our adaptation of the laser flash photolysis-resonance fluorescence (LFP-RF) technique to the study of radical-radical reactions has allowed these two reactions to be studied at higher pressures than before and without the same systematic errors inherent in discharge flow studies. A discussion of the innovations in the LFP-RF technique, as well as comparison with previous results, will appear in subsequent chapters.

The two reactions studied in this work

$$O(^3P) + HO_2 \rightarrow OH + O_2 \qquad (1)$$

$$O(^3P) + ClO \rightarrow Cl + O_2 \qquad (2)$$

are both of importance in the earth's stratosphere. The major stratospheric chemistry problem relates to ozone which, along with molecular oxygen, forms the protective ultraviolet absorption layer under which life evolved on Earth. Our knowledge of the natural dynamic balance between solar-initiated photochemistry, free radical reactions, and the background gases that are precursors of the free radicals in the stratosphere can be found described in detail in many sources.[5-10] Much of this knowledge has been gained in the last two decades from research spurred on by the recognition that the activities of man are altering the "natural" composition of the atmosphere. Of particular importance is the problem of how the introduction of additional trace species to the stratosphere changes the balance between the formation and destruction of ozone.

The formation of a roughly constant level of ozone in the stratosphere was first explained by Chapman[11] via the following mechanism:

$$O_2 + h\nu\ (< 190\text{nm}) \rightarrow 2\ O \tag{3}$$

$$O + O_2 + M \rightarrow O_3 + M \tag{4}$$

$$O_3 + h\nu\ (< 310\text{ nm}) \rightarrow O + O_2 \tag{5}$$

$$O + O_3 \rightarrow 2\ O_2 \tag{6}$$

where M represents a third-body collider (N_2 and O_2). This oxygen-only mechanism predicts concentrations of odd oxygen, O_3 and O, that are too large when compared with measured levels. It is now known that other major loss processes are extant in the stratosphere. These include the catalytic cycles

$$\begin{array}{l} X + O_3 \rightarrow XO + O_2 \\ XO + O \rightarrow X + O_2 \\ \hline O + O_3 \rightarrow 2\ O_2 \qquad \text{net} \end{array}$$

where X = OH, H, NO, Cl or Br. It should be noted that the net result of this cycle is the equivalent of reaction (6). At lower altitudes, where the partitioning between "odd" oxygen species (O_3 and O) is shifted toward the molecular species, the efficient ozone destruction cycle becomes:

$$OH + O_3 \rightarrow HO_2 + O_2 \qquad (7)$$

$$HO_2 + O_3 \rightarrow OH + 2\ O_2 \qquad (8)$$

$$2\ O_3 \rightarrow 3\ O_2 \qquad \text{net}$$

The efficiency of each cycle toward odd oxygen destruction is dependent upon the rate coefficient for the rate-determining step in each cycle and the coupling with reactions that remove the catalytic radicals. Examples of the latter include

$$Cl + CH_4 \rightarrow HCl + CH_3 \qquad (9)$$

and

$$OH + HO_2 \rightarrow H_2O + O_2 \qquad (10)$$

The major hydrogen-oxygen free radicals, OH and HO_2, play critical roles in the chemistry of the stratosphere either in catalytic cycles or through reactions that partition other species between free radicals and chemically stable forms. The dominant source of HO_x radicals throughout the stratosphere is the reaction

$$H_2O + O(^1D) \rightarrow 2\ OH \qquad (11)$$

where the excited oxygen atoms are formed by the photolysis of O_3. Reaction (1) is the rate-determining step in a catalytic cycle that leads to O_3 destruction

$$OH + O_3 \rightarrow HO_2 + O_2 \qquad (7)$$

$$O + HO_2 \rightarrow OH + O_2 \qquad (1)$$

$$O + O_3 \rightarrow 2\,O_2 \qquad \text{net}$$

Figure 1 (taken from reference 12) shows the conversion rate between OH and HO_2 as a function of altitude for all major reactions thought to interconvert these species. Note that reaction (1) is the dominant reaction converting HO_2 to OH above 40 km, i.e., in the upper stratosphere.

In 1974, Stolarski and Cicerone[13] suggested that chlorine introduced into the atmosphere in rocket exhaust could destroy O_3 by another catalytic cycle

$$Cl + O_3 \rightarrow ClO + O_2 \qquad (12)$$

$$O + ClO \rightarrow Cl + O_2 \qquad (2)$$

$$O + O_3 \rightarrow 2\,O_2 \qquad \text{net}$$

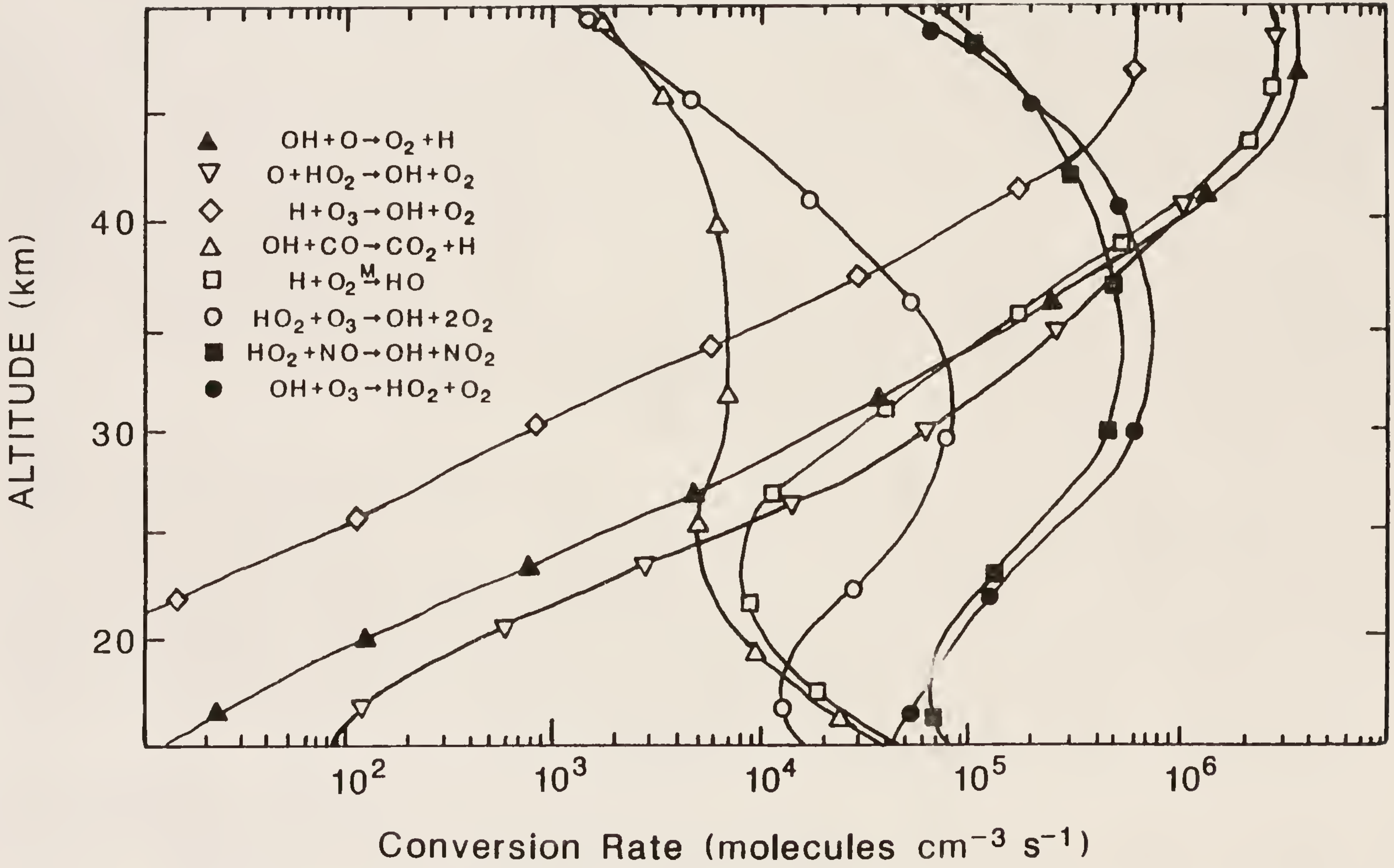

Figure 1. Conversion rates between OH and HO_2 as a function of altitude. (Figure 1-107 of Reference 12).

In this cycle, reaction (2) is rate-determining. Subsequently, Molina and Rowland[14] identified chlorofluorocarbons (CFCs) as another, much larger anthropogenic source of stratospheric Cl. In general, CFCs are defined as hydrocarbons in which all the hydrogen atoms have been replaced by either chlorine, fluorine or a combination of both. Since World War II, CFCs have been produced for use in a variety of industrial applications such as solvents and refrigerants. Relatively inert to oxidation or other loss processes in the troposphere, the CFCs mix into the stratosphere where their ultraviolet photolysis produces free chlorine atoms. Approximately 80% of the present atmospheric load of chlorine is from CFCs with the remainder coming from naturally occurring CH_3Cl.

Recent measurements have clearly shown that indeed the level of stratospheric O_3 has been negatively perturbed. Trend estimates in the loss of ozone in the mid-latitudes as measured by several methods and predicted by model calculations are shown in Figure 2 (taken from reference 15). The measurement techniques include ground based (Umkehr), balloon-borne (Payerne and Hohenpeissenberg), and satellite-borne instrumentation (SAGE). As can be seen in the figure, the measured loss of O_3 is greatest in the lower stratosphere between 15 and 20 km. More dramatic losses in the ozone column have been observed for the past several years over the continent of Antarctica in the austral spring. Heterogeneous processes that take place on polar stratospheric

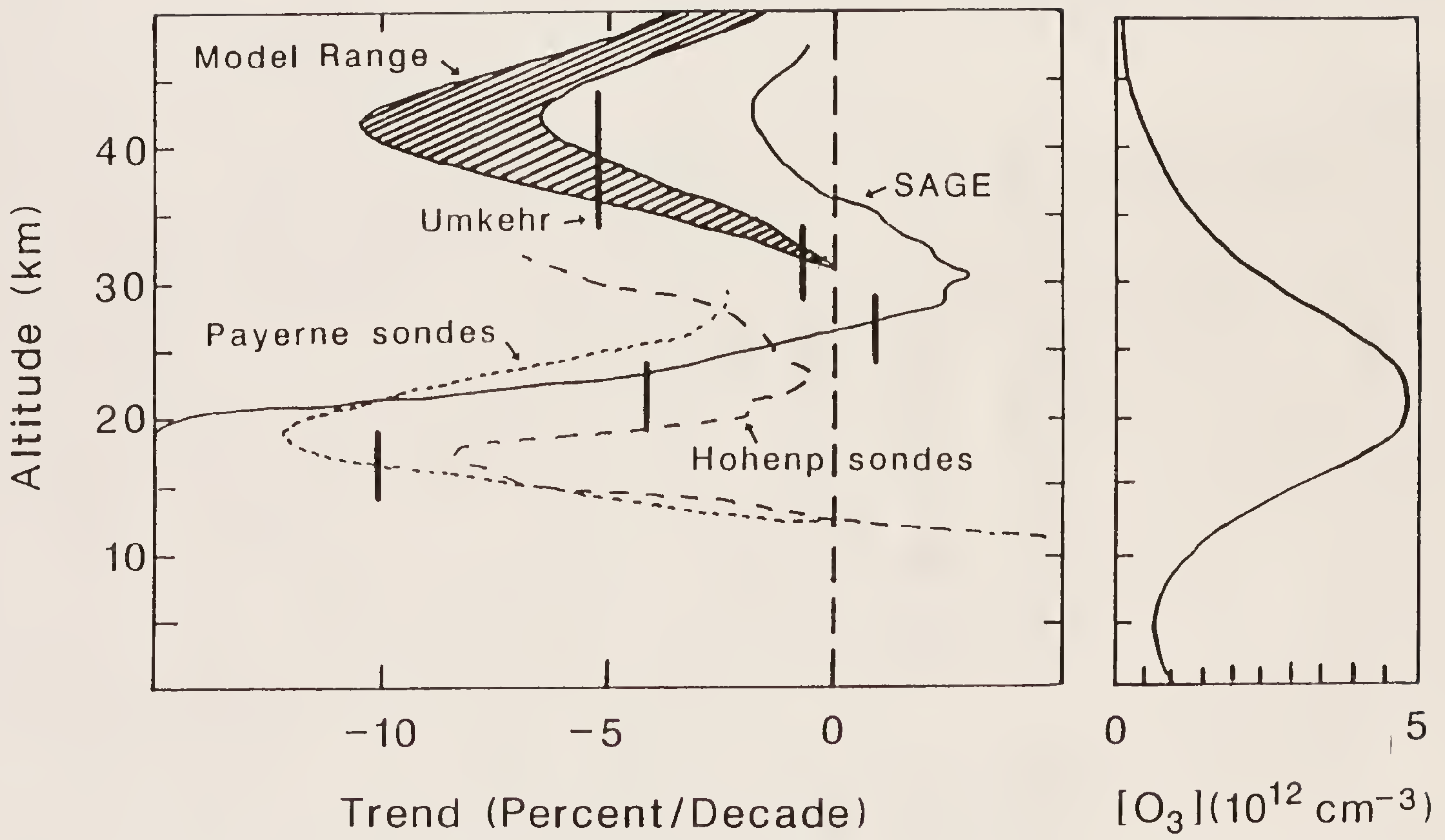

Figure 2. Comparison of ozone profile trend estimates from several measurement systems, SAGE, Umkehr, and two ozonesonde stations. SAGE data is an average over the latitude ranges 20°-50° N and 20°-50° S. The Umkehr is the average over five northern mid-latitude stations. Shaded area shows the range of two model calculations at 50° N and 50° S. The panel on the right shows a typical ozone concentration versus altitude (Figure 2-18 of Reference 15).

clouds freeing highly photoactive chlorine species (HOCl and Cl_2) followed by reactions of the oxides of chlorine are thought to be responsible for the so-called Antarctic "ozone hole."

The specific roles of reactions (1) and (2) in the chemistry of the Earth's atmosphere are discussed further in the following chapters. The study of the room temperature rate coefficient for the O + HO_2 reaction is presented in Chapter II, followed by the temperature dependence study of the same reaction in Chapter III. The study of the temperature dependence of the O + ClO rate coefficient is described in Chapter IV. Except for minor editorial changes necessary to integrate the three separate studies into a single thesis, the material in each of these chapters is taken, by permission, from three separately published journal articles.[16-18] A concluding chapter contains a summary of the work presented here as well as a discussion of pertinent information that has appeared in the literature subsequent to the publication of the three studies. Finally, there are two appendices. The first contains additional details of the experimental and calculational techniques and the second appendix lists, in numerical order, the complete set of reactions.

CHAPTER II

PULSED LASER PHOTOLYSIS STUDY OF THE REACTION BETWEEN O(^{3}P) AND HO$_2$

Introduction

Bimolecular reactions involving two free radicals are of great interest because both reactants have unpaired electrons and hence could interact at distances longer than those typical of radical-molecule encounters. Also, because of the attractive nature of the encounter, the energy barriers for the reaction can be nonexistent or small; i.e., the reaction can proceed on a purely attractive potential surface. Consequently, association reaction channels can become possible even when there exist other pathways such as simple atom transfers. The majority of radical-radical reactions have, until now, been studied using the low pressure discharge flow technique[4] which is extremely well suited for these types of reactions since the two free radicals can be created in physically separate regions and then mixed to observe the reaction of interest. However, the pressure range of discharge flow studies is presently limited to a few Torr. (Currently, a few laboratories are developing high pressure discharge flow apparatus.) Therefore, it is obvious that if the association pathways in radical-radical reactions are to be observed, especially when they are in competition with other pressure independent channels, these reactions will have to be studied at much higher pressures.

In addition to the above mentioned rationale for studying radical-radical reactions at high pressures, there is also a more practical reason for such studies. Most radical-radical reactions that are important in the atmosphere and in combustion systems take place at pressures much greater than a few Torr. If one intends to model such complex systems, it is necessary to ensure that the input rate constants are those applicable under the pressure conditions actually encountered. Also, one cannot ignore the possibility of surface enhanced reactions influencing the results of discharge flow studies even though, in principal, experimental checks for such effects can be made. Lastly, multiple studies using vastly different techniques are necessary to recognize and then (hopefully) minimize systematic errors. The last point is especially important since a great deal of reliance is placed on the absolute accuracy of kinetic data in modeling atmospheric and combustion processes.

In the past, a few high pressure studies of radical-radical reactions have been carried out. However, except for the cases of self-reactions, i.e., $R\cdot + R\cdot \rightarrow$ products (where $R\cdot$ = free radical), most of these studies have not been able to isolate the reaction of interest and therefore had to rely on modeling a complex scheme of reactions to extract the rate coefficient of interest. To worsen the situation, in many cases the modeling had to include reactions which were themselves not well understood. In some of these studies the modeling calculations showed that the experimentally measured parameters were not even very sensitive to the value of the rate constant of interest. Therefore, it is clear that experimental techniques which can directly measure radical-radical reaction rate constants at high pressures are needed.

In our laboratory, we are developing a method based on laser photolysis to selectively produce free radicals in the homogeneous gas phase in such a way as to isolate the reaction of interest and subsequently follow the course of the reaction using spectroscopic techniques. This method has become feasible because of advances in laser technology as well as improvements in our understanding of the photochemistry of precursors and kinetics of reactions from which the radicals of interest are generated. The present paper describes the first of these studies where the rate coefficient for the reaction of $O(^3P)$ with HO_2,

$$O(^3P) + HO_2 \rightarrow OH + O_2 \qquad (1)$$

has been measured at N_2 pressures ranging from 10 to 500 Torr.

Reaction (1) was chosen for the initial study for the following four reasons: (a) there is only one set of products possible for this reaction, at least at low pressures; (b) the reaction could be studied using only one photolysis laser; (c) there have been two recent studies of reaction (1) at low pressures[19,20] which are in agreement (see below) and thus provide a good basis for comparison; and (d) the chemistry in the system could be kept under very good control. Based on the above description, one might get the impression that this technique is of limited use. However, it will, in time, become evident that with carefully thought out systems and further improvements in our understanding of the photochemistry of important radical precursors, this technique will prove to be extremely powerful.

Reaction (1) has been studied at 298 K by many investigators.[19-23] The measured values of k_1 range from 2.7 to 7.0 x 10^{-11} cm^3 $molecule^{-1}$ s^{-1}. All studies,[19-23] except one,[23] have been carried out using discharge flow methods of pressures lower than 4 Torr. Some of these investigations[21,22] were indirect, i.e., k_1 was measured relative to other rate coefficients. The rate constants for the reference reactions themselves have recently been revised.[24] The high pressure study[23] was very indirect and involved the pulse radiolysis of a mixture of O_2, H_2, and Ar followed by extensive modeling to extract k_1. The most recent low pressure studies by Keyser[19] and Sridharan et al.,[20] however, were carried out such that reaction (1) was isolated and k_1 measured under pseudo-first order conditions to be $(6.1 \pm 0.4) \times 10^{-11}$ and $(5.4 \pm 0.9) \times 10^{-11}$ cm^3 $molecule^{-1}s^{-1}$, respectively. Keyser has also measured k_1 as a function of temperature and obtained a small negative activation energy for reaction (1).

In the study described here, $O(^3P)$ and HO_2 were produced by cophotolysis of O_3 and H_2O_2 in N_2 at 248.5 nm using a KrF excimer laser. Reaction (1) was studied under pseudo-first order conditions in $[O(^3P)]$ with $[HO_2] > [O(^3P)]$. $[HO_2]$ was calculated from the knowledge of various parameters. The rate coefficient for reaction (1) was measured at seven different total pressures between 10-500 Torr where the bulk of the gas was N_2 and k_1 was found to be independent of pressure with an average value of (6.2 ± 1.1) x 10^{-11} cm^3 $molecule^{-1}s^{-1}$.

Experimental Section

Reaction (1) was investigated at high pressures (10-500 Torr) where the reaction was isolated and was studied under pseudo-first order conditions in $[O(^3P)]$ with $[HO_2]$ in excess over $[O(^3P)]$. The experimental approach used in this investigation involved 248.5 nm KrF excimer laser photolysis of a mixture of H_2O_2 and O_3 in N_2 (or Ar) to produce known concentrations of HO_2 and $O(^3P)$. The temporal profile of $[O(^3P)]$ was subsequently followed using time resolved resonance fluorescence detection. The cophotolysis of H_2O_2 and O_3 in excess N_2 at 248.5 nm produces HO_2 and $O(^3P)$ via the following reactions:

$$H_2O_2 \xrightarrow[248.5]{h\nu} 2OH \tag{13}$$

$$O_3 \xrightarrow[248.5]{h\nu} O(^1D) + O_2(a^1\Delta_g) \tag{14a}$$

$$\longrightarrow O(^3P) + O_2(X^3\Sigma_g^-) \tag{14b}$$

$$OH + H_2O_2 \longrightarrow HO_2 + H_2O \tag{15}$$

$$O(^1D) + N_2 \longrightarrow O(^3P) + N_2 \tag{16}$$

$[O(^3P)]$ decays due to the following reactions:

$$O(^3P) + HO_2 \rightarrow OH + O_2 \qquad (1)$$

$$O(^3P) + H_2O_2 \rightarrow OH + HO_2 \qquad (17a)$$

$$ \rightarrow H_2O + O_2 \qquad (17b)$$

$$O(^3P) \rightarrow \text{loss from detection zone due to diffusion and reaction with background impurities} \qquad (18)$$

The concentration of HO_2 was not directly measured but was calculated based on experimentally measured and other known parameters. The criteria for producing a known concentration of HO_2 are listed below and it is worth pointing out that the accuracy of the measured value of k_1 directly depends on how well each one of these criteria is met: (i) the concentration of the photolytic precursor $[H_2O_2]$ should be measured in the system; (ii) the absorption cross section of H_2O_2 at the photolysis wavelength $\sigma(H_2O_2, 248.5$ nm) should be known; (iii) Φ_{OH}, the quantum yield for the production of OH, the precursor of HO_2, should be known at the photolysis wavelength; (iv) F, the laser fluence should be measured; and (v) the laser fluence should be "spatially uniform." If all these criteria are met, since the concentration of H_2O_2 was such that the system was optically thin at 248.5 nm, the concentration of OH formed can be calculated using the relation,

$$[OH]_o = F \times [H_2O_2] \times \sigma(H_2O_2, 248.5\ \text{nm}) \times \Phi_{OH} \qquad (I)$$

The concentration of H_2O_2 was directly measured using absorption of 202.6 nm zinc lamp radiation in a 76 cm long cell which was traversed by the reaction mixture after it exited the reactor. The absorption cross section of H_2O_2 at 202.6 nm[24] is 4.30 x 10^{-19} cm^2. The absorption cross section of H_2O_2 at 248.5 nm[24] is 8.63 x 10^{-20} cm^2 and the quantum yield for OH production from H_2O_2 at 248.5 nm[25,26] is 2. In addition, it has been shown that OH is produced in the electronic and vibrational ground state.[27] In the presence of excess N_2, the rotational and translational temperature of OH would be relaxed to that of the bath gas within a microsecond, a period very short compared to the time scale of the experiments.

Spatial uniformity of laser beams is not easy to obtain. The beam has to be reproducibly uniform for each pulse and not so merely on the average. If there is a spatial gradient (as in the case of a Gaussian beam) or if there are regions of high fluence (hot spots) then reaction (1) would proceed at different rates in different parts of the beam. The $O(^3P)$ detection zone is of finite size (~2 cm^3) and hence the measured $O(^3P)$ decay rate will be an unknown weighted average of the rates of reaction (1) in the various volumes in the detection zone. Moreover, since one cannot directly measure the fluence in the detection zone itself, if the beam were nonuniform, then the fluence measured outside the reactor could be an erroneous representation of the fluence in the detection zone. To overcome all of these problems we used a device known as a segmented aperture optical integrator to make the photolysis beam spatially uniform. The operation of this device and the extent of uniformity of the integrated beams has been described in an earlier publication from our laboratory.[28] The spatial uniformity of the beam used in the present investigation was better than 5% over its entire cross section. The beam was made to essentially fill the reactor, and the laser fluence was constant over the entire (~20 cm) length of the reactor.

The laser beam fluence was measured as the beam exited the reactor using an EG and G photodiode based radiometer capable of measuring individual pulses. Even though the calibration of this instrument is traceable to NBS standards, we carried out actinometry experiments to check the calibration. These actinometry experiments are described below.

Actinometry

Preliminary experiments using conventional actinometry techniques such as the aqueous phase ferrioxalate method or gas phase ozone photolysis followed by end product analysis showed very poor precision as well as fluence dependence. Therefore, it was clear that such methods are ill suited for measuring fluence of high powered, short pulse width lasers. To overcome this problem, we employed a very simple method where we measured the time resolved loss of O_3 due to photolysis under geometrical conditions identical to those employed in the actual kinetics experiments. The experimental set up is shown in Figure 3. A 5 cm diameter cell equipped with 2" quartz windows on opposite faces to transmit the photolysis beam and 1" windows on tubes attached to the sides of the cell to transmit the analysis beam (253.7 nm) at 90° to the photolysis beam was used. A mixture of O_3 in N_2 was slowly flowed

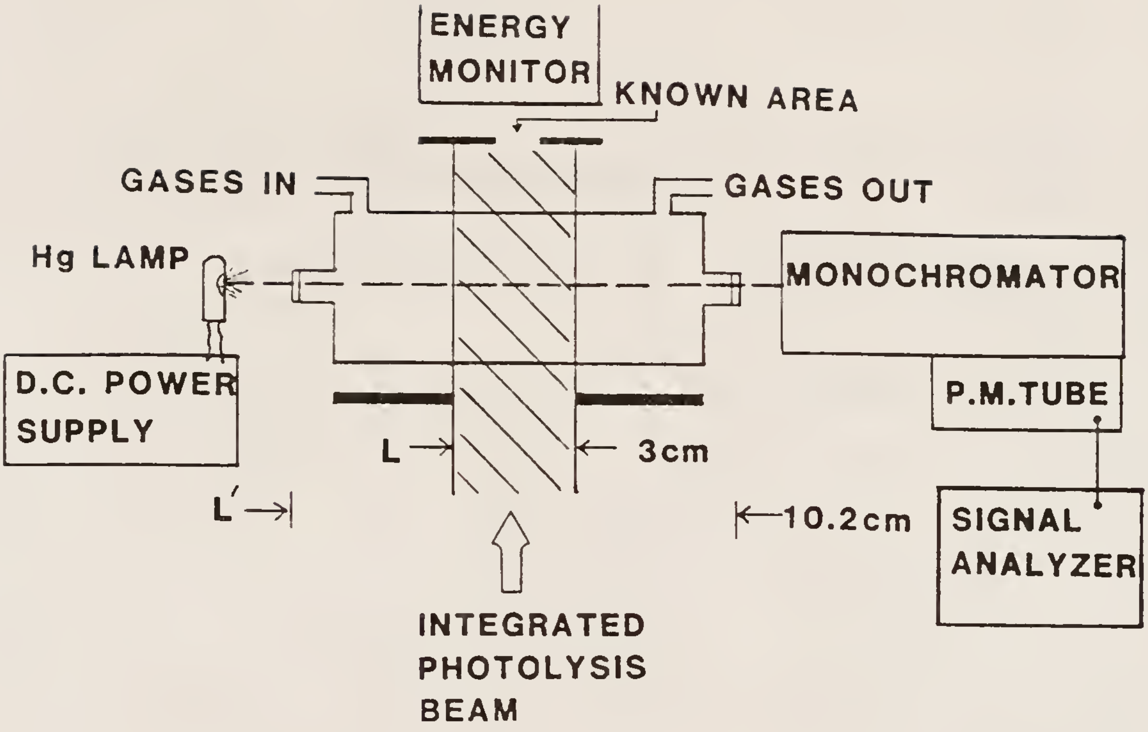

Figure 3. A schematic diagram of the apparatus used for actinometry experiments involving ozone loss measurements in real time. The gas mixture containing ozone and N_2 were premixed from measured flow rates and entered at the port marked gases in. The pressure in the system was measured at the port marked gases out. The hatched area represents the 248.5 nm photolysis beam of square cross section from the segmented aperture optical integrator. The dashed line represents the 253.7 nm Hg radiation, L is the distance the 253.7 nm beam traverses in the path of the photolysis beam and L′ is the length over which ozone absorbs.

through the cell. The 2" faces were covered by a precisely cut 3 cm x 3 cm aperture to clearly define the area of the photolysis laser beam which traversed the cell. A beam of 253.7 nm radiation from a mercury pen ray lamp run by a regulated dc power supply traversed the cell through the 1" windows, thereby crossing the 3 cm wide photolysis beam. It was passed through a monochromator and detected by a quartz enveloped 1P28 photomultiplier tube. The output of the photomultiplier tube was monitored using a signal averager operating in the peak height analysis mode.

The transmitted 253.7 nm light intensity I_o was measured with the cell flushed with N_2. Then a constant amount of ozone was added and the transmitted intensity I' measured. The ratio I'/I_o was used to calculate the concentration of ozone flowing through the cell. The photolysis laser was turned on and the integrated beam allowed to photolyze the ozone in the cell. The area of cross section of the beam was adjusted to fill the 3 cm x 3 cm aperture in front of the cell, thereby photolyzing O_3 in an identical area inside the cell. The signal averager was pretriggered and the transmitted 253.7 nm light intensity monitored. The flow rate of the O_3/N_2 mixture through the cell was such that the cell was completely replenished between laser flashes (repetition rate = 0.1 Hz). The observed temporal behavior of the transmitted 253.7 nm light intensity is shown in Figure 4. Depending on the signal level, 64 to 500 flashes were averaged. As seen in Figure 4, synchronous with the laser pulse there is a sudden jump in the transmitted intensity to I_1 followed by a slower increase to a maximum I_2. Following this maximum, the intensity

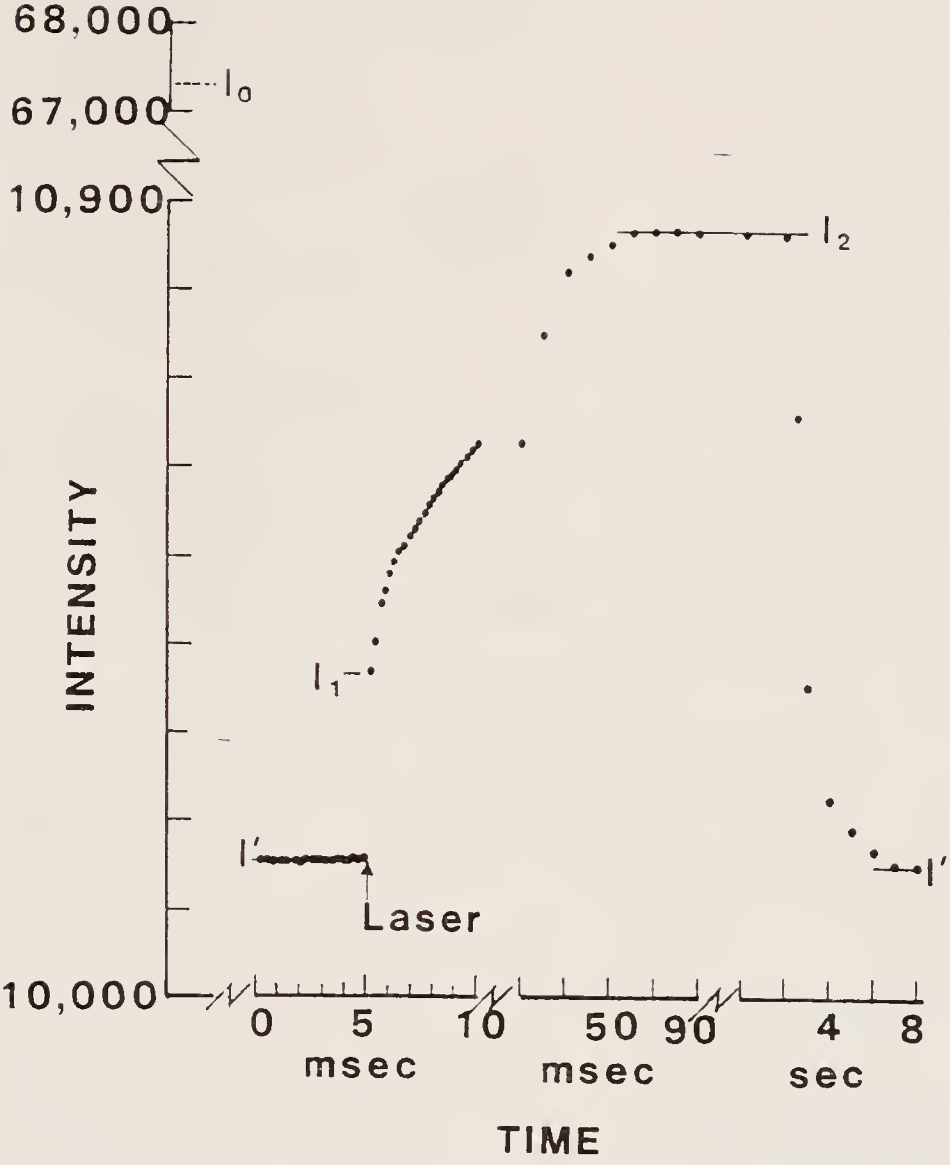

Figure 4. The temporal profile of the intensity of the 253.7 nm beam transmitted through the cell including the photolysis area. I_0 is the intensity with no ozone in the cell. I′ is the intensity after ozone has been added and its concentration has equilibrated. Notice the discontinuities in both Y and X axes. The arrow marks the time at which the photolysis laser was fired. I_1 and I_2 are the intensities immediately after photolysis and after all chemistry has stopped. The decay from I_2 to I′, in the time scale of 0-8 s, is due to refilling of the cell. For the next laser pulse, the sequence starts at time 0. I_1/I' yields the initial ozone loss and consequently the fluence while I'/I_0 yields the concentration of ozone in the cell.

slowly decreases back to I′ as the contents of the cell are swept out and filled with a fresh mixture.

The interpretation of the above result is straightforward. The sudden jump is due to the photolysis of O_3[29] to produce $O(^1D) + O_2(a^1\Delta_g)$ and $O(^3P) + O_2(X^3\Sigma_g^-)$. The primary O_3 loss is assumed to occur with a quantum yield of unity.[30] The slower ozone loss is due to the following chemistry:

$$O_3 + h\nu \rightarrow O(^1D) + O_2(a^1\Delta_g) \qquad (14a)$$

$$ \rightarrow O(^3P) + O_2(X^3\Sigma_g^-) \qquad (14b)$$

$$O(^1D) + N_2 \rightarrow O(^3P) + N_2 \qquad (16)$$

$$O(^3P) + O_3 \rightarrow 2\ O_2 \qquad (6)$$

$$O_2(a^1\Delta_g) + O_3 \rightarrow O(^3P) + 2O_2 \qquad (19)$$

It has been shown that O_3 photolysis at 248.5 nm leads to both $O(^1D) + O_2(a^1\Delta_g)$ and $O(^3P) + O_2(X^3\Sigma_g^-)$.[29] The ratio of the quantum yields of $O(^3P)$ and $O(^1D)$, $\Phi O(^3P)/\Phi O(^1D)$ has been shown[29] to be ~0.1. Therefore, the net loss of O_3 due to the secondary chemistry relative to the primary process, i.e., reaction (14) should be ~2.8. The value we obtained is 2.9 ± 0.4 which confirms that the system is behaving as expected.

The primary quantity of interest, of course, is I_1/I'. This quantity is directly related to the photon fluence in the monitoring zone of the cell by the relation

$$\ln(I_1/I') = [O_3]_{lost} \times \sigma(O_3{,}253.7\ \mathrm{nm}) \times L \tag{II}$$

where $[O_3]_{lost}$ is the decrease in $[O_3]$ due to photolysis, $\sigma(O_3{,}253.7\ \mathrm{nm})$ is the O_3 absorption cross section at 253.7 nm taken[30] to be 1.12×10^{-17} cm^2, and L is the width of the photolysis laser beam (3.0 cm). Measurement of $[O_3]_{lost}$ leads to the photon fluence F via the relationship,

$$F = \frac{[O_3]_{lost}}{\sigma(O_3{,}248.5\ \mathrm{nm}) \times [O_3]} \tag{III}$$

Simultaneous with these measurements, the transmitted laser fluence F′ (corrected as described below) was monitored by the EG and G radiometer masked by a known area (1.32 cm^2). The ratio of F/F′ was the quantity we were after since using it the photon fluence in the kinetics experiments could be directly calculated.

Four runs with varying amounts of O_3 and fluence were carried out. The average measured value of F/F′ was 1.04 ± 0.08 where the error is 2σ. (F was corrected upwards by 7.6% for the light reflected back into the cell by the back window and F′ corrected by 8% for the loss due to transmission through O_3 and the back window.) In all kinetics experiments the fluence measured by the radiometer was corrected to take the actinometry results as the primary method for fluence measurements.

The elegance of this method is clearly shown by substituting relation II into III and replacing $[O_3]$ by $\ln(I_o/I')/\{\sigma(O_3,253.7\text{ nm}) \times L'\}$, to yield,

$$F = \frac{\ln(I_1/I_o) \times L'}{\sigma(O_3,248.5\text{ nm}) \times L} \qquad \text{(IV)}$$

I_1, I_o, L', and L are all directly measured very accurately. (It should be noted that the spread in measured intensity was ~0.005%). The only quantities whose accuracies need to be relied on are $\sigma(O_3,248.5\text{ nm})$ and the quantum yield for ozone dissociation. Both of these quantities are undoubtedly accurate to better than 5% each; this leads to an accuracy of 11% in measuring F. Combining this with possible errors due to slight nonuniformities in the laser beam yields an accuracy of ~12% for the photon fluence measurements.

Kinetic Measurements

A schematic diagram of the apparatus used for carrying out kinetic measurements is shown in Figure 5. The reaction cell was 20 cm long, 3.8 cm i.d., and made of brass. Its inside was coated with FEP teflon and over coated with halocarbon wax. A mixture of H_2O_2, O_3 and N_2 was flowed through the cell. The H_2O_2 content of this mixture was measured via its absorption of 202.6 nm Zn^+ radiation from a Zn lamp in a 76 cm long absorption cell through which the reaction mixture flowed after exiting the reactor. In a previous study in our laboratory[31], it was shown that H_2O_2 does not decompose to a measurable extent in this reactor. O_3 does not interfere with the H_2O_2 measurement since (a) its concentration is very low and (b) the absorption cross section of O_3 at 202.6 nm is quite small.[30] All gas transfer lines between the source mixtures and the reactor were made of teflon connected by a few stainless steel cajon fittings to minimize H_2O_2 decomposition. The H_2O_2/N_2

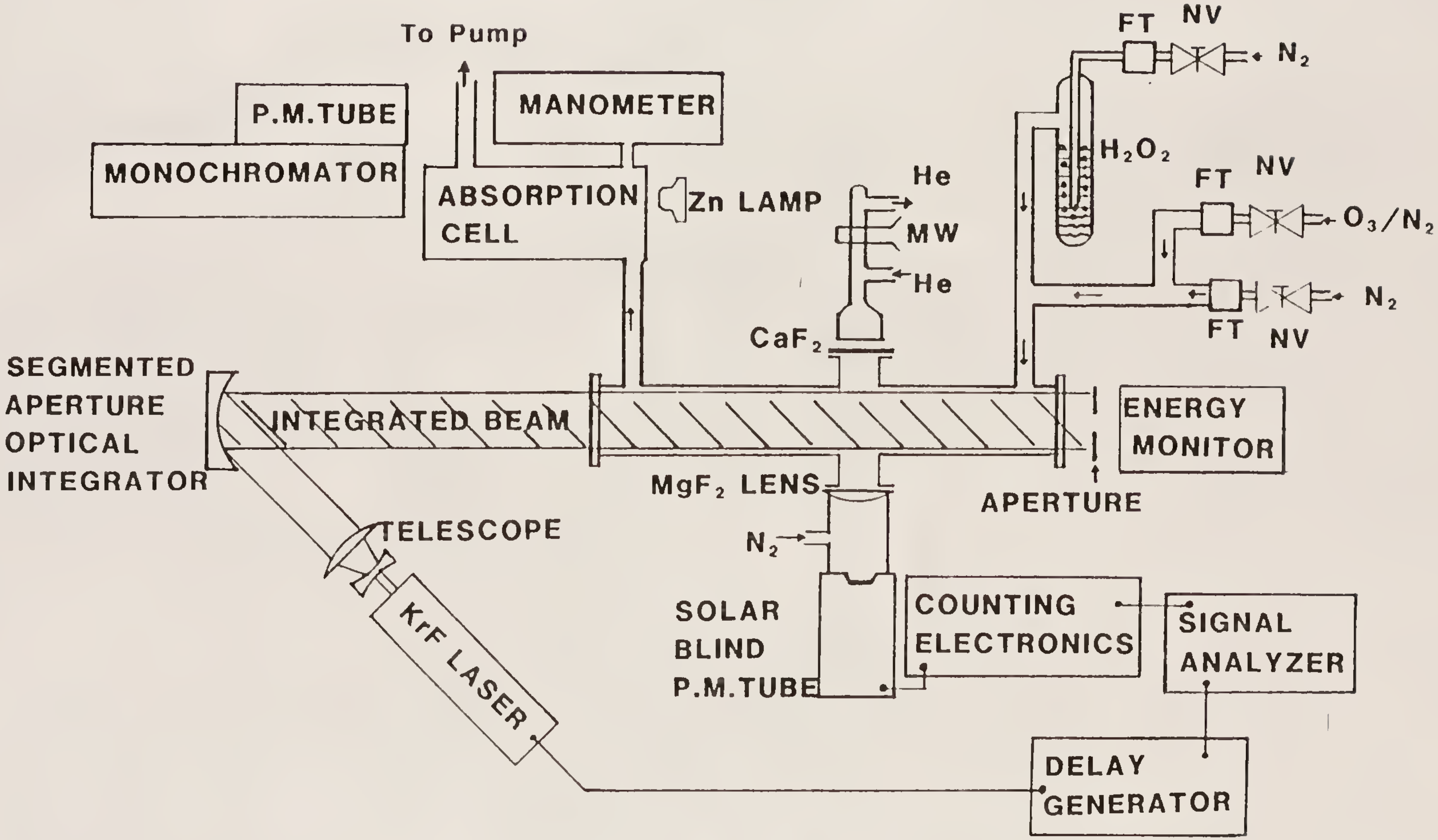

Figure 5. Schematic diagram of the pulsed laser photolysis-resonance fluorescence apparatus. To make the pictorial depiction easy, the resonance lamp is shown facing the PM tube; in the actual set up they are at 90° to each other. MW is a microwave cavity; NV is a needle valve; FT is a mass flow transducer.

mixture was generated by bubbling N_2 through a bubbler containing H_2O_2. Ninety percent pure H_2O_2 (from FMC corporation) was used after N_2 had been bubbled through it for 24 to 36 h to remove H_2O and O_2.

The O_3/N_2 mixture was stored in a 12 liter bulb. The concentration of O_3 in this mixture was measured using 253.7 nm absorption. The O_3 was prepared by passing 99.99% pure O_2 (Matheson Gas Products) through an ozonizer and collected on silica gel at 195 K. Before use ozone was liquified at 77 K and O_2 pumped out. N_2 (99.9995%) and Ar (99.9995%) were both purchased from Matheson Gas Products and used as supplied. The pressure in the system was measured as the mixture exited the reactor using a capacitance manometer. The O_3/N_2 mixture and pure N_2 were flowed through mass flow meters and their flow rates controlled by needle valves. Since H_2O_2 will decompose if passed through flow meters, a measured amount of N_2 was bubbled through the bubbler containing H_2O_2 and the mixture thus generated was added to the O_3/N_2 stream flowing into the reactor.

The reaction cell was equipped with four ports in its middle. Two ports were used to transmit the output of an oxygen resonance lamp which was filtered by a CaF_2 window to remove Lyman-α radiation. The resonance fluorescence excited by the resonance lamp beam was collected at 90° by a MgF_2 lens and focused onto the photocathode of an EMR-542G solar blind photomultiplier tube. The output of the PM tube was amplified, discriminated against noise, and fed into a signal averager operating in the multichannel scaling mode.

A typical kinetics experiment consisted of flowing 0.3-1 x 10^{13} cm^{-3} of O_3 in 10-500 Torr of N_2 through the reaction cell and the absorption cell. J_o, the intensity of the 202.6 nm Zn^+ line transmitted through the absorption cell was measured. Next, the H_2O_2/N_2 mixture was introduced into the stream of O_3/N_2

mixture, and, after equilibration of H_2O_2 with the walls, J, the transmitted 202.6 nm light intensity, was measured. Using the values of J and J_o, $[H_2O_2]$ was directly calculated; it ranged from 0.3 to 2 x 10^{16} cm^{-3}. J was continuously monitored throughout the course of the experiments. The signal averager was pretriggered 10 ms before the photolysis laser was fired to obtain the background count rate and the delay was precisely controlled by a delay generator. The photolysis beam, which had been made spatially uniform by the optical integrator, entered the reactor and initiated the chemistry. $[O(^3P)]$ was monitored as a function of time. Typically, 16 to 512 individual $O(^3P)$ temporal profiles were averaged to obtain one curve. During the averaging period, the fluence of each pulse of the photolysis beam was measured after the beam exited the reactor, using the (calibrated) E G and G radiometer. The laser fluence was then varied to produce a different concentration of HO_2. Typically, five to eight fluence values were used to create 1-10 x 10^{12} cm^{-3} of HO_2. After this series of runs were completed, the H_2O_2 flow was turned off and J_o remeasured. It should be noted that in these series of runs, for each value of HO_2, the ratio of $[HO_2]_o/[O^3P)]_o$ is not altered. To change this ratio, the composition of the mixture was varied.

During the course of each kinetic run, it is necessary that the fluence (per pulse) be constant. The KrF excimer laser used in the present experiments was equipped with a gas processor which continuously circulates the gas mixture through the laser cavity, cleans up the mixture, and replenishes F_2 such that the laser energy is extremely stable. The measured peak to peak fluctuations were typically ~2%, and the average of 10 to 512 pulses much more stable. This stability made it unnecessary to include an energy monitoring device into the circuitry triggering the signal averager to discard any individual temporal profile obtained for a given laser pulse which had not met the energy requirement.

Results and Discussion

All experiments were carried out under pseudo-first order conditions in $[O(^3P)]$ with $[HO_2]$ in excess over $[O(^3P)]$. As will be pointed out later, in this particular system it is not essential to keep $[HO_2]$ much greater than $[O(^3P)]$. If the postphotolysis chemistry is governed only by reactions (15) - (18) and reaction (1), then the temporal behavior of $[O(_3P)]$ (after all OH has been converted to HO_2) is given in Equation (V).

$$\frac{-d[O(^3P)]}{dt} = (k_1[HO_2] + k'_d)[O(^3P)] \qquad \text{(V)}$$

where $k'_d \equiv k_{17}[H_2O_2] + k_{18}$. For constant concentrations of H_2O_2 and HO_2, Equation (V) can be integrated to yield

$$[O(^3P)] = [O(^3P)]_o \exp\{(-k_1[HO_2] + k'_d)t\} \qquad \text{(VI)}$$

Figure 6 shows plots of $\ln[O(^3P)]$ versus time for three different values of $[HO_2]$ at fixed values of $[H_2O_2]$ and $[O_3]$. It is clear that Equation (VI) is obeyed. The slope of these lines yield $k' \equiv k_1[HO_2] + k'_d$. Figure 7 shows a plot of k' versus $[HO_2]$ and the slope of this line yields k_1. The value of k_1 measured using N_2 as the diluent gas under various experimental conditions are listed in Table I. Each of these values were derived by measuring at least five different k' values.

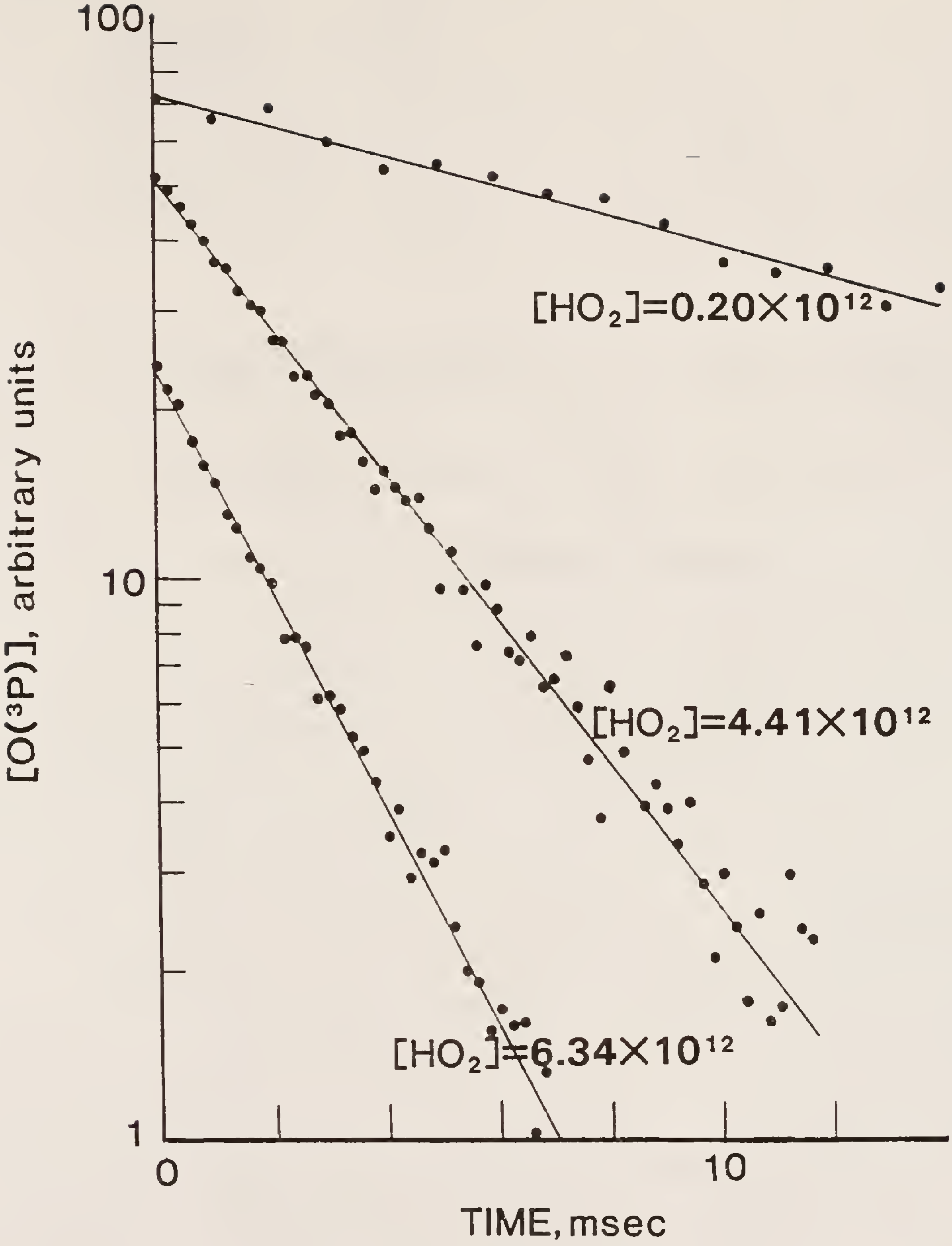

Figure 6. Temporal profile of O(^{3}P) following the photolysis of a mixture of H_2O_2, O_3 and 100 Torr N_2 at 298 K. The concentrations of HO_2 were varied by changing the fluence, and are shown next to each curve. For the sake of visual clarity, the curves are displaced on the Y axis. Different numbers of traces were averaged for each curve. The slope of each line gives k′, the measured pseudo-first order rate constant.

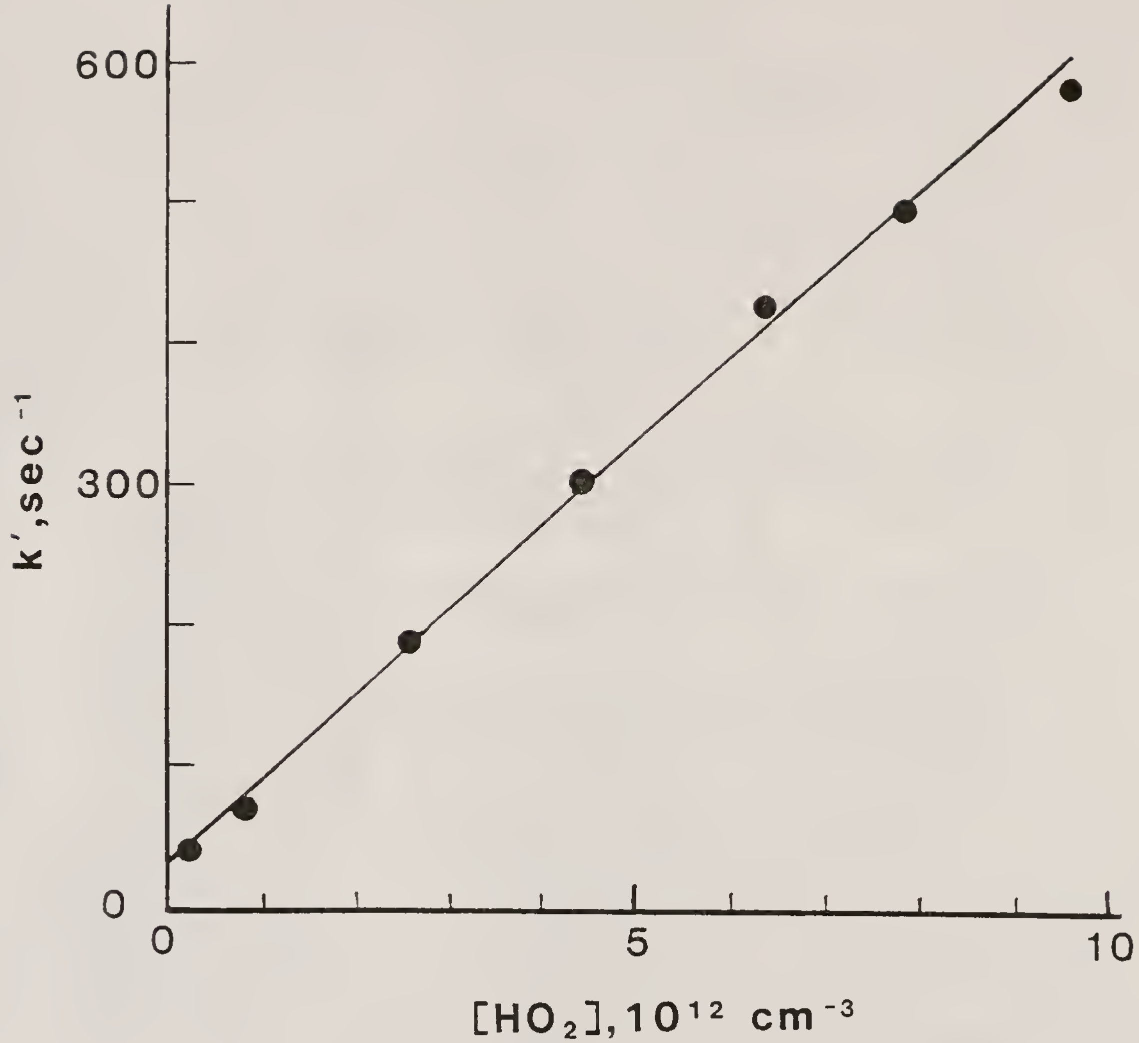

Figure 7. Plot of k′ (the measured pseudo-first order rate constant) versus [HO$_2$] at 100 Torr N$_2$ pressure and 298 K. Each [HO$_2$] has been corrected for the occurrence of the OH + HO$_2$ reaction as described in the text. The slope of the line yields k_1. The intercept represents k_d' = k_{18} + k_{17} [H$_2$O$_2$].

Table I. Summary of Rate Coefficients for Reaction (1) in N_2.

Pressure, Torr	Number of Experiments	$[H_2O_2]$, $10^{16} cm^{-3}$	$[HO_2]_o/[O(^3P)]_o$	$k_1 \times 10^{11}$ cm^3 molecule^{-1}s^{-1} (a)			
				Measured Value	Corrected(b) for reaction (22)	Average(c) value	Average(d) including systematic errors
10	9	0.75	27	6.04 ± 0.61	6.37 ± 0.64		
	6	0.84	30	6.49 ± 0.27	6.84 ± 0.28		
	5	0.80	10	5.83 ± 0.25	6.14 ± 0.26	6.47 ± 0.48	6.5 ± 1.3
20	8	0.75	22	6.15 ± 0.25	6.49 ± 0.26		
	8	0.75	26	6.03 ± 0.68	6.36 ± 0.72	6.40 ± 0.55	6.4 ± 1.3
50	5	0.82	10	5.57 ± 0.24	5.89 ± 0.25	5.89 ± 0.25	5.9 ± 1.1
100	5	0.90	15	5.58 ± 0.22	5.93 ± 0.23		
	8	0.95	17	5.49 ± 0.23	5.85 ± 0.24		
	6	0.30	5	6.54 ± 0.63	6.95 ± 0.67(e)		
	7	0.67	10	6.06 ± 0.51	6.44 ± 0.54		
	6	0.67	10	5.82 ± 0.61	6.18 ± 0.65		
	6	0.63	3	5.52 ± 0.16	5.86 ± 0.17(e)		
	8	1.00	19	5.75 ± 0.44	6.07 ± 0.47		
	7	0.92	17	5.90 ± 0.70	6.27 ± 0.74		
	5	0.85	17	5.59 ± 0.26	5.94 ± 0.28		
	6	1.71	11	5.20 ± 0.51	5.52 ± 0.54		
	6	0.68	5	5.54 ± 0.27	5.88 ± 0.29(e)	6.12 ± 0.50	6.1 ± 1.2
250	8	0.76	10	5.65 ± 0.53	6.07 ± 0.57	6.07 ± 0.57	6.1 ± 1.2
400	5	0.86	12	5.76 ± 0.26	6.27 ± 0.28	6.27 ± 0.28	6.3 ± 1.2
500	7	0.65	10	5.42 ± 0.40	5.95 ± 0.44		
	6	0.90	10	4.98 ± 0.82	5.46 ± 0.90	5.81 ± 0.72	5.8 ± 1.3

(a) All errors are 2σ.

(b) Corrected for $k_{22} = (1.6 + 2P_{atm}) \times 10^{-12}$ cm^3 molecule^{-1} s^{-1} (see the text).

(c) Averaged by weighting according to number of experiments and the precision.

(d) Includes both precision and 18% for systematic errors (see the text).

(e) Not included in the average data as $[HO_2]_o/[O(^3P)]_o$ was low.

One series of experiments was carried out with 100 Torr of Ar as the diluent gas. In these experiments, a large fraction of the $O(^1D)$ produced by O_3 photolysis reacted with H_2O_2 to produce HO_2,

$$O(^1D) + H_2O_2 \rightarrow OH + HO_2 \tag{20}$$

$$OH + H_2O_2 \rightarrow H_2O + HO_2 \tag{15}$$

This HO_2 production could not be helped since argon is a very poor quencher[32,33] of $O(^1D)$ and hence reaction (20) was competitive with the quenching. The extra production of HO_2 (2 HO_2's for each $O(^1D)$) accounted for ~12% of the net HO_2 produced. The value of k_1 obtained in 100 Torr of Ar (after correcting for certain reactions affecting $[HO_2]_o$ which will be discussed later) is $(6.27 \pm 0.68) \times 10^{-11}$ cm^3 molecule^{-1} s^{-1}.

It is necessary to mention that some preliminary measurements of k_1 were carried out using 266 nm photolysis (4th harmonic Nd:Yag) in 75 Torr of N_2. These experiments yielded a value of $(7.96 \pm 0.65) \times 10^{-11}$ cm^3 molecule^{-1}s^{-1}, (errors are 2σ and do not include systematic errors) which were reported at a recent meeting.[34] Since then we have discovered that two corrections have to be made to this number, both due to the measured fluence. First, the actinometry experiments decrease this value of k_1 by 4%. Second, we have neglected to correct for the loss in measured fluence due to the back window as well as the increase of the fluence in the reaction zone due to the reflection off the back window; this further decreases the value by ~16%, yielding $k_1 = (6.5 \pm 0.6) \times 10^{-11}$ cm^3 molecule^{-1}s^{-1} in reasonably good agreement with our other results.

Secondary Reactions that Effect [HO_2]

As mentioned earlier, during the course of this work [HO_2] was not directly measured but calculated. Therefore, a great deal of attention was paid toward recognizing, eliminating, and when unable to eliminate, accounting for HO_2 production or depletion reactions. Each of the reactions that can alter the calculated [HO_2] is considered and its possible effects on the measured value of k_1 are discussed in this section.

One of the nice features of the chemical system used in this study is that HO_2 should be regenerated after consumption in reaction (1):

$$O(^3P) + HO_2 \rightarrow OH + O_2 \tag{1}$$

$$OH + H_2O_2 \rightarrow HO_2 + H_2O \tag{15}$$

To check the effectiveness of the regeneration, a few experiments were carried out with $[HO_2]_o/[O(^3P)]_o$ ratio as low as 3. Indeed, the $O(^3P)$ decay plots were exponential and the value of k_1 thus obtained was, within experimental error, identical to those measured at higher values of this ratio (see Table I). However, most of the experiments were carried out with $[HO_2]_o/[O(^3P)]_o$ greater than 10, with an average value of 15.

Even though at first glance, looking at the exponential decays of $O(^3P)$ shown in Figure 6 and the linear variation of k' with $[HO_2]_o$ shown in Figure 7, it seems that the system is well behaved, a detailed consideration of the chemistry in the system shows that there are small contributions by some secondary reactions that do effect the calculated HO_2 concentration and they cannot be ignored. The contributions of these secondary reactions were calculated and the measured value of k_1 corrected for these complications. The corrections due to the secondary reactions are individually discussed below.

OH + HO_2 reaction. During the course of the reaction, OH was generated in reaction (1) and consumed by reaction (15). The steady state concentration of OH in the system was typically 2% of the [$O(^3P)$] and therefore no error was introduced due to the occurrence of the OH + HO_2 reaction,

$$OH + HO_2 \overset{M}{\rightarrow} H_2O + O_2 \qquad (21)$$

However, immediately after the creation of OH by H_2O_2 photolysis the concentration of OH free radicals was very high and the contribution from reaction (21) cannot be ignored. The consequence of reaction (21) is that some of the OH reacts with HO_2 and not with H_2O_2, thereby leading to an $[HO_2]_o$ value which is less than that calculated by neglecting reaction (21). To take this error into account, a numerical integration of the kinetics in the post-photolysis chemistry was carried out and the [HO_2] that is actually produced was thus calculated. The integration technique is discussed in the final section of Appendix A. The following two reaction scheme was used in the calculation:

$$OH + H_2O_2 \rightarrow HO_2 + H_2O \qquad (15)$$

$$OH + HO_2 \overset{M}{\rightarrow} H_2O + O_2 \qquad (21)$$

The recommended value[24] of k_{21},

$$k_{21} = (7 + 4\ P_{atm}) \times 10^{-11}\ cm^3\ molecule^{-1}s^{-1}$$

where P_{atm} is pressure in atmospheres, was used. The integrations showed that $[HO_2]_o$ calculated assuming reaction (21) to be negligible was as much as 8% higher than that actually produced in some of our experiments. To check for this effect, one series of experiments were carried out where ~5 x 10^{15} cm^{-3} of H_2O_2 was photolyzed at various fluence values to produce different ratios of $[H_2O_2]/[OH]_o$, some as low as 800. Figure 8 shows a plot of measured k′ versus calculated $[HO_2]_o$ (open circles). It is clear that the plot deviates from a straight line at higher $[HO_2]$ (i.e., lower $[H_2O_2]/[OH]_o$). However, when allowance is made for reaction (21), as estimated by the integration scheme, the plot is linear. Each value of $[HO_2]$ (in the kinetic runs) was corrected to allow for the occurrence of reaction (21). The corrections to $[HO_2]$ varied from 0.5% to 8% and was on the average ~3%. It should be noted that the corrections were larger for higher $[HO_2]$ since it was at these values that the $[H_2O_2]/[OH]_o$ ratios were lowest. The contribution due to reaction (21) could be made negligible by making the H_2O_2 concentration very large. However, three factors discouraged such increases. First, H_2O_2 absorbs 130.3 nm oxygen resonance radiation and increasing $[H_2O_2]$ beyond ~2 x 10^{16} cm^{-3} resulted in prohibitively degraded sensitivity for oxygen atom detection. Second, the loss of $O(^3P)$ due to reaction with H_2O_2 (reaction 17) would also increase, thereby making k'_d large. Third, the fraction of $O(^1D)$ reacting with H_2O_2 relative to that being quenched by N_2 would increase. Therefore, $[H_2O_2]$ was always held at less than 2 x 10^{16} cm^{-3}.

$O(^1D) + H_2O_2$ reaction. O_3 photolysis at 248.5 nm produces $O(^1D)$ 90% of the time.[29] In the presence of a large concentration of N_2 the majority of $O(^1D)$ is quenched to $O(^3P)$. However, a small fraction of $O(^1D)$ can react with H_2O_2 to produce two molecules of HO_2 for each $O(^1D)$ undergoing such a reaction. The extent to which reaction (20) can contribute towards the net

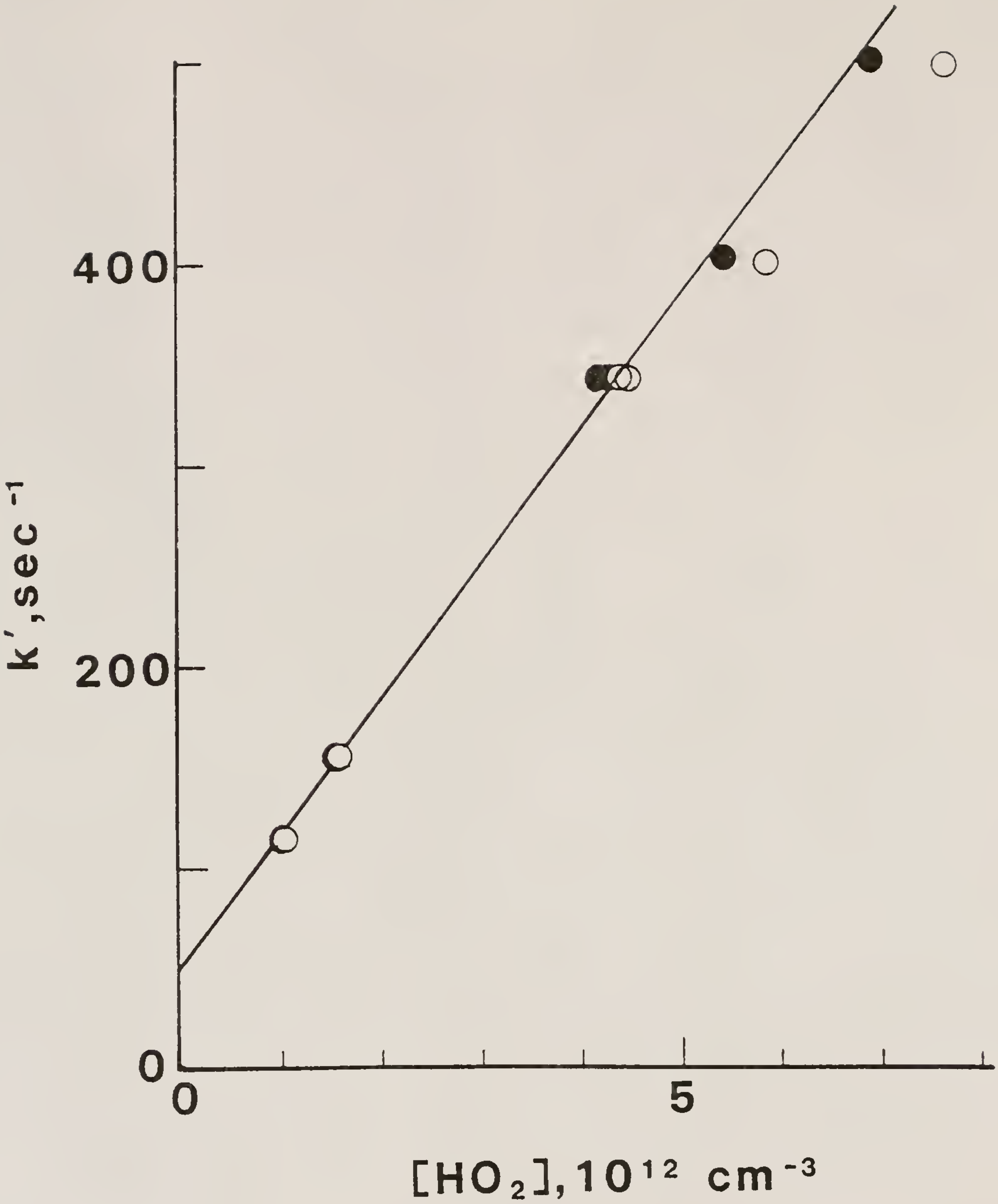

Figure 8. Plot of k′ versus $[HO_2]$ at 250 Torr and 298 K. The open circles represent $[HO_2]$ uncorrected for the occurrence of the OH + HO_2 reaction. The filled circles were obtained by correcting the HO_2 concentration as described in the text. The slope of the line yields k_1.

HO_2 produced depends on the ratio $[H_2O_2]/[N_2]$ as well as the ratio $[O_3]/[H_2O_2]$. In all experiments where N_2 was the diluent gas, except those with 10 Torr of N_2, $[HO_2]$ produced via the reaction sequence (20) followed by reaction (15) could be made less than 0.05% of that produced via H_2O_2 photolysis. In the 10 Torr experiments, however, the $[HO_2]$ produced by $O(^1D)$ reaction ranged from 0.6% to 2% of the total and this contribution was taken into account. The worst situation was in the case of one series of experiments where argon was used as the diluent gas as discussed earlier. This reaction can be made negligible by working with high $[HO_2]/[O(^3P)]_o$ as was the case in most experiments.

$O(^3P) + H_2O_2$ reaction. The reaction of $O(^3P)$ with H_2O_2,

$$O(^3P) + H_2O_2 \quad > OH + HO_2 \tag{17a}$$

$$> H_2O + O_2 \tag{17b}$$

can also increase the $[HO_2]$ during the course of reaction (1). However, this reaction is very slow, k_{17} = ~1.45×10^{-15} cm^3 molecule^{-1}s^{-1} [31]; so within the time $O(^3P)$ decays to 10% of its initial value, the maximum amount of HO_2 produced would be less than ~2% in the worst case, i.e., higher $[H_2O_2]$ (~2×10^{16} cm^{-3}) and the lowest measured decay rates (~70 s^{-1}). Therefore, the contribution due to this reaction was neglected.

HO_2 reactions with impurities. HO_2 is a reactive free radical and hence can react with impurities in the system thereby leading to an unrecognized depletion of its concentration. Keeping in mind that the only diagnostic at our disposal is the measurement of $O(^3P)$ temporal profiles, in order to check for loss of HO_2 because of reactions with impurities in the system, we varied the $[H_2O_2]$ while creating the same initial concentration of HO_2 by correspondingly varying the fluence. The measured $O(^3P)$ decay rates were not affected thereby indicating the lack of impurities coming in with H_2O_2. The $HO_2 + O_3$ reaction is too slow to deplete $[HO_2]$ and hence can be ignored. Variations in $[O_3]$ had no effect on measured $O(^3P)$ decay rates which again indicated the unimportance of HO_2 reaction with O_3 as well as with any impurities coming in with O_3. To check for impurities being swept in with the diluent gas N_2 the flow rate of the gas mixture through the cell was varied, and found to have no effect. This test, of course, does not eliminate the presence of impurities in N_2 itself. We used N_2 of the highest available purity and it seems unlikely to contain any reactive impurities. In addition, the measured value of k_1 was independent of N_2 pressure from 10 to 500 Torr. (Of course, it is possible that there can be an accidental cancellation if k_1 increases with pressure and compensates for decreases in $[HO_2]$ due to reaction of impurities. This possibility seems highly unlikely.)

$HO_2 + HO_2$ reaction. During the course of the kinetic measurements, many observations indicated the importance of the $HO_2 + HO_2$ reaction. When the $O(^3P)$ detection sensitivity was high (i.e., when all windows were clean and the resonance lamp tuned for minimal line reversal), it was clear that $O(^3P)$ decays were getting slightly nonexponential at longer reaction times with the decays getting slower as reaction (1) proceeded. The observed reaction time where this departure was evident always occurred after two 1/e times and was independent of $[HO_2]_o$. Also, these deviations were slightly more pronounced at higher pressures of N_2 than at lower pressures. Such a decrease in decay rates of $[O(^3P)]$ can be due to either the HO_2 concentration decreasing as reaction (1) proceeds or due to generation of $O(^3P)$ via secondary reactions. As will be discussed later, the second possibility can be ignored.

To take HO_2 loss via the self-reaction into account we derive the following expression for the $O(^3P)$ temporal profile based on reactions (1), (17), (18), and (22),

$$O(^3P) + HO_2 \rightarrow HO + O_2 \tag{1}$$

$$HO_2 + HO_2 \rightarrow H_2O_2 + O_2 \tag{22}$$

$$O(^3P) \xrightarrow{k'_d} \text{loss due to diffusion and reaction (17).}$$

$$\ln \frac{[O(^3P)]}{[O(^3P)]_o} = \frac{k_1}{2k_{22}} \ln(1 + 2k_{22}[HO_2]_o t) + k_d' t \tag{VII}$$

The logarithm can be expanded into a series since $-1 < 2k_{22}[HO_2]_o t < 1$, and the cubic and higher terms neglected to obtain:

$$\ln \frac{[O(^3P)]}{[O(^3P)]_o} = k_1[HO_2]_o t \times (1 - k_{22}[HO_2]_o t) + k'_d t \tag{VIII}$$

If $[HO_2]$ is indeed time independent and equal to $[HO_2]_o$, then a plot of $\ln[O(^3P)]$ versus time should be a straight line and its slope should equal $(k_1[HO_2]_o + k_d')$. In Figure 9, we have plotted $\ln([O(^3P)]/[O(^3P)]_o)$ versus time (curve a, open circles) for one experiment at 250 Torr N_2. It is seen that up to two 1/e times the decays do look exponential as does the data shown in Figure 6. However, at longer reaction times, the curve deviates from a straight line. When each $[O(^3P)]_t$ is corrected for the depletion of $[HO_2]$ using expression

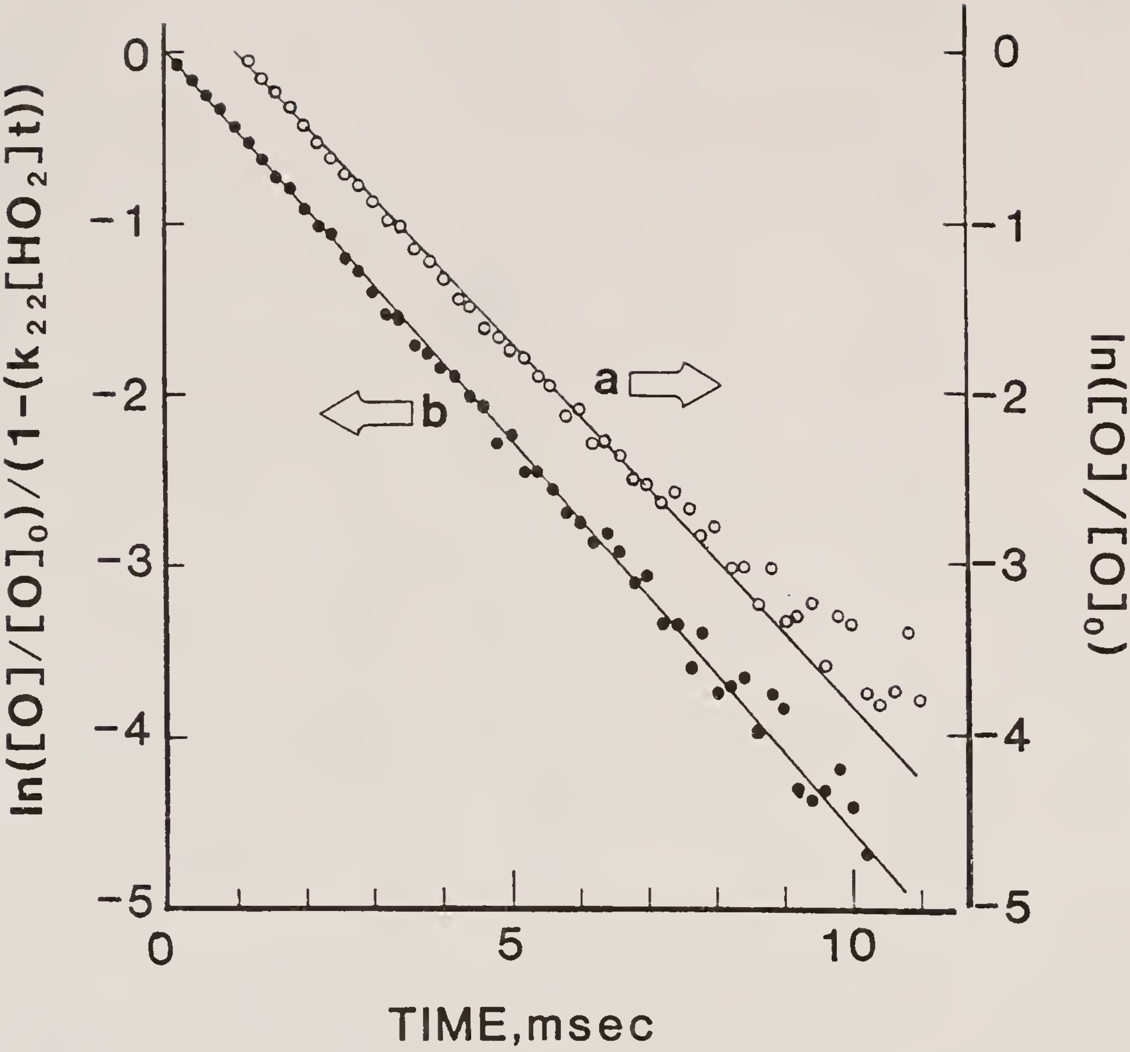

Figure 9. (a) Plot of $\ln[O]/[O]_o$ versus reaction time (open circles). The scale is on the right as shown by the arrow. The solid line is the least squares fit of this data up to two l/e times (i.e., down to $\ln[O]/[O]_o = -2$). The slope of this line is $(424 \pm 20)s^{-1}$ where the error is 2σ. Notice the deviation of the points from this line at reaction times longer than ~6 ms, (b) Plot of $(\ln[O]/[O]_o)/(1-k_{22}[HO_2]t)$ versus reaction time t. This correction accounts for the loss in HO_2 due to its self-reaction during the course of reaction (1). The scale is on the left. The solid line is the least squares fit of the data up to 10 ms. The slope of the line is $(453 \pm 13)\ s^{-1}$ where the error is 2σ. Notice the linearity of the points. The curve a has been shifted up by 1 ms for the sake of visual clarity.

VIII and we plot $\ln([O(^3P)]/[O(^3P)]_o)/(1 - k_{22}[HO_2]_o t)$ versus time, the calculated points indeed fall on a straight line (curve b). In addition, it is seen that the slope of line b is 6.8% larger than that of curve a calculated using points up to two 1/e times. It is worth noting that curve b shows what the $[O(^3P)]$ decay would be if HO_2 was not continuously decreasing due to reaction (22), but stayed constant at $[HO_2]_o$. The increase in the calculated value of k'_1 using the corrected decay curves over the uncorrected curve is ~7.8%, i.e., $(k'_{uncorrected} - k'_d)/(k'_{corrected} - k'_d) = 1.078$. This is exactly what we would get if we used the $[HO_2]$ at the point where reaction (1) has proceeded to its 1/e point. Since in all kinetic measurements we used the $O(^3P)$ decays up to two 1/e times in calculating k'_1 values, we can simply correct the $[HO_2]_o$ value to represent that at the 1/e point. The value $[HO_2]$ at the 1/e point for reaction (1), $[HO_2]'_o$, is related to $[HO_2]_o$ by the simple relation

$$[HO_2]'_o = [HO]_o/\{1 - (2k_{22}/k_1)\} \qquad \text{(IX)}$$

Most of our kinetic data were corrected using this method rather than correcting each decay curve point by point. One set of data was analyzed by correcting each decay curve and the obtained value of k_1 was indistinguishable from that obtained using the above simpler method. The correction of k_1 for this HO_2 loss process ranged from 5.4% at 10 Torr to 9.7% at 500 Torr. Both the uncorrected (column 5) and corrected values (column 6) of k_1 are listed in Table I.

Loss of HO_2 due to diffusion. It is possible for HO_2 to diffuse from the detection zone to the walls of the reactor and be lost during the course of the reaction. To minimize this possibility, the photolysis beam was made to nearly fill the reactor. $[O(^3P)]$ was monitored at the center of the beam so that HO_2

loss due to diffusion would be minimal. Therefore, HO_2 loss due to diffusion had to be quite rapid to be important. It seems unlikely to be faster than that of $O(^3P)$ which was observed to be less than ~5 s^{-1} in this system. In addition, if this loss was important, at low $[HO_2]$ the observed $O(^3P)$ temporal profiles would be nonexponential, and be unobservable at high $[HO_2]$. As discussed earlier, slightly nonexponential decays were observed at all $[HO_2]$ and were completely accounted for by reaction (22). Therefore, we conclude that HO_2 loss due to diffusion was unimportant and $[HO_2]$ was not corrected to take this process into consideration.

Secondary reactions involving $O(^3P)$. If $O(^3P)$ is either removed by reactions other than (1) and (17) or created during the course of reaction (1), our measured value of k_1 would be erroneous. The reaction of $O(^3P)$ with H_2O_2 [reaction (17)] does occur and, as pointed out earlier, merely contributes to an increased intercept. The concentration of O_3 used in these experiments (typically $< 1 \times 10^{13}$ cm^{-3}) cannot deplete $O(^3P)$ via the $O(^3P) + O_3 \rightarrow 2O_2$ reaction. Just after photolysis, a small fraction of $O(^3P)$ could react with OH,

$$O(^3P) + OH \rightarrow O_2 + H \tag{23}$$

However, the amount of OH thus depleted is negligible (~0.05%) and inconsequential since the $O(^3P)$ temporal profiles for the first 100 μs after the laser pulse was not followed. Also, any $O(^3P)$ lost by reaction (23) will regenerate an equivalent amount of HO_2 due to subsequent reactions,

$$H + HO_2 \rightarrow 2\ OH\ (H_2 + O_2,\ O + H_2O)^{20} \tag{24}$$

$$OH + H_2O_2 \rightarrow HO_2 + H_2O \tag{15}$$

Reaction (23) cannot be an important contributor to the $O(^3P)$ loss during reaction (1) since the steady state concentration of OH is very low (~10^8 - 10^9 cm^{-3}) as discussed earlier. Also, since $k_{23} \simeq k_1$,[24] reaction of $O(^3P)$ with OH would be indistinguishable from that with HO_2. The only reaction that can produce $O(^3P)$ during our experiments is that due to $O_2(a^1\Delta_g) + O_3 \rightarrow O(^3P) + 2O_2$. $O_2(a^1\Delta_g)$ is formed by ozone photolysis. The rate coefficient for this reaction[24] is too slow to be important under our experimental conditions which employed only 1 x 10^{13} cm^{-3} of ozone. Also, variations of $[O_3]$ had no effect on the measured value of k_1 implying the negligible importance of $O_2(a^1\Delta_g)$.

Possible effects of H_2O. Reactions of HO_2 are known to be enhanced by the presence of H_2O.[24] In our experiments, H_2O_2 was the source of HO_2 and it is hard to remove water from the system since H_2O_2 decomposition leads to H_2O formation. Therefore, to check for possible H_2O effects, two series of experiments using 100 Torr N_2 were carried out where up to 1.5 Torr of H_2O was added. The measured values of k_1 were, with the combined experimental error, unaltered and did not show any trends with H_2O concentration. We could not use higher concentrations of H_2O since it absorbs 130.3 nm oxygen resonance radiation, thereby severely decreasing $O(^3P)$ detection sensitivity. These experiments did show, however, that our measured values of k_1 could not have been affected by the presence of H_2O since the maximum amount of H_2O that could have been in the system was ~10% of the H_2O_2 which was usually $\leq$ 0.3 Torr.

Total error in the determination of k_1. As mentioned earlier, the total estimated error in calculating the fluence is 12%. If we add to this error, possible errors in the knowledge of $[H_2O_2]$, the quantum yield of OH production, and the uncertainties in absorption cross sections of H_2O_2 at 248.5 and 202.6 nm (5% each), the total uncertainty in our calculation of [OH] produced upon H_2O_2 photolysis would be ~15%. It is important to note here that any systematic errors in the knowledge of $\sigma(H_2O_2, 248.5\ nm)$ will be canceled out, at least partially, since we are using $\sigma(H_2O_2, 202.6\ nm)$ and as long as both numbers were taken from the same set of data the ratio $\sigma(H_2O_2, 248.5\ nm)/\sigma(H_2O_2, 202.6\ nm)$ will be much more accurate. It is this ratio that is important in calculating $[OH]_o$. However, we have conservatively assigned 5% error to each quantity.

As we discussed earlier, not all OH is converted to HO_2. The possible reduction due to reaction (21) was 8% in the worst case. In addition, the HO_2 loss due to reaction (22) varied from 5% to 9.7% with a mean value of 7.5%. These losses have been well accounted for, as described earlier. However, to be on a generously safe side, we assume that the errors in each correction could be 100%. Using all these errors in an error propagation analysis yields the net error in HO_2 concentration to be 18%. This error has been added to the precision of the measurements of k_1 and the total estimated errors are shown in the last column of Table I.

Comparison with Other Studies

Table II lists all measurements of k_1 to date. This table is essentially a duplication of that presented by Keyser[19] except that the recent results of Sridharan et al.[20] and those of the present investigation are included. The possible reasons for the discrepancies between k_1 values measured by Keyser and Sridharan et al. on one hand and all other previous measurements on the other have been discussed before[19,20] and need not be repeated. The agreement between our results and that of Keyser, $(6.1 \pm 0.4) \times 10^{-11}$ cm^3 $molecule^{-1}s^{-1}$, is extremely good. The errors quoted above for Keyser's value do not include systematic errors which he estimates to be ± 25%. The results of Sridharan et al.,[19] $(5.4 \pm 0.9) \times 10^{-11}$ cm^3 $molecule^{-1}s^{-1}$ are also in good agreement with

Table II. Comparison of Our Results for Reaction (1) with Those of Other Investigators.

Pressure, Torr	Diluent	k_1 x 10^{11} cm^3 $molecule^{-1}$ s^{-1}	Method(a)	Experimental conditions	Reference
0.8 - 2.3	He	3.7 ± 1.1(b)	DF-LMR-ESR	$[O(^3P)]>>[HO_2]$, followed $[HO_2]$	21
2.8 - 3.4	He	4.2 ± 1.5	DF-LMR-ESR	$[HO_2]>>[O(^3P)]$, followed $[O(^3P)]$	21
3.7 - 5.5	He	3.0 ± 0.9(b)	DF-LMR-ESR	Relative to reaction (23)	21
1.0	He	2.7 ± 1.0(b)	DF-LMR	Relative to reaction (23)	22
1.0	He	6.3 ± 2.0(b)	DF-LMR	Relative to reaction (15)	22
1200	$Ar(H_2,O_2)$	7 ± 2	PR-UVA	Complex chemistry modeled	23
1.0	He	6.1 ± 0.4	DR-RF	$[HO_2]>>[O(^3P)]$	19
2.5	He	5.4 ± 0.9	DF-LIF-RF	$[HO_2]>>[O(^3P)]$	20
10 - 500	N_2	6.1 ± 1.1	PLF-RF	$[HO_2]>>[O(^3P)]$	This work

(a) DF-LMR-ESR: discharge flow with LMR and ESR detection; DF-LMR: discharge flow with LMR detection; PR-UVA: pulse radiolysis with UV absorption; DF-RF: discharge flow with resonance fluorescence, DF-LIF- RF: discharge flow with laser induced fluorescence and resonance fluorescence; PLF-RF: pulsed laser photolysis with resonance fluorescence.

(b) Recalculated using currently recommended values[24] for the reference reactions.

our results considering the error limits of the two studies. (It is worth pointing out that Keyser and Sridharan et al. have not corrected their data for the occurrence of reaction (22) since they measured $[HO_2]$ and the change in $O(^3P)$ decay rates due to the continuously changing concentration of HO_2 will be small as was discussed for our measurements.) Based on the k_1 value measured by Keyser, Sridharan et al., and us, it appears that the value of k_1 is well established at 298 K and the average value is $(5.9 \pm 1.0) \times 10^{-11}$ cm^3 $molecule^{-1}s^{-1}$, independent of pressure. The atmospheric implication of this higher value of k_1 compared to previous results have been discussed by Keyser[19] and Sridharan et al.[20] and need not be repeated.

Comments on the Pressure Independence of k_1

In this study we have measured k_1 over a pressure range of 10 to 500 Torr of N_2, a factor 50 change. A plot of k_1 as a function of pressure is shown in Figure 10. The error bars that are shown represent precision only. The reason for doing so is that systematic errors are essentially the same at all pressures and therefore the relative values of k_1 at various pressures are unaffected by the systematic errors. From Figure 10, it is clear that the value of k_1 is essentially the same at all pressures within the experimental precision. The maximum range of k_1 values we observe is $5.81\text{-}6.47 \times 10^{-11}$ cm^3 $molecule^{-1}s^{-1}$. The average value falls within the error bounds of each one of the measured k_1 values (including that in 100 Torr of Ar). We prefer to quote a pressure independent value of $(6.2 \pm 1.1) \times 10^{-11}$ cm^3 $molecule^{-1}s^{-1}$ for k_1. Therefore, it is clear and worth reiterating that the value of k_1 is independent of pressure from 10 to 500 Torr.

The reaction of $O(^3P)$ with HO_2 is too fast to be understood in terms of a simple H atom abstraction reaction proceeding through a tight transition state.[19,35] $O(^3P)$ can attack HO_2 either on the H atom end to abstract the H

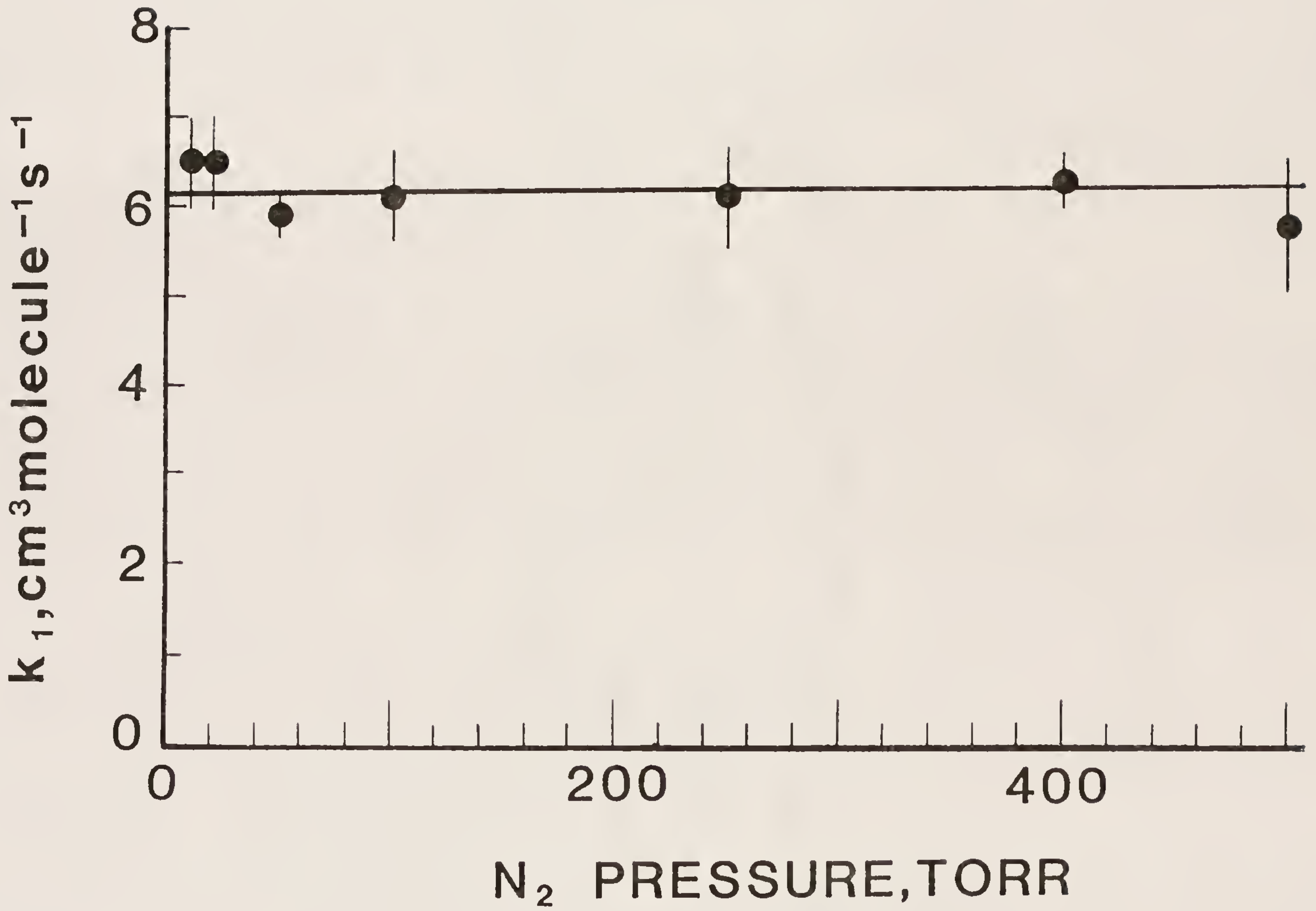

Figure 10. A plot of k_1 as a function of N_2 gas pressure. The error bars are 2σ and represent the precision of the measurements only. Notice the invariance of k_1 with N_2 pressure.

atom or on the oxygen atom end to form an H-O-O...O (not necessarily linear) complex which can decompose to give OH and O_2[19]. The latter route can proceed on a purely attractive potential energy surface since the free radical site of HO_2 is involved. If this complex is formed, it might be possible to stabilize it and decrease its decomposition back to $O(^3P)$ + HO_2. If this happens, then the observed value of k_1 should increase at high pressures. The absence of the effect of pressure on k_1 up to 500 Torr seen here indicates that, if formed, the lifetime of the complex towards decomposition into $O(^3P)$ + HO_2 should be a nanosecond or less. This short lifetime is not difficult to comprehend since the complex would be very energy rich and the energy is distributed over relatively few degrees of freedom. (A discussion of subsequent experiments that clarify the reaction pathway is presented in the next chapter.)

CHAPTER III

TEMPERATURE DEPENDENCE OF THE $O(^3P) + HO_2$ RATE COEFFICIENT

Introduction

The reaction of ground state oxygen atoms with hydroperoxyl radicals

$$O(^3P) + HO_2 \rightarrow OH + O_2 \tag{1}$$

is a major odd oxygen destruction pathway in the upper stratosphere and mesosphere. Along with the reactions

$$O(^3P) + OH \rightarrow H + O_2 \tag{23}$$

$$H + O_2 + M \rightarrow HO_2 + M \tag{25}$$

$$H + O_3 \rightarrow OH + O_2, \tag{26}$$

reaction (1) plays a major role in controlling the partitioning among H, OH, and HO_2 radicals in the upper atmosphere. Hence, accurate kinetic data for reaction (1) are needed in order to model upper atmospheric chemistry.

Several kinetics studies of reaction (1) are reported in the literature.[16,19-23,36] Four recent direct measurements of k_1 at 298 K are in excellent agreement,[16,19,20,36] with reported rate coefficients all within the range (5.2-6.2) x 10^{-11} cm^3 $molecule^{-1}s^{-1}$. However, there has been only one investigation of the temperature dependence of k_1. Keyser[19] studied reaction (1) over the temperature range 229 - 372 K in a discharge flow system at 1 Torr total pressure and observed that $k_1(T)$ increased with decreasing temperature; his reported "negative activation energy" was ~0.4 kcal/mole. Although Keyser's study of reaction (1) was a high quality experiment which appears to be free of significant systematic errors, the uncertainty in his reported activation energy will remain undesirably high[37] until independent confirmation is reported.

Several years ago, we developed a pulsed laser photolysis technique for studying the kinetics of radical-radical reactions at pressures up to 1 atm. We first applied this technique to investigate reaction (1) at 298 K over the pressure range 10 - 500 Torr.[16] In this paper, we report the results of a pulsed laser photolysis resonance fluorescence study of the temperature dependence of k_1. Our results, obtained using a much different experimental approach than that employed by Keyser,[19] confirm his reported temperature dependence and also demonstrate that k_1 is independent of pressure at subambient temperatures.

Experimental Section

With a few modifications, the experiments were carried out in the same manner as our previous room temperature study.[16] A review of the experimental approach, along with details pertinent to this investigation, is given below. A schematic of the apparatus is shown in Figure 11.

All experiments were carried out under "slow flow" conditions using a jacketed Pyrex reactor with an internal volume of 320 cm^3. The cell was maintained at a constant temperature by circulating ethylene glycol from a thermostated bath through the outer jacket. A copper-constantan thermocouple with a stainless steel jacket was inserted into the reaction zone through a vacuum seal, thus allowing measurement of the gas temperature under the precise pressure and flow conditions of the experiment.

Reactants were produced with HO_2 in excess using 248.5 nm pulsed laser photolysis of $H_2O_2/O_3/N_2$ mixtures:

$$H_2O_2 + h\nu(248.5\text{nm}) \rightarrow 2\ OH \tag{13}$$

$$O_3 + h\nu(248.5\text{nm}) \longrightarrow \begin{cases} O(^1D) + O_2(a^1\Delta_g) & \text{(14a)} \\ O(^3P) + O_2(X^3\Sigma_g^-) & \text{(14b)} \end{cases}$$

$$OH + H_2O_2 \rightarrow HO_2 + H_2O \tag{15}$$

$$O(^1D) + N_2 \rightarrow O(^3P) + N_2 \tag{16}$$

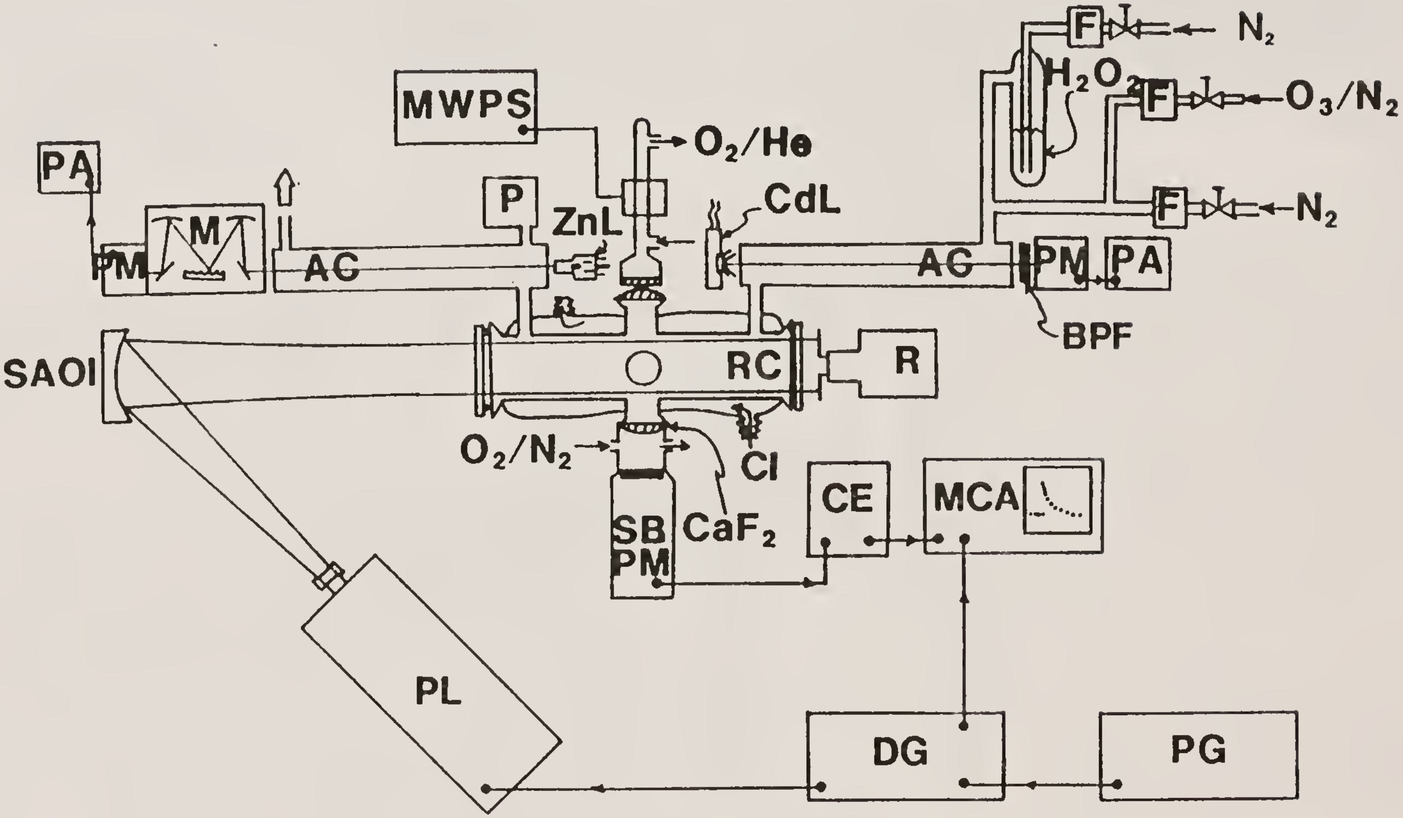

Figure 11. Schematic of the apparatus: AC, absorption cell; BPF, band-pass filter; CdL, cadmium lamp; CE, counting electronics; Cl, coolant inlet; DG, delay generator; F, flow meter; M, monochromator, MCA, multichannel analyzer; MWPS, microwave power supply; PG, pulse generator; PA, picoammeter; P, pressure gauge; PL, photolysis laser; PM, photomultiplier; R, radiometer; RC, reaction cell; SAOI, segmented aperture optical integrator; SBPM, solar blind photomultiplier, ZnL, zinc lamp. For the sake of clarity, the solar blind photomultiplier and resonance lamp are shown at 180°. In reality, the SBPM, resonance lamp, and laser beam were at right angles to each other.

A Lambda Physik model 200E KrF excimer laser was used as the photolysis light source. Kinetic data was obtained by time-resolved resonance fluorescence detection of $O(^3P)$. The laser pulsewidth was 20 ns while, under our experimental conditions, reactions (15) and (16) proceeded at rates of (3-10) x 10^3 and 7 x $10^7 s^{-1}$, respectively. $O(^3P)$ decay rates were typically in the range 30 - 500 s^{-1}.

As in our previous study, the concentration of the excess reactant, HO_2, was not directly measured but was calculated based on experimentally measured and other known parameters. To obtain $[HO_2]$ one must determine $[OH]_o$, the initial concentration of photolytically produced OH, and the yield of HO_2 from reaction (15) and competing side reactions. The chemistry of conversion of OH to HO_2 is discussed in detail in a later section. Since the concentrations of H_2O_2 and O_3 were such that the system was optically thin at 248.5 nm, $[OH]_o$ could be calculated from the following relationship

$$[OH]_o = \Phi_{OH} \times \sigma(H_2O_2, 248.5\ nm, T) \times [H_2O_2] \times F \qquad (X)$$

where Φ_{OH} is the quantum yield for OH production from 248.5 nm photolysis of H_2O_2, $\sigma(H_2O_2, 248.5\ nm, T)$ is the absorption cross section for H_2O_2 at 248.5 nm and temperature T, and F is the laser photon fluence. The determination of each factor in equation (I) is discussed in detail below.

$\underline{\Phi}_{OH}$. It is known[25,26,38] that $\Phi_{OH} \approx 2$.

$\sigma(H_2O_2$,248.5 nm,T). The absorption cross section for H_2O_2 at 248.5 nm is known to be 8.8 x 10^{-20} cm^2 at 298 K.[37] We have recently measured temperature dependent absorption cross sections for hydrogen peroxide over the wavelength range 193-350 nm.[39] At 248.5 nm, the following expression describes the observed temperature dependence (units are cm^2 molecule^{-1}):

$$\sigma(H_2O_2, 248.5\text{ nm}, T) = 1.023 \times 10^{-19} \exp\{(-45 \pm 20)/T\} \qquad \text{(XI)}$$

[H_2O_2]. Hydrogen peroxide can be lost in the slow flow system either by decomposition (particularly at higher temperatures) or by condensation (at lower temperatures). To ensure that the H_2O_2 concentration in the reactor was known, we monitored H_2O_2 by UV photometry before the gas mixture entered the reactor and after the gas mixture exited the reactor. The absorption cells were 216.2 and 90.0 cm in length. The monitoring wavelengths were 228.8 nm in the longer cell (Cd line) and 202.6 nm in the shorter cell (Zn^+ line). Both cells were kept at ambient temperature, and the absorption cross sections needed to convert absorbance data to H_2O_2 concentration were obtained by interpolation from current NASA recommendations:[37] 1.86 x 10^{-19} cm^2 at 228.8 nm and 4.31 x 10^{-19} cm^2 at 202.6 nm. When the reactor temperature was 350 K or below, the difference in H_2O_2 concentration measured in the two absorption cells was never more than a few percent. At 391 K, the highest temperature at which experiments were performed, 15-20% of the H_2O_2 was lost upon traversal of the reactor. The H_2O_2 concentration in the reaction zone was always taken to be the temperature-corrected average of the concentrations measured in the two absorption cells. Under our experimental conditions, absorption by ozone was negligible compared to absorption by H_2O_2 at 202.6 nm. At 228.8 nm, ozone made a small but significant contribution to the total absorbance. Care was taken to ensure that $[O_3]$ was constant during the I and I_o measurements required for the $[H_2O_2]$ determination.

F. The photolysis laser beam was made spatially uniform through use of a segmented aperture optical integrator.[16,28] Virtually the whole cross-sectional area of the cell was irradiated, and the depth of focus of the integrated beam was such that radical concentrations were nearly uniform down the entire length of the cell. The laser beam fluence was measured as the beam exited the reactor by using an EG&G photodiode based radiometer capable of measuring individual pulses. Pulse-to-pulse stability, a requirement for signal averaging in this type of experiment, was found to be very good. Only an occasional pulse energy deviated from the average by more than ± 5%. In order to avoid having to correct the measured fluence for reflection off the back window, an antireflection coated window with > 99.5% transmission at 248.5 nm was employed. The radiometer was calibrated by using a novel ozone actinometry method which has been described in detail previously.[16]

As mentioned above, all experiments were carried out under slow flow conditions. The linear flow velocity through the reactor was typically 12 cm s^{-1} and the laser repetition rate was typically 0.4 Hz. The reactor was 23 cm in length, so the reactor volume was completely replenished with a fresh gas mixture between laser pulses. All experiments employed nitrogen as the buffer gas at a total pressure of 80 Torr. Data were obtained over the temperature range 266-391 K. The temperature range was limited at the low end by the vapor pressure of H_2O_2 and at the high end by the thermal instability of H_2O_2.

The gases used in this study had the following stated minimum purities: N_2, 99.999%; O_2, 99.99%. Hydrogen peroxide was 90 wt % in water. It was concentrated further by bubbling N_2 through the sample for several days before experiments were undertaken and continuously during the course of the experiments. To prevent significant decomposition of H_2O_2, all components traversed by H_2O_2 between the bubbler and the exit from the last absorption cell were Pyrex or Teflon with the exception of a few stainless steel fittings. The needle valve and flowmeter in the H_2O_2 line were positioned so that N_2 flowed through these components before entering the bubbler. Ozone was prepared by passing O_2 through a commercial ozonator and was stored on silica gel at 195 K. Before use it was degased at 77 K to remove O_2. Dilute O_3/N_2 mixtures were prepared in 12 liter Pyrex bulbs for use in experiments.

A typical experiment was initiated by flowing (3-10) x 10^{12} O_3 molecules cm^{-3} in 80 Torr of N_2 through the reactor and absorption cells. I_o and J_o, the intensities of 228.8- and 202.6-nm light transmitted through the absorption cells, were measured. Next, H_2O_2 was introduced into the gas flow, the N_2 flow was reduced so the total flow rate and total pressure were the same after addition of H_2O_2 as before addition of H_2O_2, and I and J, the reduced intensities of 228.8- and 202.6 nm light transmitted through the reactor, were measured. Using the measured values of I, I_o, J, and J_o, the concentration of H_2O_2 in the gas stream entering and exiting the reactor was calculated; it ranged from (2-6) x 10^{15} molecules cm^{-3}. I and J were continuously monitored during the course of an experiment. The multichannel analyzer was pretriggered before the photolysis laser fired to obtain the background count rate. The concentration of $O(^3P)$ was monitored as a function of time after the photolysis pulse. A total of 50 - 200 laser shots were averaged to obtain one pseudo-first order kinetic decay. The fluence of each laser pulse was measured using the radiometer and a calibrated aperture. The laser fluence was varied at constant $[O_3]$ and $[H_2O_2]$ to obtain pseudo-first order decays as a function of $[HO_2]$. Five to ten fluence values were employed to determine each bimolecular rate constant, k_1, from the slope of a k' versus $[HO_2]$ plot ($k' \equiv$ the $O(^3P)$ pseudo-first order decay rate). After the fluence variations were completed, the H_2O_2 flow was turned off, the total pressure and total flow rate were readjusted, and I_o and J_o were remeasured. All HO_2 concentrations employed in the k_1 determinations were in the range (0.15-8.5) x 10^{12} molecules cm^{-3}. It should be noted that, in a series of runs involving variation of the laser fluence at constant $[O_3]$ and $[H_2O_2]$, the ratio $[OH]_o/[O(^3P)]_o$ is not altered; to change this ratio, the composition of the reaction mixture must be varied.

Results and Discussion

In the absence of competing side reactions which affect the HO_2 concentration, the kinetic system is inherently pseudo-first order, i.e., all HO_2 lost via reaction (1) is rapidly regenerated via reaction (15). However, as will be discussed in detail below, the importance of certain side reactions is suppressed when $[HO_2] >> [O(^3P)]$. Most of our experiments were carried out under experimental conditions where $[HO_2] \approx 10[O(^3P)]_o$, although this ratio was varied as a check on the kinetic model used to extract k_1. At low temperature, where relatively low H_2O_2 concentrations had to be employed, the HO_2 to $O(^3P)$ ratio was typically somewhat lower than that employed at higher temperatures.

Photolytically produced $O(^3P)$ can be lost via the following pseudo-first order processes:

$$O(^3P) + HO_2 \rightarrow OH + O_2 \tag{1}$$

$$O(^3P) + H_2O_2 \rightarrow OH + HO_2 \tag{17}$$

$$O(^3P) + O_3 \rightarrow 2O_2 \tag{6}$$

$$O(^3P) \rightarrow \text{loss by diffusion from the detector field of view and reaction with background impurities} \tag{18}$$

Under our experimental conditions, reaction (1) dominated $O(^3P)$ removal exccept at very low HO_2 levels. Reaction (6) was of negligible importance while reaction (17) was minor but not negligible.[31]. The value of k_{18} was directly measured to be ~5 s^{-1}, 1 to 2 orders of magnitude slower than $k_1[HO_2]$ under most experimental conditions.

In the absence of competing side reactions which affect the concentrations of $O(^3P)$ or HO_2, removal of $O(^3P)$ should obey first order kinetics

$$\ln\{[O(^3P)]_o/[O(^3P)]\} = (k_1[HO_2] + k_d)t \equiv k'_{exptl}t \qquad \text{(XII)}$$

where

$$k_d \equiv k_{17}[H_2O_2] + k_6[O_3] + k_{18} \qquad \text{(XIII)}$$

Figure 12 shows typical plots of ln $[O(^3P)]$ versus time. Equation XII does indeed appear to be obeyed. If side reactions were unimportant, the bimolecular rate coefficient would be obtained from the slope of a k'_{exptl} versus $[OH]_o$ plot, such as shown in Figure 13.

Secondary Chemistry

In the paper describing our 298K study of reaction (1), possible side reactions were considered in detail.[16] It was concluded that two reactions could significantly affect the HO_2 temporal profile:

$$OH + HO_2 \rightarrow O_2 + H_2O \qquad (21)$$

$$HO_2 + HO_2 \rightarrow H_2O_2 + O_2 \qquad (22)$$

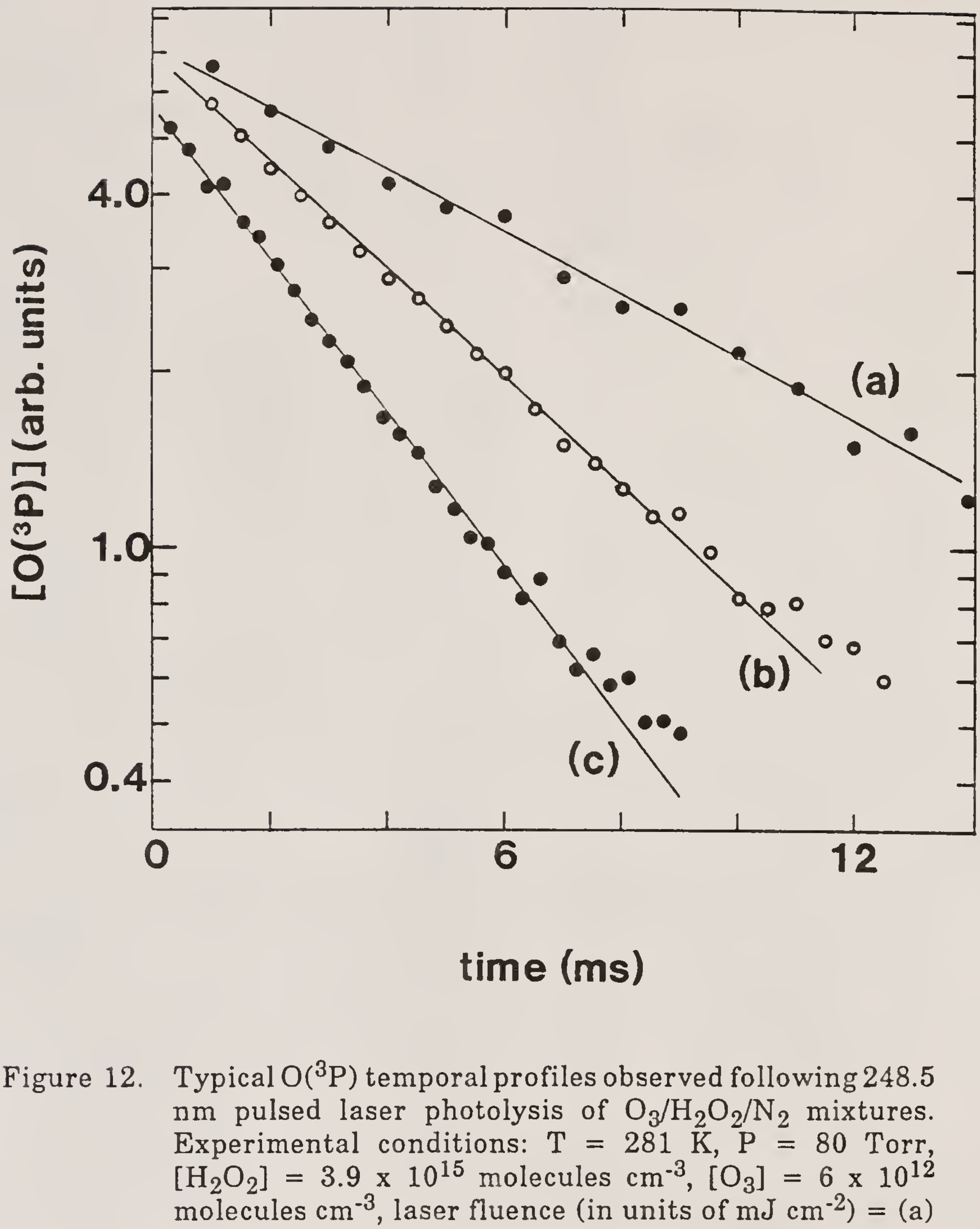

Figure 12. Typical O(^{3}P) temporal profiles observed following 248.5 nm pulsed laser photolysis of $O_3/H_2O_2/N_2$ mixtures. Experimental conditions: T = 281 K, P = 80 Torr, $[H_2O_2] = 3.9 \times 10^{15}$ molecules cm^{-3}, $[O_3] = 6 \times 10^{12}$ molecules cm^{-3}, laser fluence (in units of mJ cm^{-2}) = (a) 1.95, (b) 4.55, and (c) 6.31. Solid lines are obtained from least squares analyses of the first two 1/e times of O(^{3}P) decay and give the following pseudo-first order decay rates (k'_{exptl}): (a) 111 s^{-1}, (b) 210 s^{-1}, (c) 303 s^{-1}.

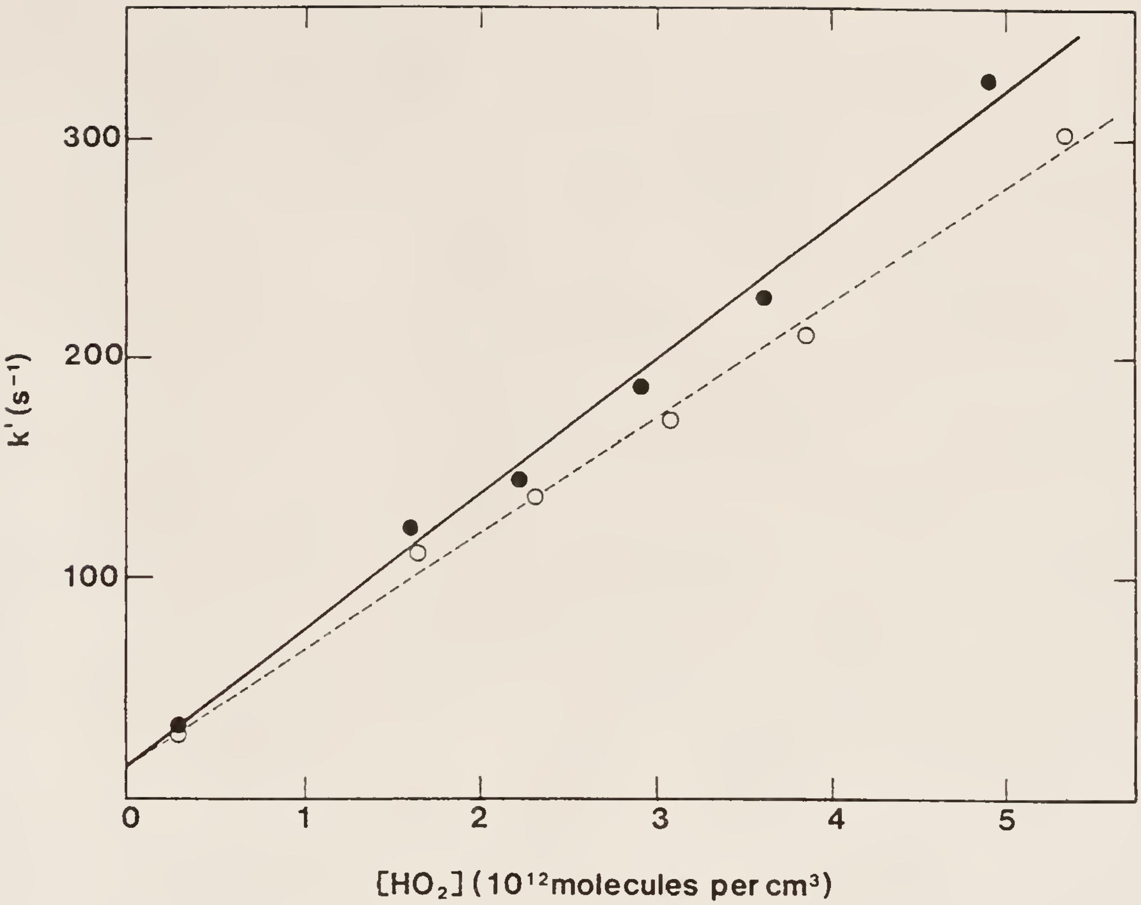

Figure 13. Typical plots of k'_{exptl} versus $[OH]_o$ (open circles) and k' versus $[HO_2]_{max}$ (closed circles). Experimental conditions: T = 281 K, P = 80 Torr, $[H_2O_2] = 3.9 \times 10^{15}$ molecules cm^{-3}, $[O_3] = 6 \times 10^{12}$ molecules cm^{-3}. The dashed line is obtained from a linear least squares analysis of the k'_{exptl} versus $[OH]_o$ data and gives the "uncorrected" rate coefficient $(5.24 \pm 0.38) \times 10^{-11}$ cm^3 $molecule^{-1}$ s^{-1}. The solid line is obtained from a linear least squares analysis of the k' versus $[HO_2]_{max}$ data and gives the "corrected" rate coefficient $(6.15 \pm 0.54) \times 10^{-11}$ cm^3 $molecule^{-1}$ s^{-1}.

To quantify the roles of reactions (21) and (22) in our kinetics experiments, a series of computer simulations were carried out where the temporal profiles of key species were calculated under a variety of experimental conditions by numerical integration of the appropriate rate equations. (The final section of Appendix A contains a discussion of the integration procedure.) For completeness, a number of reactions which were expected to play very minor roles in the $O(^3P)$ and HO_2 kinetics were included in the mechanism. The complete set of reactions and rate coefficients used in the simulations is given in Table III.

Reaction (21) competes with reaction (15) during the period immediately after the laser pulse when OH is being converted to HO_2. Each time reaction (21) occurs, two HO_2 radicals are lost which otherwise would have been present to react with $O(^3P)$. Reaction (21) is most important at high laser fluence (i.e., high $[OH]_o/[H_2O_2]$) and at low temperature. From the computer simulations, a set of curves were constructed which relate $[HO_2]_{max}$, the peak amount of HO_2 present after all photolytically produced OH has reacted away but before appreciable HO_2 loss via processes such as reaction (22) has occurred, to $[OH]_o$. Representative correction curves are plotted in Figure 14. For the 101 experiments used in the $k_1(T)$ determinations, the average value for $[HO_2]_{max}/[OH]_o$ was 0.947 while the minimum value under any set of experimental conditions was 0.845.

As pointed out above, loss of $O(^3P)$ via reactions (1), (6), (17) and (18) occurs on a time scale which is long compared to the time scale for HO_2

Table III. Reaction Set for Computer Simulations.

Reaction	Rate Coefficient[(a,b)]
$O + HO_2 \rightarrow OH + O_2$	$k_1 = 3 \times 10^{-11} \exp(200/T)$
$O + OH \rightarrow H + O_2$	$k_{23} = 2.2 \times 10^{-11} \exp(117/T)$
$H + O_3 \rightarrow OH + O_2$	$k_{26} = 1.4 \times 10^{-10} \exp(-470/T)$
$OH + H_2O_2 \rightarrow HO_2 + H_2O$	$k_{15} = 3.1 \times 10^{-12} \exp(-187/T)$
$O + H_2O_2 \rightarrow OH + HO_2$	$k_{17} = 1.4 \times 10^{-12} \exp(-2000/T)$
$O + O_3 \rightarrow 2\ O_2$	$k_6 = 8 \times 10^{-12} \exp\ (-2060/T)$
$O \rightarrow$ loss	$k_{18} = 5\ s^{-1}$
$OH + HO_2 \rightarrow O_2 + H_2O$	$k_{21} = 1.7 \times 10^{-11} \exp(416/T) + 3 \times 10^{-31}[M] \exp(500/T)$
$HO_2 + HO_2 \rightarrow H_2O_2 + O_2$	$k_{22} = 2.3 \times 10^{-13} \exp(590/T) + 1.7 \times 10^{-33}[M] \exp(1000/T)$
$HO_2 \rightarrow$ loss	$k_{27} = 5\ s^{-1}$
$HO_2 + O_3 \rightarrow OH + 2\ O_2$	$k_8 = 1.4 \times 10^{-14} \exp(-580/T)$
$H + HO_2 \rightarrow 2\ OH$	$k_{24} = 6.4 \times 10^{-11} \exp(0/T)$

(a) All rate coefficients are taken from reference 37 except k_{18} which was measured and k_{27} which was set equal to k_{18}.

(b) All rate coefficients except k_{18} and k_{27} are in units of cm^3 $molecule^{-1}$ s^{-1}.

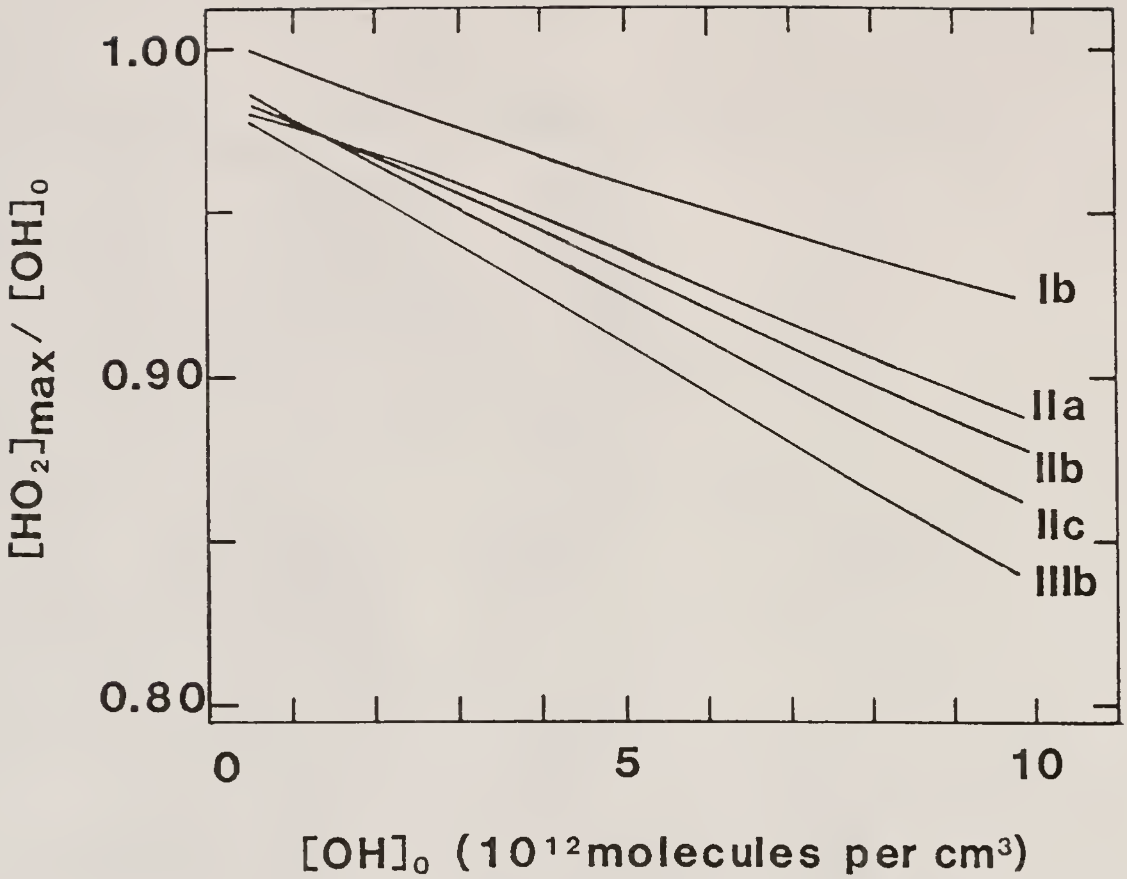

Figure 14. Typical correction curves (obtained from computer simulations) which relate $[HO_2]_{max}$ to $[OH]_o$. All curves shown in the figure are from simulations with $[H_2O_2]$ = 4 x 10^{15} molecules cm^{-3}. Temperature: I, 400 K; II, 300 K; III, 260 K. $[OH]_o/[O(^3P)]_o$: a, 10^4; b, 10; c, 4.

formation. Hence, if the concentration of HO_2 were constant over the time period of $O(^3P)$ removal, k_1 could be obtained from the slope of a k'_{exptl} versus $[HO_2]_{max}$ plot. Unfortunately, small but significant time variation of $[HO_2]$ can result from the occurrence of reactions (17), (22), and (27). Reactions (17) and

$$HO_2 \rightarrow \text{loss by diffusion from the reaction zone and reaction with background impurities} \tag{27}$$

(27) are most important at low laser fluences, i.e., low $[HO_2]$. Reaction (17) is strongly temperature dependent and increases in importance at high temperature. Reaction (17) is also a more important source of HO_2 when $[OH]_o/[O(^3P)]_o$ is relatively low. Reaction (22) becomes an important HO_2 removal mechanism at relatively high HO_2 concentrations. To avoid large corrections for HO_2 loss via reaction (22), all experiments were carried out with $[HO_2]_{max} < 9 \times 10^{12}$ molecules cm^{-3} and all data analyses were restricted to two 1/e times of $O(^3P)$ decay; i.e., no data where $[O(^3P)]/[O(^3P)]_o < 0.13$ were used in the data analysis. Computer simulations were carried out under a variety of experimental conditions. The first two 1/e times of the slightly nonexponential computer generated $O(^3P)$ temporal profiles were least squares fit to an exponential decay to obtain k'_{sim}, the simulated decay rate. The simulated decay rates were then compared to the "real" decay rates, k'_r, to obtain a set of correction curves, some of which are shown in Figure 15.

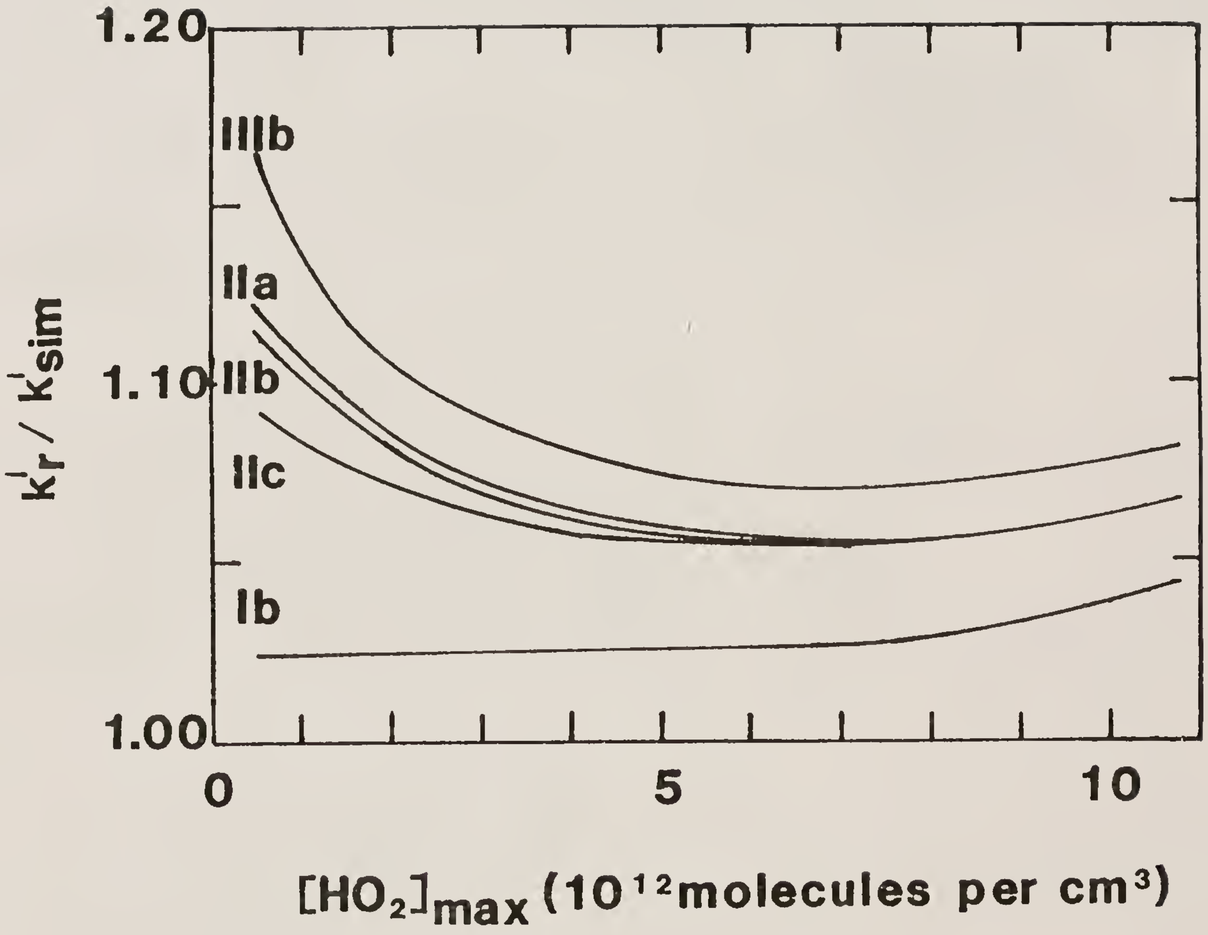

Figure 15. Typical correction curves (obtained from computer simulations) which relate k'_{exptl} to k' via equation VI. All curves shown in the figure are from simulations with $[H_2O_2]$ = 4×10^{15} molecules cm^{-3}. Temperature: I, 400 K; II, 300 K; III, 260 K. $[OH]_o/[O(^3P)]_o$: a, 10^4; b, 10; c, 4.

$$k'_r \equiv k_1[HO_2]_{max} + k_{17}[H_2O_2] + k_6[O_3] + k_{18} \qquad \text{(XIV)}$$

The first two 1/e times of each experimental $O(^3P)$ temporal profile were least squares fit to equation (XII) to obtain k'_{exptl}. A corrected value of k′ was then computed from the expression

$$k' = k'_{exptl}(k'_r/k'_{sim}) \qquad \text{(XV)}$$

One source of uncertainty in the computer simulations concerns the fact that k_{27} was not measured; it was estimated that $k_{27} = k_{18} \approx 5\ s^{-1}$. Lack of knowledge of the exact value of k_{27} increases the uncertainty in the k'_r/k'_{sim} factors at low concentrations of HO_2. The low $[HO_2]$ data are relatively unimportant in defining k_1, so the uncertainty of k_{27} makes only a minor contribution to the overall undertainty in k_1. For the 101 experiments used in the $k_1(T)$ determinations, the average value of k'_r/k'_{sim} was 1.06 and the maximum value under any set of experimental conditions was 1.18.

As discussed above, k_1 values corrected for secondary chemistry were obtained from the slopes of plots of k′ versus $[HO_2]_{max}$. Typical data are shown in Figure 13. For all 15 rate coefficients measured, the corrected k_1 values were larger than the values which would have been obtained from plots of k'_{exptl} versus $[OH]_o$ (see Figure 13, for example). The magnitude of the secondary chemistry corrections was largest at the lowest temperatures. For the 15 rate coefficients reported, the average difference between the corrected and uncorrected bimolecular rate coefficients was 16% while the largest difference was 26%.

Summary of Results

The experimental results are summarized in Table IV. Errors quoted for individual "corrected" k_1 determinations are 2σ and refer only to the precision of the k' versus $[HO_2]_{max}$ data. The absolute accuracy of our k_1 determinations is limited not only by precision but also by uncertainties in measurement of the laser photon fluences (F), the H_2O_2 concentration, the correction factor used to obtain $[HO_2]_{max}$ from $[OH]_o$, the correction factor used to obtain k' from k'_{exptl} (i.e., k'_r/k'_{sim}), and unidentified systematic errors. We estimate the pertinent 2σ uncertainties to be as follows: F, 10%; $[H_2O_2]$, 5%; $[HO_2]_{max}/[OH]_o$ 5%; k'_r/k'_{sim}, 10% at 266K and 5% at 298K and above; unidentified systematic errors, 5%. Precision did not appear to be temperature dependent and averaged 9%. Hence, the absolute accuracy of an individual k_1 determination is estimated to be $\pm$ 23% at 266 K and $\pm$ 21% at 298 K and above.

An Arrhenius plot of our results is shown in Figure 16. An unweighted linear least squares analysis of the $\ln k_1$ versus $1/T$ data gives the following expression (units are cm^3 $molecule^{-1}$ s^{-1}):

$$k_1(T) = (2.91 \pm 0.70) \times 10^{-11} \exp[(228 \pm 75)/T] \qquad \text{(XVI)}$$

Table IV. Summary of Our O + HO_2 Kinetic Data

T,K	No. of expts[(a)]	$[H_2O_2]$, $10^{15}cm^{-3}$	$[OH]_o/[O]_o$	Range of k′, s^{-1}	k_1, $10^{-11}cm^3molelcule^{-1}s^{-1}$, $\pm 2\sigma$[(b)]	
					uncorrected[(c)]	corrected[(d)]
266	6	2.98	5.0	100-268	5.22 ± 0.51	7.00 ± 0.70
266	6	2.37	6.8	28-209	5.92 ± 0.39	7.14 ± 0.52
275	6	5.61	12	57-608	5.58 ± 0.54	6.60 ± 0.75
281	6	3.90	11	33-327	5.24 ± 0.38	6.15 ± 0.54
298	5	4.22	10	56-558	5.29 ± 0.65	6.30 ± 0.91
300	10	3.57	7.1-17	51-487	5.16 ± 0.30	6.16 ± 0.73
300	6	2.05	6.8	32-293	5.21 ± 0.73	6.34 ± 0.73
300	7	3.81	6.9	66-358	4.81 ± 0.52	5.69 ± 0.56
318	6	5.46	13	73-547	5.48 ± 0.13	6.28 ± 0.09
328	8	3.07	8.0	66-326	5.44 ± 0.24	6.24 ± 0.28
354	6	3.90	16	55-418	5.14 ± 0.45	5.86 ± 0.54
359	5	4.63	15	92-368	4.52 ± 0.69	5.11 ± 0.70
374	8	4.62	15	75-361	4.40 ± 0.40	4.87 ± 0.43
380	7	4.71	19	72-466	5.11 ± 0.39	5.63 ± 0.40
391	9	4.94	11	111-438	4.87 ± 0.32	5.28 ± 0.38

(a) Experiment ≡ determination of one pseudo-first order rate.

(b) Errors represent precision only.

(c) Obtained from the slopes of k'_{exptl} versus $[OH]_o$ plots.

(d) Obtained from the slopes of k′ versus $[HO_2]_{max}$ plots.

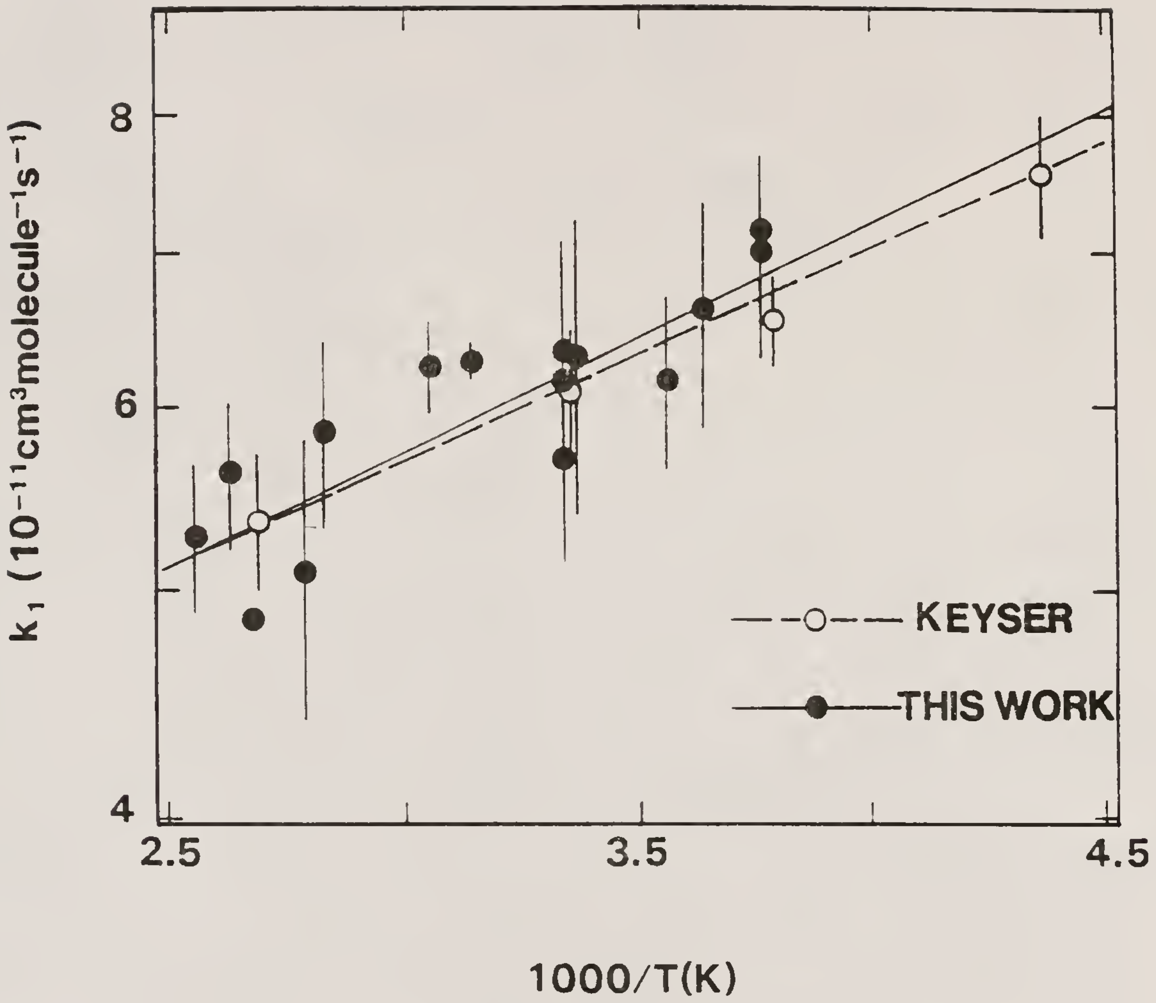

Figure 16. Arrhenius plot for the O(^{3}P) + HO_2 reaction.

The uncertainties quoted in the above expression are 2σ and represent precision only.

Comparison with Previous Work

Our results are compared with those reported by other investigators in Table V. The 298 K value reported in this paper is identical with our previously reported value[16] and at the upper end of the group of recent direct determinations[16,19,20,36] which span the range (5.2-6.2) x 10^{-11} cm^3 $molecule^{-1}$ s^{-1}. Other than our studies, the other recent direct measurements all employed low pressure discharge flow systems, all measured not only $O(^3P)$ but also HO_2 (either directly or indirectly by conversion to OH), and all carefully considered the role of competing side reactions. Hence, there is no obvious reason to prefer one value over another. The early work of Burrows et al.[22] and Hack et al.[21] give k_1(298 K) values which are considerably lower than those reported in references 16, 19, 20, and 36. Possible reasons for the apparently erroneous results reported in references 22 and 21 are discussed elsewhere.[19] Lii et al.[23] obtained a value for k_1 by comparing computer simulations with HO_2 and O_3 concentration profiles observed following pulsed radiolysis of $O_2/H_2/Ar$ mixtures. Their reported rate coefficient agrees well with our results. However, as pointed out by Keyser,[19] the experimental data of Lii et al. are very insensitive to the value of k_1; hence, their error limits should be ~500% rather than the reported 30%.

Very little temperature dependent data are available for reaction (1). Values for k_1 of 8 x 10^{-11} $cm^3 molecule^{-1} s^{-1}$ at 1600 K[40] and 6 x $10^{-11} cm^3$

Table V. Comparison of Our Results With Those of Other Investigators.

Range of T,K	Range of P, Torr	M	Experimental method(a)	Experimental conditions	A(b)	E/R,K	k_1(298K)(b)	Ref.
298	1.0	He	DF-LMR	relative to k_{23} relative to k_{15}			2.7 $\pm$ 1.0(c) 6.3 $\pm$ 2.0(c)	22
298	0.8 - 2.3 2.8 - 3.4 3.7 - 5.5	He	DF-LMR/ESR	$[O(^3P)]>>[HO_2]$ $[HO_2]>>[O(^3P)]$ relative to k_{23}			3.7 $\pm$ 1.1 4.2 $\pm$ 1.5 3.0 $\pm$ 0.9(c)	21
298	1200	$Ar/H_2/O_2$	PR-UVA	k_1 extracted by modeling complex chemistry			7 $\pm$ 2	23
296$\pm$2	2.5	He	DF-RF/LIF	$[HO_2]>>[O(^3P)]$			5.4 $\pm$ 0.9	20
229-372	1.0	He	DF-RF	$[HO_2]>>[O(^3P)]$	3.1 $\pm$ 0.3	200 $\pm$ 28	6.1 $\pm$ 0.4	19
298	10 - 500	N_2	PLP-RF	$[HO_2]>>[O(^3P)]$			6.1 $\pm$ 1.1(d)	16
300	1.0 - 4.0	He	DF-LMR/RF/RA	$[O(^3P)]>>[HO_2]$ $[HO_2]>>[O(^3P)]$			5.2 $\pm$ 0.8	36
266-391	80	N_2	PLP-RF	$[HO_2]>>[O(^3P)]$	2.9 $\pm$ 0.7	228 $\pm$ 75	6.2 $\pm$ 1.0	This Work

(a) DF, discharge flow; LMR, laser magnetic resonance; ESR, electron spin resonance; PR, pulsed radiolysis; UVA, ultraviolet absorption; RF, resonance fluorescence; LIF, laser-induced fluorescence; PLP, pulsed laser photolysis; RA, resonance absorption.

(b) Units are $10^{-11} cm^3 molecule^{-1} s^{-1}$.

(c) k_1 recalculated with presently recommended (ref. 37) values for the reference reactions.

(d) Corrected downward from reported value by 1.5% to account for small change in recommended H_2O_2 absorption cross section.

molecule^{-1}s^{-1} at 1050 K[41] have been inferred from flame studies. The only previous temperature dependence study in the atmospheric temperature regime is that of Keyser.[19] As seen from the comparisons in Table V and Figure 14, our results are in excellent agreement with those of Keyser. Since our experiments were very different in methodology from Keyser's and are subject to different sources of systematic errors, the uncertainty of $k_1(T)$ for atmospheric modeling purposes is now greatly reduced. Keyser's study employed helium buffer gas at a pressure of 1.0 Torr while our study employed nitrogen buffer gas at a pressure of 80 Torr. Thus, agreement between the two studies strongly suggests that k_1 is independent of pressure over the relevant upper atmospheric temperature and pressure ranges.

Reaction (1) could proceed via a hydrogen abstraction mechanism (1a) or via formation of an energized HOOO "pseudo-intermediate" (1b):

$$O + HO_2 \rightarrow O\cdots HO_2 \rightarrow OH + O_2 \tag{1a}$$

$$O + O_2H \rightarrow O\cdots OOH \rightarrow O_2 + OH \tag{1b}$$

Sridharan et al.[42] recently reported an elegant experiment in which ^{16}OH and ^{18}OH products from the reaction of ^{18}O with HO_2 were monitored in a discharge flow system. They found that only ^{16}OH was produced, implying that O reacts with HO_2 via channel (1b). Thermochemical estimates suggest that HOOO is bound relative to O + HO_2, but is ~12 kcal mol^{-1} less stable than the

$OH + O_2$ products.[43,44] Mozurkewich[45] points out that since HOOO is bound relative to $O + HO_2$, we might expect to find a long-range interaction that would produce a transition state for reaction (1) very similar to that expected from formation of HOOO. Mozurkewich's RRKM calculations yield a rate constant for formation of HOOO of $5.5 \times 10^{-11} cm^3 molecule^{-1} s^{-1}$ independent of temperature.[45] The observed negative activation energy for reaction (1) could probably be reproduced if a small barrier were assumed in the HOOO → OH + OH_2 reaction path.[46]

Implications for Atmospheric Chemistry

Model calculations of OH and HO_2 concentration profiles in the upper stratosphere are very sensitive to the choice of $k_1(T)$. Kaye and Jackman,[47] considering both sensitivity of their model to various parameters and uncertainties in these parameters, have concluded that the uncertainty of k_1 contributes more to the uncertainty in [OH] and [HO_2] at 35°N, 40 km altitude than any parameter in their model except k_{21}. The currently recommended value[37] for $k_1(T)$ is

$$k_1(T) = 3.0 \times 10^{-11} \exp[(200 \pm 200)/T] \ cm^3 molecule^{-1} s^{-1} \qquad (XVII)$$

The results reported in this paper will have little effect on the recommended A factor and activation energy, but will substantially reduce the uncertainty in the above expression; this will, in turn, significantly reduce the overall uncertainty in model calculations of upper stratospheric OH and HO_2 concentrations and facilitate meaningful comparisons of stratospheric measurements with photochemical models.

Jackman et al.[48] have recently compared O_3 concentrations at 5°N and 43 km altitude measured by LIMS (limb infrared monitor of the stratosphere) with those calculated from a photochemical model using LIMS measurements of H_2O, HNO_3, NO_2, and temperature and SAMS (stratospheric and mesospheric sounder) measurements of CH_4 as input. The model predicted lower O_3 levels than those actually observed. A sensitivity analysis showed that the overall uncertainty in the model calculation was a factor of 1.7, about the same magnitude as the discrepancy between model and measurement. Of the many parameters used in the model, the uncertainty of k_1 was found to make the sixth largest contribution to the overall uncertainty of the calculation. Our results will therefore result in a small but significant reduction in the model uncertainty.

CHAPTER IV

PULSED LASER PHOTOLYSIS KINETICS STUDY OF THE $O(^3P)$ + ClO REACTION

Introduction

The reaction of ground state oxygen atoms $O(^3P)$ with ClO radicals is the rate determining step in the dominant catalytic cycle via which chlorine atoms destroy odd oxygen in the middle stratosphere:

$$O + ClO \rightarrow O_2 + Cl \qquad (2)$$

$$Cl + O_3 \rightarrow ClO + O_2 \qquad (12)$$

$$\overline{\qquad\qquad\qquad\qquad\qquad}$$

$$O + O_3 \rightarrow 2O_2 \qquad \text{net}$$

The primary source of stratospheric chlorine atoms is the photolysis of anthropogenic chlorofluorocarbons.

Seven measurements of k_2(298 K) are reported in the literature.[49-56] There is agreement among the five most recent studies that k_2(298 K) lies in the range 3.5 - 4.2 x 10^{-11} $cm^3molecule^{-1}s^{-1}$. The activation energy for reaction (2) is known to be small,[50-56] but its value is not as well defined as would be desirable for such an important stratospheric reaction. In fact, it is not clear if $k_2(T)$

increases or decreases with decreasing temperature. In addition to the abovementioned studies of reaction (2) at atmospheric temperatures, one high temperature (1250 K) shock tube measurement of k_1 has been reported,[57] as has one theoretical calculation of $k_2(T)$ over the temperature range 220-1000 K.[58]

Because predictions of chlorine catalyzed ozone loss are very sensitive to the value of $k_2(T)$ used in model calculations, it is important that this rate coefficient be determined with high precision at stratospheric temperatures. Studies employing a variety of experimental techniques are desirable in order to uncover possible systematic errors. All previous studies of reaction (2) at ambient and subambient temperatures[49-56] employed discharge flow systems which were limited to total pressures of 10 Torr or less. It is interesting to note that reaction (2) occurs on a potential energy surface with a minimum along the reaction coordinate, i.e., the intermediate complex ClOO is a bound species whose ground state correlates with $O(^3P) + ClO(X^2\pi)$[59]. Reactions which occur on potential energy surfaces of this type often exhibit negative activation energies and pressure dependent rates.

We have recently developed a pulsed laser photolysis method for carrying out direct kinetics studies of radical-radical reactions at pressures up to one atmosphere, and applied this method to study the temperature and pressure dependences of the $O + HO_2$ reaction.[16,17] Using an extension of the technique employed in the $O + HO_2$ investigations, we have studied the kinetics of reaction (2) in N_2 buffer gas over the temperature and total pressure ranges 231-367 K and 25-500 Torr. Our results, which include observation of a significant negative activation energy, are reported in this paper.

Experimental

A schematic of the apparatus appears in Figure 17. The two radical species were created via a scheme involving two separate photolysis lasers. Under "slow flow" conditions, a gas mixture containing Cl_2 and O_3 in a large excess of N_2 buffer gas was first subjected to photolysis by a XeF excimer laser,

$$Cl_2 + h\nu \ (351 \text{ nm}) \rightarrow 2Cl \tag{28}$$

The combination of the excimer laser fluence and $[Cl_2]$ was always large enough for the condition $[Cl]_o > [O_3]_o$ to hold. During a predetermined delay period, t', the reaction

$$Cl + O_3 \rightarrow ClO + O_2 \tag{12}$$

was allowed to go to completion. At this time the ozone in the reaction cell had effectively been titrated by Cl atoms and the initial value of $[O_3]_o$ could be related to $[ClO]_{t'}$. At the end of this delay a second laser pulse, the fourth harmonic of the fundamental wavelength from a Nd:YAG laser, photolyzed a small fraction of the ClO,

$$ClO + h\nu(266 \text{ nm}) \rightarrow Cl + O \tag{29}$$

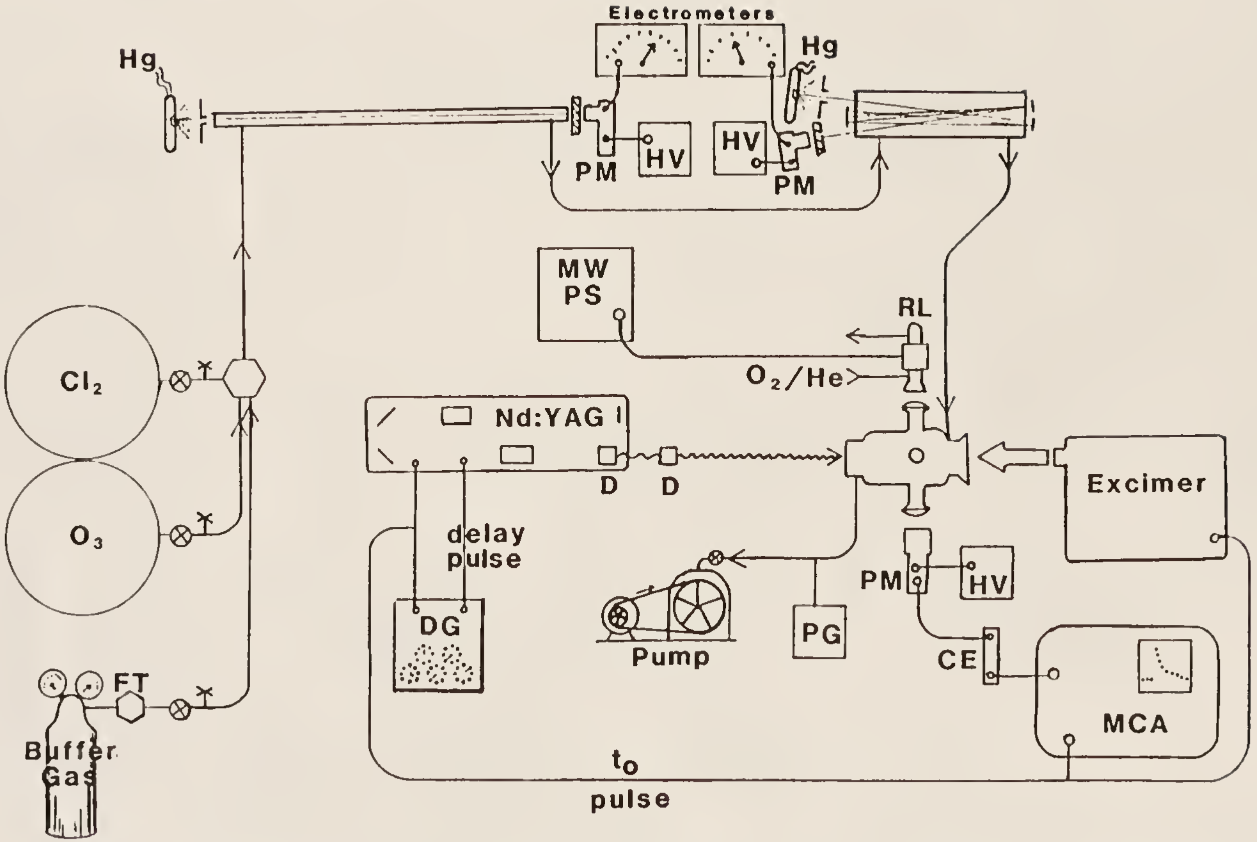

Figure 17. Schematic diagram of the experimental apparatus. The abbreviations used are as follows: FT - flow transducer; Hg - mercury pen-ray lamp; PM - photomultiplier tube; HV - high voltage power supply; MWPS - microwave power supply; RL - resonance lamp; DG - delay generator; PG - pressure gauge; MCA - multichannel analyzer; D - doubling crystal; CE - counting electronics. For the sake of clarity, the resonance lamp and photomultiplier tube are shown facing each other when, in fact, they were mounted at 90° to each other and perpendicular to the direction of the laser beams.

The decay of oxygen atoms in the presence of excess ClO was followed by monitoring the time dependence of fluorescence signal which was continuously excited by a microwave discharge resonance lamp. The lamp was operated with a low pressure of helium (<1 Torr) containing a small fraction of O_2.

The ozone storage bulb contained a mixture of 1% to 2% O_3 in nitrogen, while the Cl_2 was stored neat. These species were leaked through needle valves into the main gas flow. Ozone in the gas flow was measured in a 35.0 cm absorption cell that was placed within a multipass optical arrangement. Using modified White cell optics, 30 passes of the 254 nm Hg line from a pen-ray lamp were sent through the absorption cell for an effective path length of 10.50 m. The chlorine was measured in a 216 cm absorption cell using a single pass of the 366 nm Hg line, also from a pen-ray lamp. Both atomic lines were isolated using suitable band pass filters. Typically, the absorption cells were upstream from the reaction cells, although in a few experiments the Cl_2 and O_3 were measured after the flow exited the reaction cell. Because Cl_2 absorbance at 254 nm was not totally negligible [$\sigma = 1.6 \times 10^{-21}$ cm^2 (Ref. 60)], the reference light intensity for the [O_3] determination was always measured with Cl_2 flowing. The Cl_2 absorption cross section at 366 nm and the O_3 absorption cross section at 254 nm were taken to be 1.01×10^{-19} cm^2 (Ref. 60) and 1.147×10^{-17} cm^2 (Ref. 61-63), respectively.

The Pyrex reaction cell measured 16 cm along its longer axis and had an internal diameter of 4 cm. The two laser beams counterpropagated along the longer axis. Around the middle of the cell were four 1.5 cm diameter side arms, each perpendicular to the long axis of the cell and at 90° to each other. The resonance lamp radiation entered the cell through one of the side arms and the fluorescence signal was collected through a neighboring arm. The central portion of the cell was surrounded by a jacket through which thermostated liquids were flowed to control the temperature of the gas mixture inside the reactor. The gas mixture entered the cell through several ports very near the window at one end of the long axis and exited the cell through similar ports near the opposite window. Because the chemistry initiated by the excimer laser beam completely titrated one component (O_3) of the gas mixture within much of the cell volume, the cell was designed to have minimum total volume and low dead space, i.e., gas flowed through all volume elements of the cell at approximately equal rates. The typical linear flow rate through the cell was 14 cm s^{-1} and the repetition rate of the two laser sequence was usually 0.4 Hz. Therefore, the gas mixture within the entire volume of the reaction cell was replenished between excimer laser pulses. The temperature of the gas mixture was measured by replacing one of the end windows with an acrylic flange through which a copper-constantan thermocouple could be inserted. The errors in the reported temperatures are estimated to be no more than ± 1.0 K at the extreme temperatures and less at intermediate temperatures.

Oxygen resonance lamp radiation was focused into the reaction zone by a 2-inch focal length MgF_2 lens. The reaction zone was viewed by a solar blind photomultiplier tube through a similar lens. The volumes between the resonance lamp and the reaction cell, and between the reaction cell and the photomultiplier tube were purged with a mixture of 1% O_2 in nitrogen. This excluded room air and also acted as a filter of extraneous emissions from the resonance lamp. A CaF_2 window between the cell and the photomultiplier tube eliminated the possibility of hydrogen atom detection. Fluorescence signals were accumulated using photon counting techniques in conjunction with multichannel scaling. Each sweep of the analyzer was triggered simultaneously with the excimer laser. From 50 to 500 flashes were averaged to obtain sufficient signal to noise ratio for quantitative kinetic analysis.

The total pressure in the flow system was measured with a capacitance manometer. Due to the necessarily fast flow rate and the small (4.0 mm i.d.) tubing connecting the various components of the flow system, there were measurable pressure gradients between the absorption cells and the reaction cell. Quantitative adjustments were made for these gradients in the calculation of the Cl_2 and O_3 concentrations in the reaction cell under each set of conditions. The magnitude of the adjustment was largest at the lowest pressure (15% at 25 Torr) and negligible at the highest (1% at 200 Torr). The nitrogen buffer gas comprised at least 94% of the mixture for all experiments and its flow rate was monitored using a calibrated electronic mass flowmeter.

The concentration of ClO, the excess species in this technique, was derived from the concentration of ozone as measured *in situ*. Therefore, it was not necessary to have an absolute calibration of the photolysis laser fluences. However, it was important to know that following the excimer laser pulse the condition $[Cl] > [O_3]$ held throughout the reaction zone. Therefore, the excimer laser fluence was measured in each experiment. As will be discussed below, it was also important to monitor the 266 nm laser fluence. Both of these quantities were determined using a photodiode-based calibrated radiometer. With the front optic of the excimer laser approximately 2 m from the center of the reaction cell, the beam was rectangular in cross section and measured 2.0 cm by 4.0 cm. When measured through a 0.5 cm diameter aperture, the fluence peaked at the center of the beam and dropped off by 10% per 0.5 cm distance from the center in both the vertical and horizontal directions. The beam from the Nd:YAG laser was aligned at the center of the volume irradiated by the excimer laser. It was estimated to be 0.4 ± 0.1 cm in diameter.

The reagent purities and sources were as follows: N_2 (99.999%, Spectra Gases, Inc.); Cl_2 (99.9%, Matheson Gas Products, Inc.); O_2 (99.99%, Spectra Gases, Inc.). Ozone was prepared in a commercial ozonator using UHP oxygen. It was stored at 195 K on silica gel and degassed at 77 K before use. The other gases were used without further purification.

Results

In the absence of competing reactions that either deplete or enhance the ground state oxygen atom ($O(^3P)$) concentration, the temporal behavior of $[O(^3P)]$ following the 266 nm laser pulse can be described by the relationship

$$\ln \{[O(^3P)]_t/[O(^3P)]_{t'}\} = - (k_2[ClO] + k'_d)(t - t') = - k'(t-t') \qquad (XVIII)$$

where

$$k'_d = k_{30}[Cl_2] + k_{18} \qquad (XIX)$$

In Equation XIX, k_{30} and k_{18} are the rate coefficients for the following processes:

$$O(^3P) + Cl_2 \rightarrow \text{products} \qquad (30)$$

$$O(^3P) \rightarrow \text{loss by diffusion from the viewing zone and reaction with background impurities} \qquad (18)$$

A typical experimental $O(^3P)$ temporal profile is shown in Figure 18. Unexpectedly, a significant build-up and decay of $O(^3P)$ occured before the 266 nm laser fired; possible sources of this $O(^3P)$ and its implications for our study of reaction (2) are discussed below. It should be noted that the vertical axis in Figure 18 has units of concentration. To construct Figure 18, the fluorescence signal before the 266 nm laser fired was scaled to account for the fact that the 351 nm laser photolyzed the entire field of view of the detection system, while the 266 nm laser photolyzed only 15% of the detector viewing zone. The size of the viewing zone was estimated by placing a series of apertures in front of the 351 nm beam and noting the variation of fluorescence signal strength with beam size.

Typical decays of $O(^3P)$ generated by the 266 nm laser pulse are shown in Figure 19. At each temperature and pressure a minimum of five and an average of eight experiments were performed at various values of $[O_3]_o$. Because the Nd:YAG laser fluence was measured in each experiment, the amount of ClO lost via 266 nm photolysis could be quantified. The expression

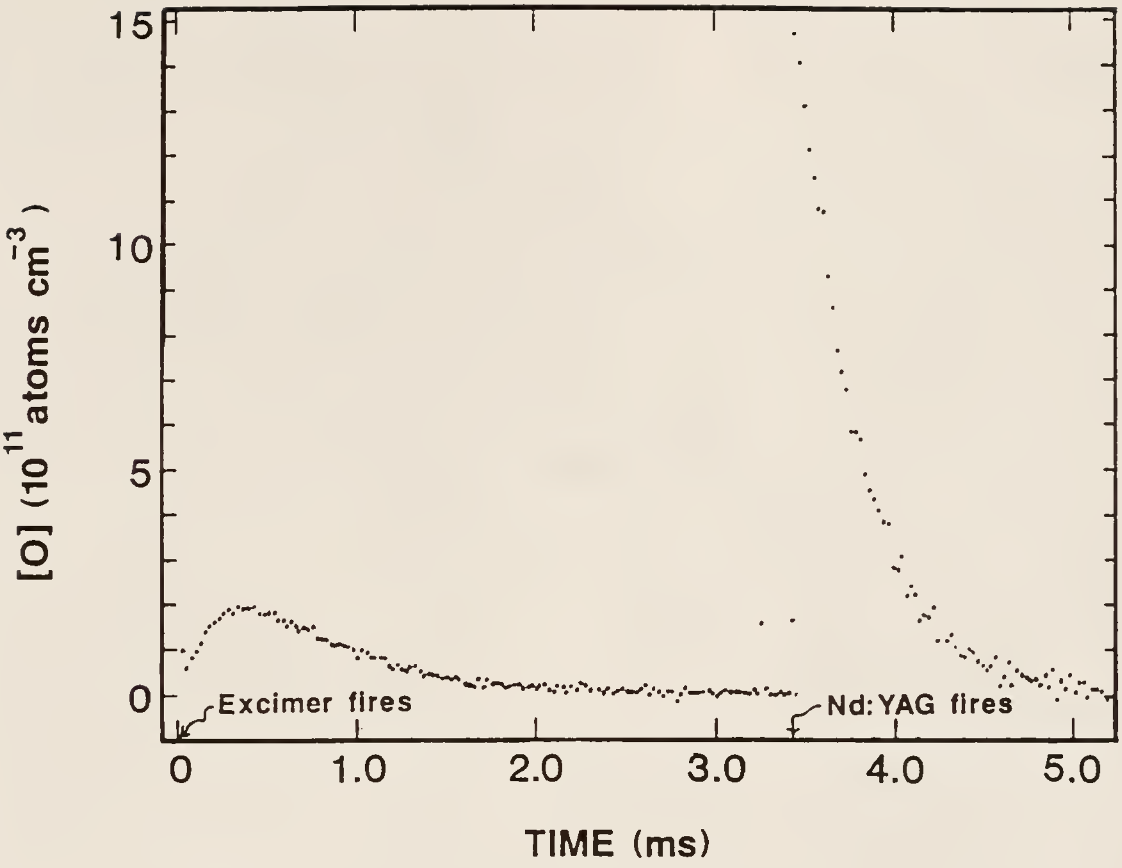

Figure 18. An experimental O atom temporal profile obtained under the following conditions: $[Cl_2]$ = 1.40 x 10^{16} molecules cm^{-3}; $[O_3]_o$ = 7.27 x 10^{13} molecules cm^{-3}; $[Cl]_o$ = 1.82 x 10^{14} molecules cm^{-3}; total pressure = 25 Torr; temperature = 298 K; multichannel scalar dwell time = 25 microseconds.

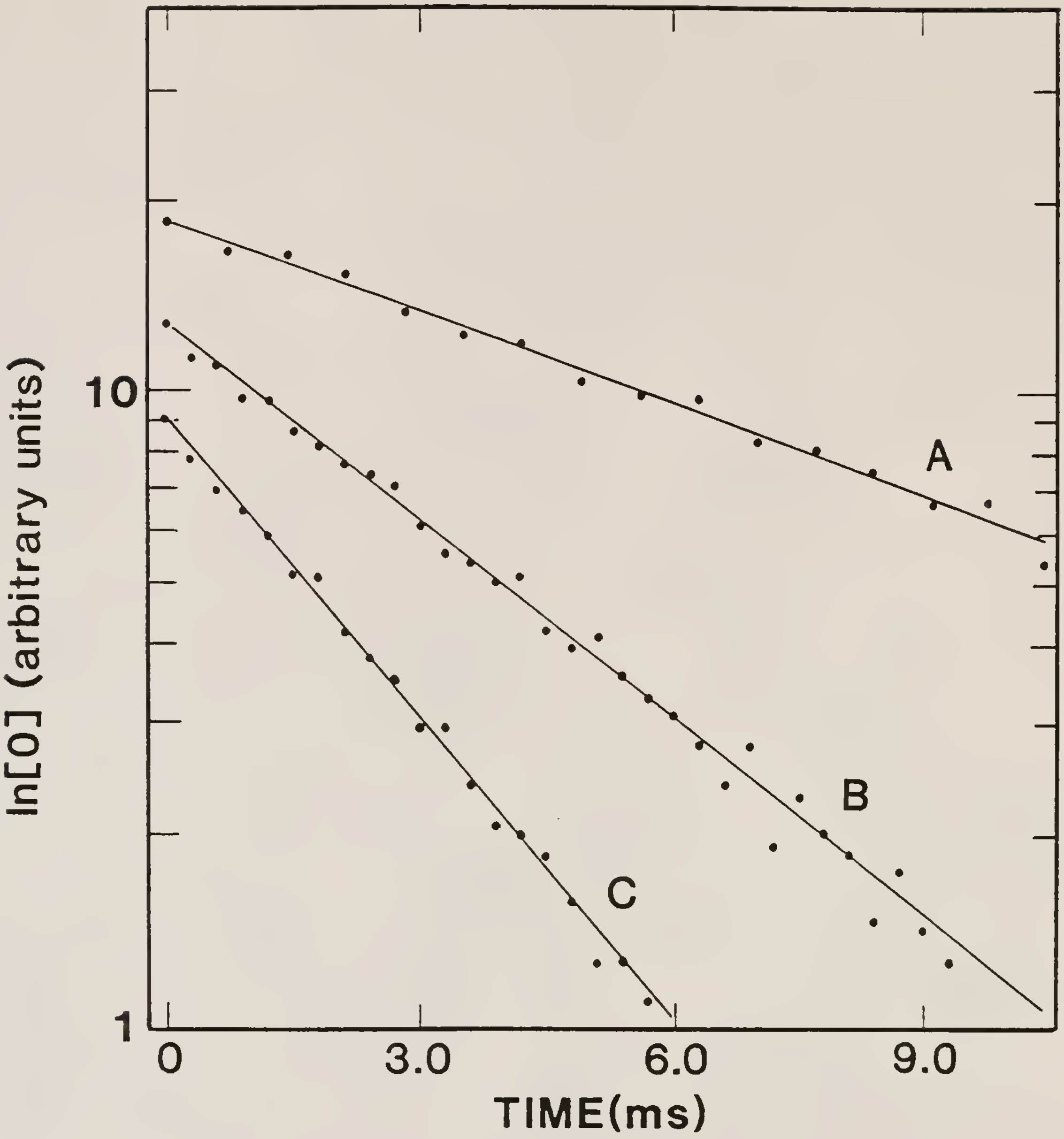

Figure 19. Typical O atom temporal profiles. These experiments were carried out under the following conditions (all concentrations expressed in molecules cm^{-3}): 25 Torr total pressure; T = 298 K; $[Cl_2] = 9.8 \times 10^{15}$; $[O_3]_o = 1.73 \times 10^{13}$ (A), 5.15×10^{13} (B), 8.76×10^{13} (C); and $[Cl]_o = 1.10 \times 10^{14}$ (A), 1.66×10^{14} (B), 2.29×10^{14} (C).

$$[ClO]_t = [O_3]_o - [O(^3P)]_{t'} \qquad (XX)$$

was used to calculate the ClO concentration under the assumption that no loss of ClO occurred during the delay between photolysis laser pulses. The ratio $[O(^3P)]/[ClO]$ immediately following the 266 nm laser pulse was determined for each experiment, and was typically in the range 0.01- 0.04. Hence, it was appropriate to correct each measured decay rate for slight deviations from pseudo-first order conditions. These corrections were derived from computer simulations of reactions (2), (30) and (18) under the range of experimental conditions employed. (A discussion of the computer simulations appears in Appendix A.) Best fit values for each decay rate (k′) were obtained from linear regression analyses of the experimental data over at least two 1/e times. Each value of k′ was then increased by 2% or less using the appropriate nonpsuedo-first order correction. Representative plots of [ClO] versus k′ are shown in Figure 20. These data were subjected to linear least squares analyses to give values for k_2. The results are presented in Table VI. Note the separate columns for k_2(uncorrected) and k_2(corrected). The former represents the best fit to the data when k′ was not corrected for nonpseudo-first order behavior and [ClO] was set equal to $[O_3]_o$ less the amount photolyzed to produce $[O(^3P)]$. The latter k_2 values include the small nonpseudo-first order correction to k′ and additional corrections to [ClO] discussed below.

The absorption cross section used to calculate the amount of ClO photolyzed by the Nd:YAG laser was estimated experimentally. The signal level

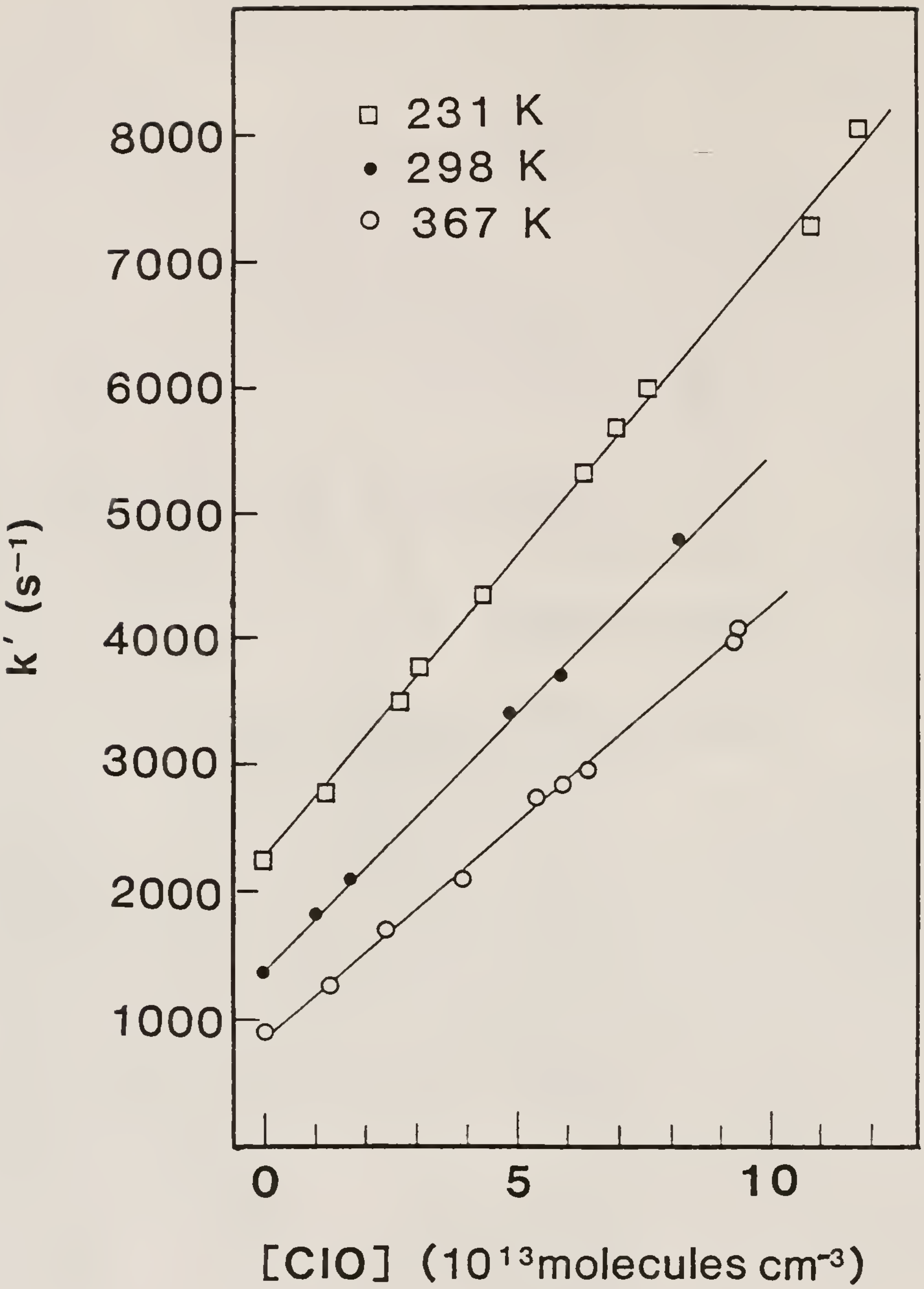

Figure 20. A k′ versus [ClO] plot of typical data taken at 25 Torr total pressure of N_2 and at three temperatures. Note that the 298 and 231 K data have been displaced upward by 1000 and 2000 s^{-1}, respectively. Solid lines are obtained from linear least squares analyses and give the following rate coefficients (in units of 10^{-11} cm^3 $molecule^{-1}$ s^{-1}): 4.99 at 231 K, 4.07 at 298 K, 3.44 at 367 K.

Table VI. Summary of k_2 Determinations

Temperature (K)	Pressure (Torr)	$k_2 \times 10^{11}$ (uncorrected)(a,b) (cm^{3}molecule^{-1}s^{-1})	$k_2 \times 10^{11}$ (corrected)(a) (cm^{3}molecule^{-1}s^{-1})
231	25	4.64 ± 0.16	4.99 ± 0.17
238	25	4.25 ± 0.43	4.47 ± 0.43
252	200	3.10 ± 0.22	3.97 ± 0.30
255	25	4.15 ± 0.20	4.42 ± 0.20
255	200	3.25 ± 0.20	3.95 ± 0.32
257	25	3.86 ± 0.15	4.10 ± 0.11
257	25	4.30 ± 0.15	4.47 ± 0.19
275	25	3.94 ± 0.17	4.10 ± 0.16
298	25	3.55 ± 0.21	3.84 ± 0.14
298	25	3.47 ± 0.25	3.59 ± 0.25
298	25	3.51 ± 0.14	3.62 ± 0.13
298	25	3.87 ± 0.36	3.93 ± 0.36
298	25	3.89 ± 0.15	4.07 ± 0.17
298	50	3.91 ± 0.23	4.07 ± 0.24
298	50	3.62 ± 0.15	3.98 ± 0.18
298	50	3.70 ± 0.12	3.91 ± 0.11(c)
298	50	3.53 ± 0.19	3.76 ± 0.14
298	50	3.76 ± 0.16	3.98 ± 0.14
298	100	3.73 ± 0.68	3.97 ± 0.67
298	200	3.39 ± 0.27	3.73 ± 0.24

(a) Errors are 2σ.

(b) Uncorrected values have not been adjusted for non pseudo-first order conditions and [ClO] loss by reaction (31). See text for details.

(c) Carried out with 283 nm photolysis of ClO, under "reversed" and "normal" flow conditions.

Table VI. (Continued)

Temperature (K)	Pressure (Torr)	$k_2 \times 10^{11}$ (uncorrected)$^{(a,b)}$ ($cm^3molecule^{-1}s^{-1}$)	$k_2 \times 10^{11}$ (corrected)$^{(a)}$ ($cm^3molecule^{-1}s^{-1}$)
298	200	3.39 ± 0.28	3.71 ± 0.24
298	200	3.55 ± 0.12	3.76 ± 0.13
298	500	3.18 ± 0.16	4.03 ± 0.20
338	25	3.16 ± 0.60	3.26 ± 0.12
359	200	2.99 ± 0.14	3.09 ± 0.15
360	25	2.89 ± 0.13	2.96 ± 0.12
367	25	3.35 ± 0.13	3.44 ± 0.13

(a) Errors are 2σ.

(b) Uncorrected values have not been adjusted for non pseudo-first order conditions and [ClO] loss by reaction (31). See text for details.

immediately after the Nd:YAG laser fired was directly proportional to the concentration of oxygen atoms. If the Nd:YAG laser was not preceded by a pulse from the excimer laser, then the photolyte was O_3. If all the O_3 had been converted to ClO via reaction with Cl atoms created in the 351 nm excimer pulse, then the signal was due to ClO photolysis. Therefore, in back-to-back experiments with constant $[Cl_2]$, $[O_3]$ and 266 nm fluence, the ratio of $O(^3P)$ signal with and without 351 nm photolysis should be identical to the ratio of the ClO and O_3 absorption cross sections at the Nd:YAG laser wavelength (the $O(^1D)$ product of O_3 photolysis is rapidly quenched to $O(^3P)$ by N_2). This experiment resulted in a value of 0.35 for the signal ratio. If $\sigma(O_3,266\ \text{nm})$ is taken to be $9.0 \times 10^{-18}\ \text{cm}^2$ (Ref. 60) then $\sigma(\text{ClO},266\ \text{nm})$ is approximately $3.1 \times 10^{-18}\ \text{cm}^2$. This is somewhat lower than the low resolution cross section at this wavelength that is reported in the literature.[64] However, we carried out the identical signal level comparison near 283 nm, a wavelength where the high resolution cross section has been characterized.[65] Using a frequency doubled, Nd:YAG pumped tunable dye laser the rotational structure in the ClO spectrum was reproduced by observing the resonance fluorescence signal as the wavelength was scanned. At 282.95 nm, the peaks of the R(19.5) and P(16.5) lines of the $A^2\pi_{3/2} - X^2\pi_{3/2}$ 9-0 band, we observed a factor of 1.65 ± 0.20 more fluorescence signal when the excimer laser photolyzed Cl_2 than when the excimer laser beam was blocked. Based on the dye laser linewidth employed and the literature values for the ozone and ClO cross sections, we expected a ratio of 1.80 ± 0.40. This result confirms our value for $\sigma_{266}(\text{ClO})$.

As mentioned above, the delay between the two laser pulses, t′, was adjusted to be long enough for reaction (12) to go to completion. The value of the Cl + O_3 rate constant is reasonably well known[60] so an appropriate delay time could be calculated. As a check the delay time was varied until a constant signal and decay rate were observed, indicating that all the O_3 had been converted to ClO. The majority of experiments were carried out with delay periods of either 3.4 ms or 6.4 ms.

The temporal behavior of ClO could be monitored by following both the $O(^3P)$ signal level produced by 266 nm photolysis and the measured value of k′. For some conditions (lower temperature, higher pressures) it was observed that ClO was decreasing on the time scale of the delay between the two lasers. The disappearance of ClO is probably due to self-reaction, a process that has not been completely characterized.[66] In order to make a correction for the amount of ClO lost during the delay between laser pulses and also during the O atom decay, a series of experiments were carried out in which the delay time was varied at fixed $[O_3]$, $[Cl_2]$ and laser fluences.

For the process

$$ClO + ClO \rightarrow \text{products} \qquad (31)$$

the time dependence of [ClO] is described by the relationship

$$2k_{31}t = [ClO]_t^{-1} - [ClO]_o^{-1} \qquad (XXI)$$

If we define $k_{31'}$ to be the second order rate coefficient for ClO removal under our experimental conditions, then plotting $[ClO]_t^{-1}$ versus time should yield a straight line of slope $2k_{31'}$ and intercept equivalent to $[ClO]_o^{-1}$. The absolute concentration of ClO needed to determine k_{31} was deduced in two manners. In the first method, Equation XVII was rearranged to calculate [ClO]. Here k_2 was taken from fixed delay experiments at the same experimental temperature and pressure. $k_{31'}$ was determined from Equation XXI. Then the values for [ClO] in the fixed delay experiments were adjusted to account for the loss of ClO during the delay. This procedure was iterated until constant values of k_2 and $k_{31'}$ were obtained. The second method involved relating the signal level immediately following the 266 nm laser pulse to the value of [ClO]. The signal calibration could be arrived at by two procedures. When enough data was available under the same experimental conditions, a [ClO] versus signal calibration curve was constructed. Otherwise, signal versus delay time was plotted and extrapolated to time zero and that signal level normalized to $[O_3]_o$. This normalization factor was then used to put the signal level at each delay time on an absolute concentration scale. Because of the reciprocal relation in Equation XXI, the value of $k_{31'}$ is quite sensitive to the scaling factor used in setting the value of [ClO]. Also the signal level is quite dependent on the operating conditions of the resonance lamp. Therefore, the values of $k_{31'}$ determined from the first method are more precise. However, when using k′ as a measure of [ClO], we assume that O atoms are removed only by reaction with ClO and Cl_2; this assumption appears to be justified. A typical plot of $[ClO]^{-1}$

versus time appears in Figure 21. The end results of a number of such experiments appear in Table VII. These results are presented only as a measure of the phenomenological loss rate of ClO in our system, not as a definitive measurement of k_{31}.

Hayman et al.[66] report 298 K values for k_{31} which are substantially faster than the values for $k_{31'}(298 \text{ K,P})$ we have determined. However, our 255 K results appear to agree reasonably well with the low temperature values of k_{31} of Hayman et al. According to Hayman et al.,[66] reaction (31) has an important branch to form a weakly bound dimer which can either decompose or react rapidly with chlorine atoms. The relevant reaction scheme is given below:

$$\mathrm{ClO + ClO + M \leftrightarrow (ClO)_2 + M} \qquad (31a,-31a)$$

$$\mathrm{ClO + ClO \rightarrow OClO + Cl} \qquad (31b)$$

$$\mathrm{ClO + ClO \rightarrow other\ products} \qquad (31c)$$

$$\mathrm{Cl + (ClO)_2 \rightarrow Cl_2 + ClOO} \qquad (32)$$

$$\mathrm{ClOO + M \rightarrow Cl + O_2 + M} \qquad (33)$$

$$\mathrm{Cl + ClOO \rightarrow Cl_2 + O_2\ (major)} \qquad (34a)$$

$$\mathrm{Cl + ClOO \rightarrow 2ClO\ (minor)} \qquad (34b)$$

$$\mathrm{Cl + OClO \rightarrow 2ClO} \qquad (35)$$

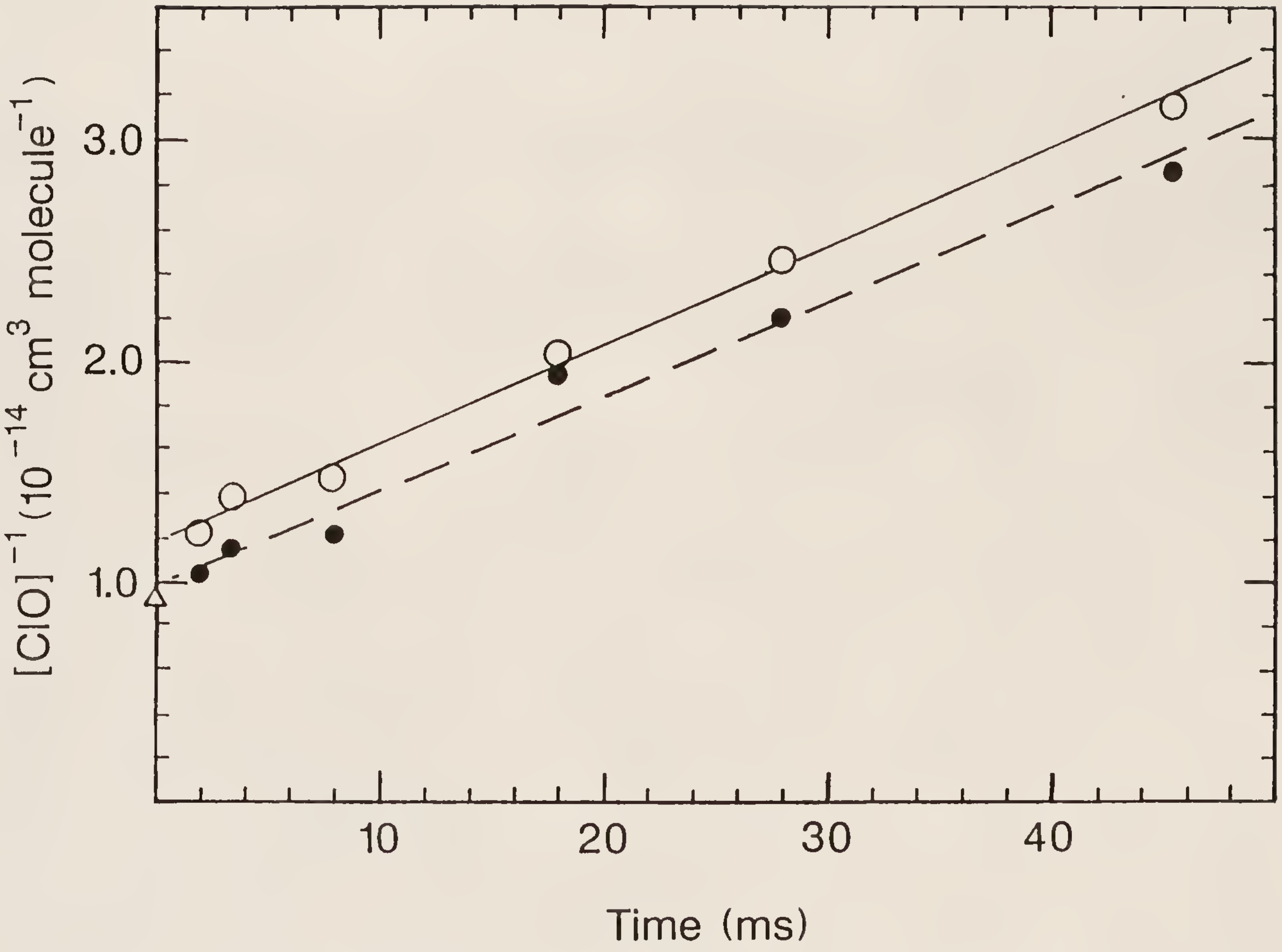

Figure 21. A plot of $[ClO]^{-1}$ versus delay time. The open circles are based on ClO concentrations calculated from the O atom decay at each delay and the closed circles are based upon the fluorescence signal immediately following the 266 nm laser pulse. The triangular point on the abscissa represents $[O_3]_o^{-1}$. Experimental conditions: T = 252 K; P = 200 Torr.

Table VII. Summary of $k_{31'}$ Determinations

T (K)	P (Torr)	$10^{-14}[Cl]_o$ (a)	$10^{-13}[O_3]$ (a)	No. of Experiments	Range of t′(ms)	$10^{13}k_{31'}$ (b,c)
252	200	4.0 - 4.8	10.4	6	1.5 - 45	2.27 ± 0.18
255	25	4.0 - 5.1	9.8	6	3.0 - 45	0.47 ± 0.19
255	200	3.4 - 4.7	12.2	8	3.0 - 50	2.47 ± 0.18
298	16	1.7 - 2.5	7.3	7	1.5 - 60	0.17 ± 0.12
298	50	4.3 - 7.8	13.0	6	5.0 - 60	0.40 ± 0.09
298	50	2.2 - 5.2	8.3	8	1.5 - 60	0.36 ± 0.09
298	200	1.9 - 4.6	9.7	12	1.5 - 60	1.12 ± 0.11
298	200	2.6 - 3.9	6.15	6	1.5 - 60	0.92 ± 0.18
298	500	3.2 - 3.4	11.8	6	2.0 - 45	1.63 ± 0.17
298	500	3.7 - 4.0	5.9	5	1.5 - 35	2.94 ± 0.63
359	200	2.0 - 2.5	9.3	5	3.0 - 45	0.38 ± 0.15

(a) Units are molecules per cm^3.
(b) Units are $cm^3 molecule^{-1} s^{-1}$.
(c) Errors are 2σ, precision only.

Hayman et al.[66] obtained their kinetic data from a molecular modulation study. They observed much smaller apparent values for k_{31} during the lights-off cycle (no chlorine atoms present) than during the lights-on cycle (large concentration of chlorine atoms present). Hence, a plausible explanation for the difference between our $k_{31'}$(298 K) determinations and the k_{31}(298 K) values reported by Hayman et al.[66] is that k_{-31a}(298 K) was substantially faster than k_{32}[Cl] under our experimental conditions, thus facilitating ClO regeneration by dimer decomposition; this is, of course, a favorable situation for measurement of k_2 but would result in systematic underestimation of k_{31}. No clear variation of $k_{31'}$ with [Cl] is evident in our data, although our experiments spanned a rather narrow range of chlorine atom concentrations (Table VII).

In order to make appropriate corrections for the loss of ClO during the delay between laser pulses, a reaction system consisting of reactions (12) and (31) was modeled under a variety of initial conditions using literature values for $k_{12}(T)$[60] and setting $k_{31} = k_{31'}$. (A discussion of how this reaction sequence was modeled can be found in Appendix A.) From these calculations a set of correction factors (F) could be derived:

$$F_{t'} = [\mathrm{ClO}]_{t'}/[\mathrm{O_3}]_o \qquad \text{(XXII)}$$

Values of $F_{t'}$ at $t' = 3.4$ ms are given in Table VIII as a function of temperature, pressure, $[O_3]_o$, and $[Cl]_o/[O_3]_o$. Note that the maximum correction is made for the highest value of [ClO] for a given experiment; also,

Table VIII. Correction Factors for Loss of ClO Via Reaction (31) as a Function of Temperature, Pressure, $[O_3]_o$ and $[Cl]_o/[O_3]_o$.

$[O_3]_o$	$[Cl]_o/[O_3]_o$ [(a)]	255 K		298 K			363 K	
		25 Torr	200 Torr	25 Torr [(b)]	200 Torr	500 Torr	25 Torr	200 Torr
2.0×10^{13}	10	0.993	0.970	0.996	0.986	0.970	0.997	0.994
2.0×10^{13}	5	0.961	0.943	0.976	0.968	0.956	0.987	0.984
6.0×10^{13}	6	0.983	0.918	0.990	0.962	0.919	0.992	0.985
6.0×10^{13}	2	0.930	0.887	0.952	0.933	0.901	0.969	0.964
1.2×10^{14}	5	0.965	0.845	0.979	0.926	0.849	0.984	0.970
1.2×10^{14}	2	0.964	0.864	0.979	0.934	0.877	0.985	0.973

(a) Typical range of values for $[Cl]_o/[O_3]_o$ employed in k_2 determinations.

(b) $k_{31'}$ determined by interpolation to be $3 \times 10^{-14} cm^3 molecule^{-1} s^{-1}$.

the longer the delay used in an experiment the larger the correction applied. For a few experimental conditions where $k_{31'}$ was great enough (i.e., high pressure, low temperature) a correction was made to the observed k′ for loss of ClO during the decay itself; this correction never exceeded 1.4%.

As a further check on the consistency of our experiments, the rate coefficient for reaction (2) was determined at 298 K in 50 Torr N_2 using 283 nm photolysis of ClO rather than 266 nm photolysis. The additional photolysis wavelength was provided by the frequency doubled, Nd:YAG pumped tunable dye laser. Also, to ensure that neither O_3 nor Cl_2 were being lost in the flow system, a measurement of k_2(298 K) was carried out with the two absorption cells plumbed downstream from the reaction cell rather than in the "normal" upstream position. Neither of these variations in experimental parameters affected the observed kinetics.

As mentioned above, a significant O atom signal was generated subsequent to the excimer laser pulse (Figure 18). Leu[52] and Vanderzanden and Birks[67] have observed O atoms from the reaction of chlorine atoms with ozone. The following chemistry was proposed to explain their observations:

$$Cl + O_3 \rightarrow ClO + O_2(b^1\Sigma_g^+) \tag{12'}$$

$$O_2(b^1\Sigma_g^+) + O_3 \rightarrow O + 2O_2 \tag{36}$$

Subsequently, Choo and Leu[68] monitored $O_2(b^1\Sigma_g^+)$ directly by observing its near infrared emission and put an upper limit of ~0.05% on the $O_2(b^1\Sigma_g^+)$ yield from reaction (12). Such a yield is much too small to account for the observed levels of $O(^3P)$ produced in the Cl + O_3 studies.[52,67] Choo and Leu have suggested that the O atoms may be generated by reactions of vibrationally excited ClO formed in reaction (12), i.e.,

$$\mathrm{Cl} + \mathrm{O_3} \rightarrow \mathrm{ClO^*}(v' \leq 18) + \mathrm{O_2} \tag{12''}$$

followed by

$$\mathrm{ClO^*}(v' \geq 12) + \mathrm{O_3} \rightarrow \mathrm{O_2} + \mathrm{O} + \mathrm{ClO} \tag{37}$$

or

$$\mathrm{ClO^*}(v' \geq 3) + \mathrm{Cl} \rightarrow \mathrm{Cl_2} + \mathrm{O} \tag{38}$$

In our system Cl atoms are in excess over O_3 and, therefore, in excess over the ClO created in reaction (12). Also, the occurence of reaction (38) results in loss of two ClO molecules which otherwise would have been present at t′ while the occurence of reaction (37) results in loss of only one ClO molecule. Hence, reaction (38) would potentially have the larger effect on the ClO concentration in our experiments. To examine the potential role of reaction (38) in consuming ClO, we simulated the system chemistry using a Gear routine (see Appendix A) to solve the rate equations numerically. The following scheme was modeled:

$$Cl + O_3 \rightarrow ClO^* + O_2 \qquad (12'')$$

$$Cl + ClO^* \rightarrow Cl_2 + O \qquad (38)$$

$$ClO^* + M \rightarrow ClO + M \ (M{=}N_2) \qquad (39)$$

$$O + ClO \rightarrow O_2 + Cl \qquad (2)$$

$$ClO + ClO \rightarrow \text{products} \qquad (31')$$

$$O + Cl_2 \rightarrow ClO + Cl \qquad (30a)$$

Although reactions (12″) and (38) may have other channels, this scheme was devised to have the greatest impact on the [ClO] at the end of the reaction period; therefore, only the branches that deplete ClO were used. It should be noted that a large dependence of the extraneous $O(^3P)$ signal on the total pressure in the system was observed. This observation would be consistent with quenching of either ClO* or $O_2(b^1\Sigma_g{}^+)$ by N_2. k_2 and k_{30} are known, and the other rate coefficients were adjusted to reproduce the magnitude and temporal behavior of the O atom signal observed. Typical results are shown in Figure 22. It was found that the above reaction scheme led to no more than a two percent perturbation in the concentration of ClO. Of course there is no direct proof that the assumed reaction scheme is correct. However, it is the

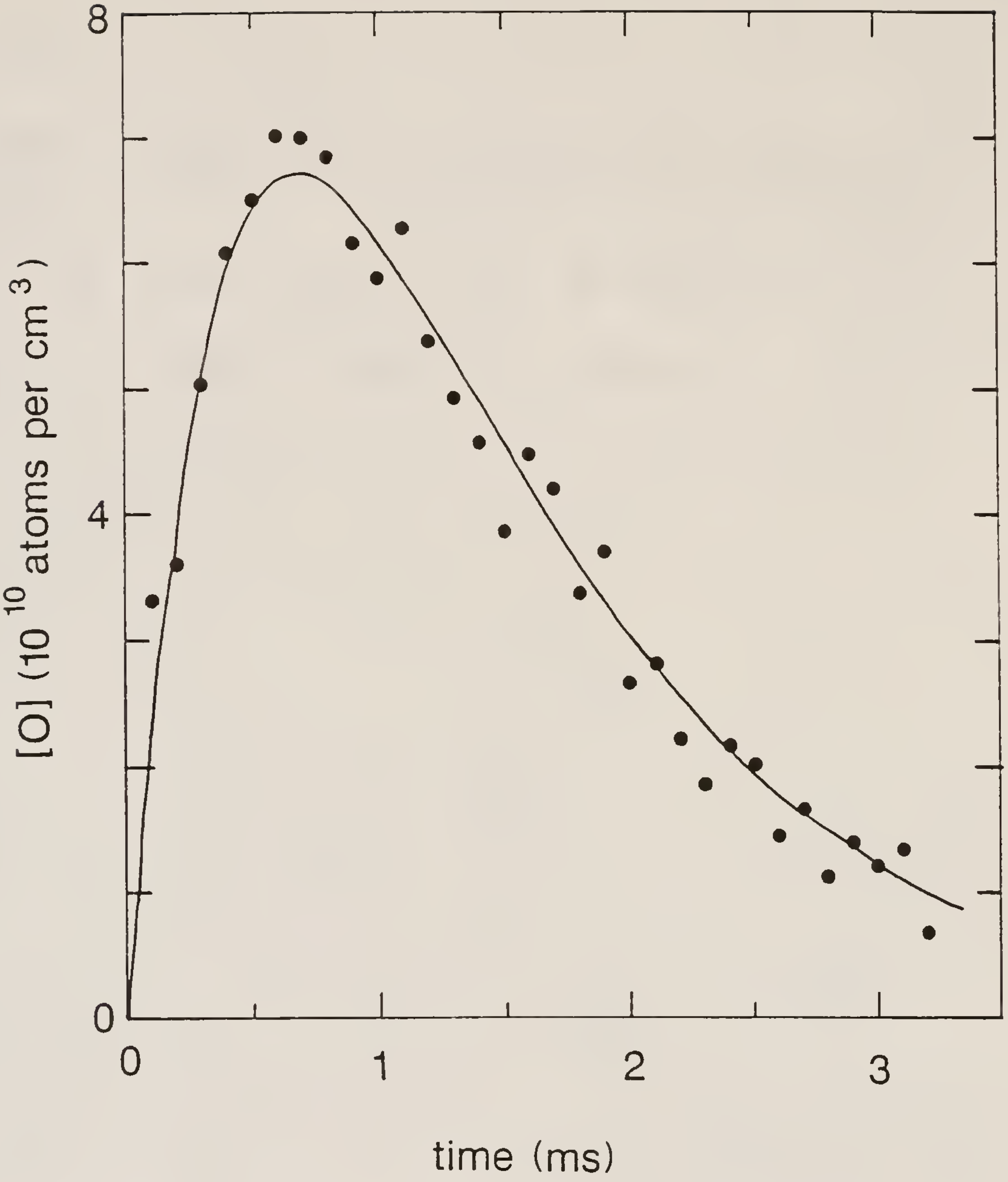

Figure 22. Comparison of oxygen atom temporal profile immediately following 351 nm laser pulse to computer simulation of reaction scheme discussed in the text. Experimental conditions are as follows: T = 298 K; $[O_3]_o$ = 1.65 x 10^{13} molecules cm^{-3}; $[Cl_2]$ = 1.42 x 10^{16} molecules cm^{-3}; $[Cl]_o$ = 1.81 x 10^{14} molecules cm^{-3}; pressure = 25 Torr. The reaction rate coefficients used in the simulation are: k_2 = 3.66 x 10^{-11}; $k_{12''}$ = 1.18 x 10^{-11}; k_{30} = 2.91 x 10^{-14}; $k_{31'}$ = 3.0 x 10^{-14}; k_{37} = 2.0 x 10^{-11}; k_{38} = 5.8 x 10^{-13}. All rate coefficients are in units of cm^3 $molecule^{-1}$ s^{-1}.

worst case of the suggested possibilities and any corrections would be quite small. Since the mechanism for O atom formation following the excimer laser pulse is not well understood, the effect of this chemistry on the ClO concentration was not taken into account in the determination of "corrected" values for k_2 (Table VI).

The combination of Cl_2 photolysis, Cl + O_3 reaction, and ClO photolysis could result in some heating of the gas in the reaction zone. Calculations which assume worst case conditions, i.e., P = 25 Torr N_2, $[Cl]_o = 6 \times 10^{14}$ molecules per cm^3, $[O_3] = 1 \times 10^{14}$ molecules per cm^3, $[O]_{t'} = 2 \times 10^{12}$ atoms per cm^3, and all excess energy dissipated as heat, show that laser heating of the reaction zone could not have exceeded 2 Kelvin in any experiment. This potential systematic error is negligibly small so it was not incorporated into the data analysis.

As discussed above, several corrections were made to either the observed k′ values or in the calculation of [ClO] from $[O_3]_o$. For clarity this set of corrections is reiterated:

a) A quantitative correction was made in k′ for nonpseudo-first order conditions during the O atom decay. In only a few cases did this exceed a 1% adjustment.

b) [ClO] was corrected for the amount of ClO lost to photolysis at 266 nm. This correction was dependent upon knowledge of the laser fluence, which was monitored in every experiment using a calibrated radiometer, and on our estimated value of σ_{266}(ClO). Because there was only a small adjustment to [ClO] (on the average 3%) the final results were not very sensitive to this correction. For example, in an experiment where the fraction of ClO photolyzed was above the average, an increase in σ_{266}(ClO) of a factor of 2 was found to change the final value of k_2 by only 4%.

c) Using the loss rate of ClO determined in the same system, a correction was made to [ClO] for the ClO that undergoes self-reaction (or other loss processes) during the delay time between laser firings. The largest corrections were made at higher pressures, lower temperatures and in long delay experiments. Because the simulation of the production and loss of ClO was sensitive to the errors in our measurements of $k_{31'}$, this correction has a rather large uncertainty.

d) A few decays were corrected for ClO loss during the decay itself; however, this correction was insignificant under most experimental conditions.

e) It was concluded that of the known possibilities for the source of O atoms prior to ClO photolysis, none could have had more than a two per cent effect on $[\mathrm{ClO}]_{t'}$; no corrections were made for this chemistry.

Even though there were several corrections made in order to reach a final value for k_2 at each temperature and pressure, the magnitudes of the corrections were small in most cases (see Table VI), the corrections could be quantitatively applied, and in general, the results are self-consistent. An

Arrhenius plot of our data appears in Figure 23. An unweighted least squares analysis of all data yields the expression

$$k_2(T) = (1.68 \pm 0.31) \times 10^{-11} \exp\{(241 \pm 53)/T)\} \text{ cm}^3\text{molecule}^{-1}\text{s}^{-1} \quad \text{(XXIII)}$$

where the errors represent 2σ, precision only, and $\sigma_A \equiv A\sigma_{\ln A}$. For the 25 Torr data only, the expression

$$k_2(T) = (1.55 \pm 0.33) \times 10^{-11} \exp\{(263 \pm 60)/T)\} \text{ cm}^3\text{molecule}^{-1}\text{s}^{-1} \quad \text{(XXIV)}$$

is obtained from an unweighted least squares analysis. The difference between the Arrhenius expression obtained from the 25 Torr data and that obtained from the complete data set is primarily due to the slightly lower rate coefficients obtained at high pressure (200 Torr) and low temperature (252-255 K). These rate coefficients required rather large corrections for contributions from reaction (31) and, therefore, are more likely to be in error than rate coefficients obtained at higher temperatures and/or lower pressures. For this reason, we believe the Arrhenius expression obtained from the 25 Torr data only should be preferred. The absolute accuracy of k_2 at any temperature within the range studied is estimated to be ± 20%.

Discussion

In all prior investigations reaction (2) was studied by flow tube techniques at pressures less than 10 Torr. The results of all studies are summarized in

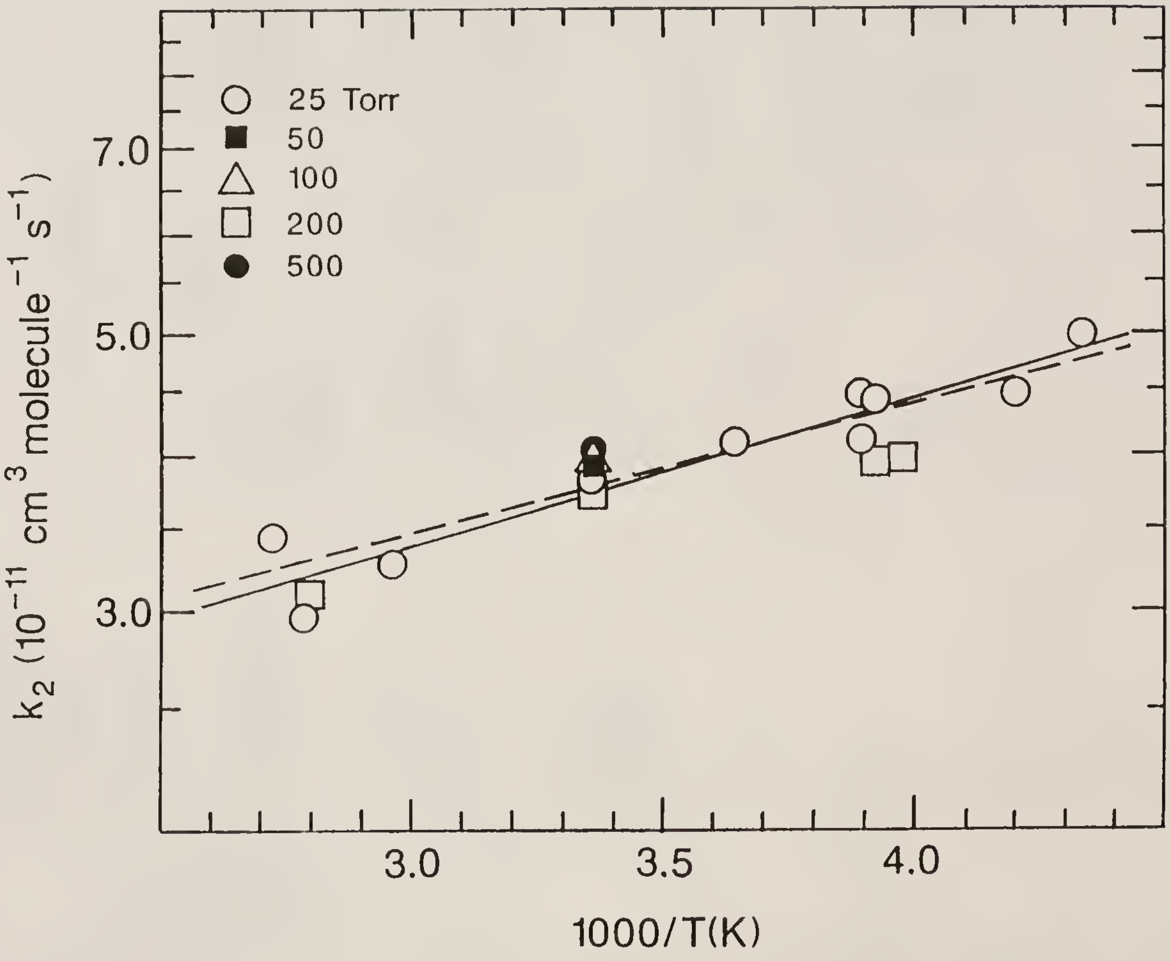

Figure 23. Arrhenius plot of our results for k_2 (T,P). The dashed line represents an unweighted least squares analysis of the 25 Torr data only while the solid line includes all data.

Table IX. In the earliest study Bemand et al.,[49] measured k_2(298 K) using resonance fluorescence to monitor $O(^3P)$ in excess ClO. The ClO was produced by the reaction

$$Cl + OClO \rightarrow 2\ ClO \qquad (35)$$

assuming a stoichiometric factor of 2. These workers reported k_2(298 K) = 5.3 ± 0.8) x 10^{-11} $cm^3 molecule^{-1} s^{-1}$. They also measured the rate coefficient by following the decay of ClO mass spectrometrically in excess oxygen atoms and obtained the result (5.7 ± 2.3) x 10^{-11} $cm^3 molecule^{-1} s^{-1}$. In a subsequent study in the same laboratory Clyne and Nip[50] measured the temperature dependence of k_2. Again, $O(^3P)$ was monitored by resonance fluorescence in excess ClO, the latter species being generated via reaction (12). The room temperature rate coefficient was in good agreement with their previous study. They report a significant activation energy and quote the Arrhenius expression $k_2(T) = (1.07 \pm 0.30) \times 10^{-10} \exp\{-(224 \pm 76)/T\}$ $cm^3 molecule^{-1} s^{-1}$.

Zahniser and Kaufman[51] measured the temperature dependence of the ratio k_2/k_{12}. Using a value of k_{12} measured directly in the same system these workers report $k_2(T) = (3.38 \pm 0.50) \times 10^{-11} \exp\{(75 \pm 40)/T\}$ $cm^3 molecule^{-1} s^{-1}$.

The next reported investigation of $k_2(T)$ was performed by Leu[52] using resonance fluorescence detection of $O(^3P)$ in excess ClO. The ClO radicals were

Table IX. Comparison of Measurements of k_2.

					$k_2(10^{-11}cm^3molecule^{-1}s^{-1})$(c)		
Investigators	Ref.	Experimental Method(a,b)	Temperature Range (K)	Pressure Range (Torr)	210 K	250 K	298 K
Bemand, Clyne & Watson	49 49	DF-RF(O) DF-MS(ClO)	298 298	~1.0 0.75	--- ---	--- ---	5.3 ± 0.8 5.7 ± 2.3
Clyne & Nip	50	DF-RF(O)	220-426	0.90	3.68	4.37	5.05
Zahniser & Kaufman	51	DF-RF(Cl)(d)	220-298	2.0-4.0	4.84	4.56	4.35
Leu	52	DF-RF(O)	236-422	1.0-3.5	3.17	3.41	3.62
Schwab, Toohey, Brune & Anderson	53	DF-LMR(ClO) DF-RF(O)	252-347	0.8-2.0	3.50	3.50	3.50
Ongstad & Birks	54,55	DF-CL(O)(e)	220-387	2.3	4.14	3.85	3.61
Margitan	56	DF-LFP-RF(O)	241-298	10	4.20	4.20	4.20
Nicovich, Wine & Ravishankara	This Work	LFP-RF(O)	231-367	25-500 25	5.29 5.42	4.41 4.44	3.77 3.75

(a) DF - discharge flow; RF - resonance fluorescence; MS - mass spectrometry; LMR - laser magnetic resonance; CL - chemiluminescence; LFP - laser flash photolysis.

(b) The monitored species is given in parentheses.

(c) Calculated from reported Arrhenius expressions.

(d) $k(O + ClO)$ measured relative to $k(Cl + O_3)$.

(e) NO added to produce chemiluminescence via $O + NO + M > NO_2^* > h\nu + NO_2$.

produced using three different source reactions in order to validate stoichiometric assumptions necessary to arrive at ClO concentration levels. Reactions (12), (35) and

$$Cl + Cl_2O \rightarrow ClO + Cl_2 \tag{40}$$

were the three sources used at room temperature. Reaction (12) was used at all other temperatures. Leu's value for k_2(298 K) is lower than the previously reported values and he measured a small positive activation energy with $k_2(T) = (5.0 \pm 1.0) \times 10^{-11} \exp\{-(96 \pm 20)/T\}$ cm^{3}molecule^{-1}s^{-1}. The use of reaction (12) as the only ClO source in all experiments at $T \neq 298$ K could result in a systematic error in Leu's reported temperature dependence. At the low pressures employed in Leu's study, the ClO* + Cl reaction may have competed favorably with ClO* deactivation, thus leading to overestimation of [ClO]. Since the ratio of k_{38}/k_{39} may be temperature dependent, such an effect could have been more important at one end of the investigated temperature range than at the other end. It should be emphasized that while the abovementioned systematic error in Leu's [ClO] determination is possible, there currently exists insufficient information concerning ClO* chemistry to prove or disprove this conjecture.

Schwab et al.[53] employed an experimental apparatus in which both reactants (ClO by laser magnetic resonance and O(^{3}P) by resonance fluorescence) and one product (Cl atoms by resonance fluorescence) could be monitored. [Interestingly, this is the only O + ClO study where ClO was directly measured in the reaction zone.] Again, a somewhat lower value was measured ($k_2(298\ K) = (3.5 \pm 0.5) \times 10^{-11}\ cm^3 molecule^{-1} s^{-1}$) and these workers observed essentially no temperature dependence for k_2.

Ongstad and Birks[54,55] measured $k_2(T)$ in a discharge flow system using the same three sources of ClO as Leu[52]. $O(^3P)$ was followed via the chemiluminescence from NO_2^* generated by reacting the oxygen atoms with NO added to the detection region of their flow tube. These workers measured $k_2(T)$ directly and also relative to the reaction

$$O + NO_2 \rightarrow NO + O_2 \qquad (41)$$

In a successive measurement scheme $k_{41}(T)$ was also measured. The relative measurements yielded somewhat higher values presumably due to nonpure source gases (Cl_2O, ClO_2, O_3) or other channels for the source reactions. Ongstad and Birks measured a value for $k_2(298\ K)$ that agrees with the other more recent studies and a small "negative activation energy." They reported the expression $k_2(T) = (2.61 \pm 0.60) \times 10^{-11} \exp\{(97 \pm 64)/T\}\ cm^3 molecule^{-1} s^{-1}$.

The only other study of k_2 at or near room temperature reported in the literature was by Margitan.[56] ClO radicals were generated in a flow tube via reaction (40). Downstream from this source $O(^3P)$ was created by laser photolysis of the ClO and followed by resonance fluorescence. The ClO concentration was measured directly in the flow by absorption. However, large corrections (up to 20%) had to be made for ClO loss between the ClO detection region and the $O(^3P)$ detection region. Margitan used literature values for k_{31} to make these corrections. Given the recent advances in our understanding of reaction (31),[66] a large uncertainty must be associated with the magnitude of Margitan's correction for ClO loss via the self-reaction. His results are also very dependent on the value chosen for the ClO absorption cross section. Margitan reports that E/R lies within the range $\pm$ 200 K and $k_2(298\ K) = (4.2 \pm 0.8) \times 10^{-11}\ cm^3 molecule^{-1} s^{-1}$.

As seen by the comparison in Table IX, there is very little difference between the value of $k_2(298\ K)$ from our experiments and from any of the other recent studies. However, at the lower temperatures typical of the middle stratosphere our results indicate significantly faster values for $k_2(T)$ than any of the other recent investigations (see Table IX). Hence, model calculations which employ our expression for $k_2(T)$ would predict somewhat larger ozone depletion due to chlorofluorocarbon injection than calculations which take $k_2(T)$ from previously available data.

Summary

We have measured k_2 as a function of temperature and pressure. Our results indicate a lack of any pressure dependence at 298 K over the range 25 Torr to 500 Torr. Although our 298 K rate coefficient agrees well with previous studies, our observation of an activation energy that is more negative than any previously reported leads to a significant difference between our result and other recent measurements at temperatures relevant to stratospheric chemistry.

CHAPTER V

CONCLUSIONS

In the preceding chapters, our studies of the temperature dependence of the rate coefficients for the reactions

$$O + HO_2 \rightarrow OH + O_2 \qquad (1)$$

and

$$O + ClO \rightarrow Cl + O_2 \qquad (2)$$

are presented. Each chapter contains a comparison of our measurements with all previously published work on these reactions. Subsequent to publication of our results, there have been no additional measurements of these rate coefficients. However, it is useful to discuss the current "evaluated" rate coefficient for each reaction, as well as recent developments relevant to our studies.

As discussed in Chapter III, there is very good agreement on the room temperature value of k_1 among the recent direct measurements.[16,17,19,20,36] Also, the temperature dependence for k_1 observed in our study is essentially identical with that seen by Keyser.[19] Therefore, the current NASA evaluation[69] of $k_1(T)$ is an average of the five studies at room temperature fitted to the temperature dependence from our work and that of Keyser.[19]

In order to extract a value for $k_1(T)$ from our data, small corrections were made for some secondary chemistry. The set of reactions that were included in our modeling of the secondary processes is given in Table III in Chapter III. The values for the rate coefficients listed in Table III are very nearly identical with the current NASA evaluations[69] except for the rate coefficient for reaction (21).

$$OH + HO_2 \rightarrow H_2O + O_2 \tag{21}$$

A recent study by Keyser[70] demonstrated that previous low pressure studies of reaction (21) in discharge flow experiments had been subject to secondary chemistry problems leading to low values for the rate coefficients (see Ref. 69 for discussion). The current NASA[69] recommended value at room temperature is approximately 50% faster than the value of k_1 used in our study. A re-evaluation of the effect of the secondary chemistry listed in Table III but with the current value for k_{21} leads to no more than a few percent change in the worse case for any rate coefficient determination; therefore, it is not necessary to make any changes in our reported results. The methods used to simulate the secondary chemistry in these studies is discussed in the final section of Appendix A.

For reaction (2), the NASA evaluation[69] is based on a least squares analysis of the seven most recent measurements of k_2.[18,51-56] There is reasonable agreement for k_2(298 K) but some uncertainty still exists as to the magnitude and direction of the temperature dependence.

In the $O(^3P) + ClO$ study small corrections were made for the amount of ClO lost to 266 nm photolysis. These corrections were based on an absorption cross section value that is somewhat lower than that given in a recent evaluation[69] of the literature on the ClO absorption spectrum. However, as was pointed out in Chapter IV, a factor of 2 increase in the value of σ(ClO,266 nm) changes k_2 by only 4 percent. Recently, the ClO cross section at 266 nm, near the peak of the continuum, has been found to be independent of temperature.[69] Temperature independence had been assumed in our study.

During our study of reaction (2) (see Chapter IV), we were able to estimate values for the process

$$ClO + ClO \rightarrow \text{product} \qquad (31)$$

under different conditions of temperature and pressure. These results are presented in Table VII. When our study was completed, only the work of Hayman et al.[66] was available for comparison. Subsequently, two more measurements of k_{31} have appeared in the literature.[71,72] The results of each of these studies of k_{31}(P,T) are compared with our reported values in Table X. The reasonably good agreement between our reported values for the phenomenological loss of ClO and the recent literature values for k_{31} give support to the interpretation of the ClO loss in our experiments.

In summary it can be stated that two of the main goals of this research have been reached. The temperature dependence of the rate coefficients for the atmospherically important reactions (1) and (2) have been measured. Our values for $k_1(T)$ and $k_2(T)$ are currently included in the primary chemical kinetic database for use in stratospheric modeling. Secondly, we have clearly demonstrated that laser flash photolysis-resonance fluorescence is a viable technique for use in kinetics studies of radical-radical reactions. Also, it has been demonstrated that neither of these radical-radical reactions are pressure dependent. Even though the entrance channel for the reactions are attractive, the possible bound species, HO_3^* and ClO_2^*, are not stabilized on the time scale of collisions at pressures approaching one atmosphere.

Table X. Comparison of Literature Values of k_{31}.

	k_{31}(10^{-13} $cm^3 molecule^{-1} s^{-1}$)				
	Hayman and Cox[(a)]	Sander et al.[(b)]	Trolier et al.[(c)]	NASA[(d)]	Nicovich et al.[(e)]
200K					
25 Torr	1.70	0.82	1.36	0.97	-
200 Torr	13.6	5.02	5.29	5.96	-
255K					
25 Torr	0.82	0.28	0.61	0.31	0.47
200 Torr	6.42	1.98	2.01	2.20	2.47
298K					
25 Torr	0.55	0.14	0.38	0.15	0.23[(f)]
200 Torr	4.00	1.03	1.07	1.09	1.02

(a) Calculated from low pressure limit plus bimolecular channel as reported in Reference 66.
(b) Calculated from parameterized fall-off expression reported in Reference 71.
(c) Calculated from parameterized fall-off expression reported in Reference 72.
(d) Calculated from parameterized fall-off expression given in latest NASA evaluation (Reference 69). This expression is based on an average of data from Sander et al.[71] and Trolier et al.[72]
(e) Experimental data from this work.
(f) This value was interpolated graphically from data given in Table VII, Chapter IV.

APPENDIX A

FURTHER DETAILS OF THE EXPERIMENTAL METHODS

Introduction

One of the shortcomings of most journal articles in experimental physical chemistry is that space only permits a cursory treatment of the experimental method employed in the work. A reader interested in more details is left with options such as searching out any references to similar experiments, generalized descriptions of the method in textbooks or review articles, or establishing direct contact with the researchers. Because the work described in the preceding three chapters represents a somewhat innovative approach to studies of radical-radical reactions, more information was given concerning the experimental method (especially in Chapter II) than would be found in a published account of a more standard flash photolysis resonance fluorescence experiment. However, many details were excluded. This appendix contains additional information about some aspects of the experiments and should redress some of the deficiencies of the experimental method sections of the preceding three chapters.

Flow Systems

The components of the various gaseous reaction mixtures were leaked into the flow system through needle valves and monitored using calibrated electronic mass flowmeters (Matheson Gas Products, Inc.). Using 1/4" o.d. teflon tubing with either Swagelock or Cajon fittings, the separate components were combined and flowed through a sequence of cells (the reaction cell and UV absorption cells). The gas mixture was exhausted through a rotary vane mechanical pump (Sargent Welch Model 1402 or 1397). The pressure of the system and flow rate through the reaction cell was controlled by adjusting the flow of each component into the system and by use of a throttle valve on the exhaust port. A separate, larger exhaust valve could be used to bypass the throttle valve to facilitate leak testing and flushing of the system. A Pyrex trap held at the boiling point of nitrogen (77 K) was plumbed directly above the vacuum pump. This prevented corrosive condensibles (H_2O_2, O_3, Cl_2) from reaching the pump and degrading the pump oil. The cold trap also prevented volatile components of the pump oil from backstreaming into the system under pump down. It is worth noting that ozone has a significant vapor pressure at 77K and therefore cannot be completely trapped. O_3 is particularly damaging to red rubber vacuum hose, with small perforations appearing in the tubing even after limited exposure. However, the O_3 can be destroyed in a length of heated copper tubing plumbed upstream of any hose and the pump.

All experiments were carried out under "slow flow" conditions. This prevented the depletion of any components of the reaction mixture and the build-up of reaction products that might become involved in secondary chemical processes. The experiments were conducted in a signal averaging mode, i.e., signal traces following individual, sequential laser pulses were accumulated to improve the counting statistics. Therefore, the lower limit of the flow rate was set by the condition that every laser flash encountered a fresh gas mixture. Because the photolysis was down the long axis, the entire volume of the cell had to be replenished between laser shots. This was especially critical in the case of the O + ClO study. As explained in Chapter IV, one component of the gas mixture, O_3, was completely titrated after each laser pulse. Therefore, for the O + ClO experiment, a low volume, low dead space cell was designed that would ensure total flushing of the cell volume in a convenient time period. The linear flow rate was typically 14 cm/s and the laser repetition rate was 0.4 cm/s in the O + ClO experiments. In the O + HO_2 studies, only a small fraction of the gas mixture was photolyzed so that the condition of complete gas exchange between laser pulses was not as stringent.

The flowmeters were calibrated during each study using one of two different techniques. In the first technique, the pressure drop in a known volume was timed while monitoring the flowmeter reading generated by a fixed flow out of that volume. In the second method, the gas output of the flowmeter was passed through a buret fitted with a latex reservoir filled with soap solution. Introduction of a small amount of the soap into the gas flow created thin soap films across the buret that could be timed as the ‘bubble’ rose through the buret. It is worth pointing out that as long as all the flowmeters used in an experiment were calibrated near the same time with the same method, then the meters should be well calibrated relative to each other. Calibration on an absolute scale was not necessary because it was the fractional flow through each flowmeter that was used in any concentration determination. In none of these studies were the measured rate coefficients directly dependent on the calibration of the flowmeters. In the $O + HO_2$ studies the $[H_2O_2]$ was measured *in situ* by UV photometry. The flowmeter readings were used to calculate total flow rate and the value of $[O_3]$ in each experiment. In the $O + ClO$ study both Cl_2 and O_3 were monitored via UV photometry. In fact, for most experiments neither the Cl_2 flow nor the flow of the O_3/N_2 mixture were even measured by flowmeters. These flows were only a small fraction of the total flow and more constant concentrations of Cl_2 and O_3 were possible when the concentrated O_3 flow and pure Cl_2 flow were not passed through the heated and restrictive stainless steel flowmeters.

Direct measurement of the critical low concentration components in the flow greatly reduces the uncertainty in any measured rate coefficient. Any systematic loss of these components due to dark reactions, heterogeneous processes, or thermal decomposition will be detected and taken into account. Of course, accurate absorption coefficients are then important. In the O + HO_2 studies, however, it is actually the ratio of the H_2O_2 absorption coefficients at the monitoring wavelength and at the photolysis wavelength that is critical. If the wavelengths are reasonably close and the cross sections are taken from a single study, then the ratio of cross sections can be more accurate than either individual cross section. Because a titration was used in the O + ClO study, the rate coefficient was only directly dependent upon the concentration of a single species and, therefore, a single absorption cross section, i.e., that of O_3 at 253.7 nm.

The pressure in the system was measured with an absolute capacitance manometer (MKS Instruments Model 220). Because small tubing connected the larger components of the flow system and the flow rate was relatively large, a pressure gradient existed between the absorption cell(s) and the reaction cell. Therefore, the concentration of the species measured by photometry were corrected by the appropriate ratio of pressures. The pressure ratios were measured by alternately coupling the pressure gauge directly to the reaction cell and the absorption cell for each set of pressure and flow conditions used in the experiments.

Resonance Lamps

The lamp itself is essentially the same as described by Davis and Braun.[73] A 1" diameter MgF_2 window is attached to one end of the lamp using Torr Seal low vapor pressure epoxy (Varian Associates). Compared to MgF_2, LiF is more transmitting in the vacuum UV, but it is a much weaker material. Helium containing a small amount of O_2, either as an impurity or from a separate reservoir, is flowed rapidly through the lamp at low pressure, a few Torr. Helium is used rather than argon in order to avoid the extraneous emissions of the latter. For these experiments, a rotary vane pump (Sargent Welch Model 1397) pulled the helium through the lamp and a LN_2 cooled trap. A 100 watt, 2.45 GHz microwave power supply (KIVA Instruments Model MPG4) was used to maintain the discharge in an Evenson cavity[74] (Ophthos Instruments). For atomic species, the gas flow through the discharge should always be in the direction away from the window in order to lessen reabsorption by ground state atoms. Emissions by other species can be reduced by using higher purity gases or possibly filtering the lamp emissions. The quality of the resonance fluorescence signal is very dependent upon the operation of the lamp. The concentration of O_2 in the helium, the total pressure, the power level of the discharge, the position of the discharge along the axis of the lamp and the tuning of the cavity are all factors in determining the detection sensitivity of O atoms. The optimum set of conditions can only be found by systematically varying all these parameters and empirically arriving at the best signal level. While there is a temperature difference maintained between the emitting atoms in the lamp and the absorbing atoms in the reaction cell, the fluorescence will still be proportional to the concentration of atoms in the cell as long as the emission profile of the lamp does not change during the measurement. By merely replacing oxygen with another appropriate precursor, the lamps can be used as sources of resonance radiation for any number of elements. Two final points are noted on the operation of these lamps. The transmission of the window may degrade under use due to production of trapped absorbers in the crystal. Also, care must be taken to keep all exposed surfaces clean, since almost any adsorbed contaminate will have a vacuum UV absorption.

Fluorescence Detection

The fluorescence from the O atoms in the reaction cell excited by the resonance lamp was detected using a solar blind photomultiplier tube (either a Thorn EMI Model G26L314LF or EMR Schlumberger Model 5181ER or 542G). The photocathode material in these end-on tubes is CsI coated on the inside of the MgF_2 window. The detector was mounted perpendicular to both the path of the photolysis laser and the direction of light from the resonance lamp. Because the resonance wavelengths are in the vacuum UV (130-135 nm), MgF_2 or CaF_2 optics were employed to couple light into and out of the reaction cell. The space between the resonance lamp output window and the reaction cell as well as the space between the cell and the window of the photomultiplier tube were purged with a gas transparent to the resonance wavelengths. The purge gas, N_2, excluded room air, which contains O_2, H_2O and other absorbers. Helium should never be used as a component of the purge gas in front of a photomultiplier tube, because it can permeate the window, or window seals, hence, destroying the tube. A small controlled amount of a filter gas, O_2, could be added to one or both of the purges to increase the ratio of the resonance radiation to the background emissions from the lamp. Because light was coupled into and out of the reaction cell using MgF_2 lenses (ca. 2" focal length), the distances of the resonance lamp discharge and the photoactive area of the PM tube from the reaction zone were also critical parameters in the detection of O atoms.

Signal Acquisition

Data were accumulated in a fashion usually referred to as photon counting. Weak pulses from the photomultiplier tube were fed into a photon discriminator (Mechtronics Nuclear Model 551). To bias against the weaker signal arising mostly from thermal processes, only pulses larger than an adjustable threshold level triggered the discriminator to output a TTL logic pulse. These logic pulses were the input for the signal analyzer (either a Tracor Northern TN-1500 or NS-570) operating in the multichannel scaling (MCS) mode. The analyzer accumulates the data in a time versus signal counts grid. The time axis is subdivided into equal increments sized to match the rate of the decay process observed.

An external trigger signal marked the start of each MCS sweep. Multiple sweeps were accumulated in order to improve the signal statistics. The scheme used to synchronize the MCS sweep with the laser pulses was different in each of the studies. In the first O + HO_2

experiment, a Lumonics Model TE-261-2 was used as the photolysis laser. Timing pulses from a pulse generator in the laser power supply were routed to a digital delay generator (California Avionics Laboratories Model 101AR). The delay generator put out two pulses, a t_0 pulse that was practically synchronous with the faster pulse from the laser triggered the signal analyzer and a delayed pulse triggered the firing of the laser. The delay between these pulses was typically 10 ms. Triggering the analyzer prior to the laser flash allows determination of the background light prior to generation of O atom signal. In the second O + HO_2 experiment, a Lambda-Physik EMG200 excimer laser was employed. A separate pulse generator (Global Specialties Model 4001) was used for the master pulse. This triggered the digital delay generator which again put out a t_0 pulse to the signal analyzer and a delayed pulse to the laser. In the O + ClO experiment, two lasers were used but a similar scheme was employed. A pulse generator integral to the power supply of the Nd:YAG laser (Quantel 481A) supplied the master pulse to trigger the delay generator. In this case, the delay generator t_0 pulse triggered both the Lambda-Physik excimer laser and the signal analyzer. A delayed pulse then triggered the flash lamps of the YAG laser.

After sufficient signal had been accumulated, the background was subtracted in the signal analyzer and the data downloaded. In the first two studies, a printout of signal counts versus channel number was obtained. As a first cut analysis, this data was hand plotted on semilogarithmic graph paper. Because the signal decays were expected to be exponential then a plot of the natural logrithm of the signal versus time yields a line whose slope is equal to the decay rate for that experiment. Later, more precise analysis was performed by entering the data into a personal computer for linear least squares analysis. In the O + ClO experiment, an interface was devised that allowed direct transfer of the data from the TN-1500 signal analyzer into a Radio Shack Color Computer II for subsequent analysis.

UV Photometry

In all the experiments described in the preceding three chapters, the concentrations of the minor, but critical, constituents in the gas flow were monitored by UV photometry. As discussed above, the accuracy of the measured rate coefficient is determined in part by the accuracy in the concentration of critical components in the gas mixture. In the O + HO_2 studies, $[H_2O_2]$ was monitored directly in the gas flow via its absorption at either 202.6 nm or 228.8 nm. The concentration of ozone, the other minor component of the gas mixture in the O + HO_2 experiments, was calculated based on the total pressure in the system and the fractional flow from a dilute O_3/N_2 mixture. However, the fractional concentration of O_3 in the 12 liter Pyrex storage bulb containing the ozone mixture was periodically determined by measuring the absorption at 253.7 nm due to a known pressure of the mixture. For the O + ClO study, both Cl_2 and

O_3 were monitored *in situ* via absorption at 366 nm and 254 nm, respectively.

The absorption cells were Pyrex tubing with size 25 O-ring joints as end pieces and 1/4" o.d. side tubes near each end to allow for the gas flow. UV quality quartz windows were clamped across each of the O-ring joints. Depending on the wavelength to be monitored, three different lamps were used. A zinc hollow cathode lamp was the source of a zinc ion line at 202.6 nm. Because the output of the zinc lamp includes several other strong lines in the same wavelength region it was necessary to isolate the 202.6 nm line with a monochromator. Typically, the lamp was mounted 6" from a 1 cm^2 aperture on one window of the absorption cell. The entrance slit of a 1/4 m Jarrell-Ash monochromator was positioned near the other window of the cell. With the slits used in these measurements, the monochromator was able to completely resolve the 202.6 nm Zn^+ line from the nearest line at 206.2 nm (also Zn^+). A quartz envelope photomultiplier tube (RCA 1P128 or similar) in a light tight box was mounted directly to the monochromator at the exit slit. The high voltage (typically 700 V d.c.) was divided equally down the dynode chain and the current measured with an electrometer. For a larger absorption cell, 100 cm or more, a few tenths of a microamp of signal could be expected for the unattenuated light level.

At the other photometric wavelengths, the light sources were brighter and the spectra less congested near the analytical wavelengths.

Therefore, the desired lines could be isolated using commercially available bandpass filters. A mercury pen-ray lamp (UV Photonics) was used to monitor ozone at 254 nm and also for chlorine at 366 nm. The former line dominates the lamp output and care should be taken to avoid having too much light entering the absorption cell. Distance and black vinyl masks are useful means of attenuation. The bandpass filters were obtained from Acton Research Corporation. Both filters had stated maximum bandwidths of 12 nm (full width at half maximum). The 254 nm filter is approximately 10% transmitting at the peak, while the 365 nm filter is 25% transmitting. The bandpass filters were mounted directly over the opening in the box containing the PM tube and this assembly positioned near the exit window of the absorption cell. Typically, more signal at lower voltages could be expected for detection of the Hg atomic lines than for the zinc line described above. The lamp output at 366 nm is actually three separate lines at 365.0 nm, 365.5 nm, and 366.3 nm. The Cl_2 spectrum is quite broad in this region, therefore, resolution of this triplet feature is not necessary.

In the O + ClO study, it was necessary to have quite a long path length for the measurement of ozone. This was accomplished by passing the 254 nm output of the Hg lamp 30 times through a 35 cm long absorption cell. The multipassing was done using modified White cell optics.[75] The White cell mirrors had a broad band reflective coating that included 254 nm and the windows of the cell anti-reflection coated at 254 nm. In order to accommodate the large number of passes, a wide aperture was needed. Therefore, the cell was made with size 50 O-ring joints on each end.

There is a common interference associated with the use of the 254 nm line from the mercury pen-ray lamp. The output also contains a strong emission at 185 nm, which is attenuated by O_2 in room air. Photolysis of O_2 leads to a production of O_3 which then attenuates the 254 nm line. The interference can be eliminated by constantly replenishing the air between the lamp and the absorption cell, i.e., directing a small fan toward this region.

For the actinometry experiments carried out in conjunction with the $O + HO_2$ studies, the ozone concentration was determined in much the same fashion as described above. However, because the emission was monitored on short times scales, it was more convenient to operate the lamp on a direct current (dc) power supply rather than the usual alternating current (ac) transformer. The lamp was started using the arc from a Tesla coil instead of the high voltage pulse provided by the standard ac supply. Under dc operation, the lamp intensity eventually diminished due to distillation of the Hg to one side of the lamp. Periodically, the measurement was halted, the polarity reversed, and the lamp restarted.

Numerical Simulations

Numerical integrations were used at several junctures in these studies to assess and quantify interferences in the rate coefficient measurement due to secondary chemistry. It is worthwhile to give a brief description of these simulation techniques. Because the chemistry to be simulated was relatively simple and more sophisticated programs were not available in our laboratory at the time of the initial studies, a simple brute force approach was taken in writing the integration programs. Initially, a differential equation was written to express the change in concentration with time for each species (dX_i/dt). This set of equations was integrated by repeatedly calculating the change in each concentration (ΔX_i) over small time steps (Δt), correcting each concentration for the change ($X_i + \Delta X_i$), and calculating the concentration change for the next time step. As long as the time step is small compared to the rate at which the chemistry is occurring, the integration will be accurate.

More elegant programming contains an algorithm for adjusting the time steps to match the rates as the integration proceeds, making for a more efficient program. However, for the relatively simple reaction schemes discussed in the preceding chapters, the running time of the integration on a personal computer using the simple approach was not a major constraint. In each case, the appropriateness of the time step was checked by demonstrating that a smaller time step gave the same result. A discussion of a re-evaluation of the secondary chemistry effecting the measurement of the O + HO_2 rate coefficient appears in the final chapter. In this case, the integration was performed with the program QCMP022 purchased from the Quantum Chemistry Program Exchange at Indiana University. The agreement between the results of this latter integration with the results of simpler calculations discussed in Chapters II and III confirms the validity of our initial conclusions.

APPENDIX B

LIST OF REACTIONS

For the convenience of the reader a list of the chemical reactions in numerical order is given in Table XI.

Table XI. List of Reactions

1. $O(^3P) + HO_2 \rightarrow OH + O_2$

2. $O(^3P) + ClO \rightarrow Cl + O_2$

3. $O_2 + h\nu \rightarrow 2\ O$

4. $O + O_2 \xrightarrow{M} O_3$

5. $O_3 + h\nu \rightarrow O + O_2$

6. $O + O_3 \rightarrow 2\ O_2$

7. $OH + O_3 \rightarrow HO_2 + O_2$

8. $HO_2 + O_3 \rightarrow OH + 2\ O_2$

9. $Cl + CH_4 \rightarrow HCl + CH_3$

10. $OH + HO_2 \rightarrow H_2O + O_2$

11. $H_2O + O(^1D) \rightarrow 2\ OH$

12. $Cl + O_3 \rightarrow ClO + O_2$

13. $H_2O_2 + h\nu \rightarrow 2\ OH$

14. $O_3 + h\nu \rightarrow O(^1D)+O_2(a^1\Delta_g)$
    $\rightarrow O(^3P)+O_2(X^3\Sigma_g^-)$

15. $OH + H_2O_2 \rightarrow HO_2 + H_2O$

16. $O(^1D) + N_2 \rightarrow O(^3P) + N_2$

17. $O(^3P) + H_2O_2 \rightarrow OH + HO_2$
    $\rightarrow H_2O + O_2$

18. $O(^3P) \rightarrow$ bckgrd loss

19. $O_2(a^1\Delta_g) + O_3 \rightarrow O(^3P) + 2\ O_2$

20. $O(^1D) + H_2O_2 \rightarrow OH + HO_2$

21. $OH + HO_2 \xrightarrow{M} H_2O + O_2$

22. $HO_2 + HO_2 \rightarrow H_2O_2 + O_2$

23. $O(^3P) + OH \rightarrow O_2 + H$

24. $H + HO_2 \rightarrow 2\ OH$

25. $H + O_2 \xrightarrow{M} HO_2$

26. $H + O_3 \rightarrow OH + O_2$

27. $HO_2 \rightarrow$ bckgrd loss

28. $Cl_2 + h\nu \rightarrow 2\ Cl$

29. $ClO + h\nu \rightarrow Cl + O$

30. $O(^3P) + Cl_2 \rightarrow$ products

31. $ClO + ClO \rightarrow$ products

32. $Cl + (ClO)_2 \rightarrow Cl_2 + ClOO$

33. $ClOO \xrightarrow{M} Cl + O_2$

34. $Cl + ClOO \rightarrow Cl_2 + O_2$
    $\rightarrow 2\ ClO$

35. $Cl + OClO \rightarrow 2\ ClO$

36. $O_2(b^1\Sigma_g^+) + O_3 \rightarrow O + 2\ O_2$

37. $ClO^*(v' \geq 12) + O_3 \rightarrow$
    $O_2 + O + ClO$

38. $ClO^*(v' \geq 3) + Cl \rightarrow Cl_2 + O$

39. $ClO^* \xrightarrow{M} ClO$

40. $Cl + Cl_2O \rightarrow ClO + Cl_2$

41. $O + NO_2 \rightarrow NO + O_2$

REFERENCES

1. M.J. Howard and I.W.M. Smith, Prog. Reaction Kinetics 12, 55 (1983).

2. L.F. Keyser, J. Phys. Chem. 88, 4750 (1984).

3. J.P.D. Abbatt, K.L. Kemerjian, and J.G. Anderson, J. Phys. Chem. 94, 4566 (1990).

4. C.J. Howard, J. Phys. Chem. 83, 3 (1979).

5. R.P. Wayne, Chemistry of Atmospheres (Clarendon Press, Oxford, 1991).

6. P. Warneck, Chemistry of the Natural Atmosphere (Academic Press, San Diego, 1988).

7. G. Brasseur and S. Solomon, Aeronomy of the Middle Atmosphere (D. Riedel, Boston, 1984).

8. H.S. Johnston, Ann. Rev. Phys. Chem. 35, 481 (1984).

9. J.G. Anderson, Ann. Rev. Phys. Chem. 38, 489 (1987).

10. B.A. Thrush, Rep. Prog. Phys. 51, 1341 (1988).

11. S. Chapman, Mem. Roy. Meterol. Soc. 3, 103 (1930).

12. The Stratosphere 1981, Theory and Measurements (World Meteorological Organization, Geneva, 1992).

13. R.S. Stolarski and R.J. Cicerone, Can. J. Chem. 52, 1510 (1974).

14. M. Molina and F.S. Rowland, Nature 249, 810 (1974).

15. The Stratosphere 1991, Theory and Measurement, (World Meteorological Organization, Geneva, 1992).

16. A.R. Ravishankara, P.H. Wine, and J.M. Nicovich, J. Chem. Phys. 78, 6629 (1983).

17. J.M. Nicovich and P.H. Wine, J. Phys. Chem. 91, 5118 (1987).

18. J.M. Nicovich, P.H. Wine, and A.R. Ravishankara, J. Chem. Phys. 89, 5670 (1988).

19. L.F. Keyser, J. Phys. Chem. 88, 3439 (1982).

20. U.C. Sridharan, L.X. Qui, and F. Kaufman, J. Phys. Chem. 86, 4469 (1982).

21. W. Hack, A.W. Preuss, F. Temps, H. Gg. Wagner, Ber. Bunsenges. Phys. Chem. 83, 1275 (1979).

22. J.P. Burrows, D.I. Cliff, G.N. Harris, B.A. Thrush, and J.P.T. Wilkinson, Proc. R. Soc. London Ser. A 368 463 (1979).

23. R.R. Lii, M.C. Sauer, Jr., and S. Gordon, J. Phys. Chem. 84, 817 (1980).

24. Chemical Kinetics and Photochemical Data for Use in Stratospheric Modeling, JPL Publication No. 82-57 (NASA, Jet Propulsion Laboratory, 1982).

25. D.H. Volman, Adv. Photochem. 1, 43 (1963).

26. N.R. Greiner, J. Chem. Phys. 45, 99 (1966).

27. G. Ondrey, N.J. Van Veen, and R. Bersohn, J. Chem. Phys. 78, 3732 (1983).

28. A.R. Ravishankara, F.L. Eisele, N.M.Kreutter, and P.H. Wine, J. Chem. Phys. 74, 2267 (1981).

29. P.H. Wine and A.R. Ravishankara, Chem. Phys. 69, 365 (1982) (and references therein).

30. M. Nicolet, *Etude des reactions chimiques de lozone dans la Stratosphere* (Institut Royal Meterologiue de Belgique, 1980).

31. P.H. Wine, J.M. Nicovich, R.J. Thompson, and A.R Ravishankara, J. Phys. Chem. 87, 3748 (1983).

32. R.F. Heidner III and D. Husain, Int. J. Chem. Kinet. 6, 77 (1974).

33. Davidson, H.I. Schiff, T.J. Brown, G.E. Streit, and C.J. Howard, J. Chem. Phys. 69, 1213 (1978).

34. A.R. Ravishankara and P.H. Wine, 7th International Symposium on Gas Kinetics, Gottingen, West Germany, August 23-27, 1982.

35. M. Weissman, L.G.S. Shum, S.P. Heneghan, and S.W. Benson, J. Phys. Chem. 85, 2863 (1981).

36. W. H. Brune, J.J. Schwab, and J.G. Anderson, J. Phys. Chem. 87, 4503 (1983).

37. Chemical Kinetics and Photochemical Data for Use in Stratospheric Modeling, JPL Publication No. 85-37, (NASA, Jet Propulsion Laboratory, 1975).

38. G.L. Vaghjiani and A.R. Ravishankara, J. Geophys. Res. 94, 3487 (1989).

39. J.M. Nicovich and P.H. Wine, J. Geophys. Res. 93, 2417 (1988).

40. J. Peeters and G. Mahnen, Symp. (Int.) Combust., [Proc.] 14, 133 (1972).

41. M.J. Day, K. Thomson, and G. Dixon-Lewis, Symp. (Int.) Combust., [Proc.], 14, 47 (1972).

42. U.C. Sridharan, F.S. Klein, and F. Kaufman, J. Chem. Phys. 82, 592 (1985).

43. P.S. Nangia and S.W. Benson, J. Phys. Chem. 83, 1138 (1979).

44. S.W. Benson, Oxid. Commun. 2, 169 (1982).

45. M. Mozurkewich, J. Phys. Chem. 90, 2216 (1986).

46. M. Mozurkewich and S.W. Benson, J. Phys. Chem. 88, 6429 (1984).

47. J.A. Kaye and C.H. Jackman, J. Geophys. Res. 91, 1117 (1986).

48. C.H. Jackman, R.S. Stolarski, and J.A. Kaye, J. Geophys. Res. 91, 1103 (1986).

49. P.P. Bemand, M.A.A. Clyne, and R.T. Watson, J. Chem. Soc. Faraday Trans. 1 69, 1356 (1973).

50. M.A.A. Clyne and W.S. Nip, J. Chem. Soc. Faraday Trans. 1 72, 2211 (1976).

51. M.S. Zahmiser and F. Kaufman, J. Chem. Phys. 66, 3673 (1977).

52. M.T. Leu, J. Phys. Chem. 88, 1394 (1984).

53. J.J. Schwab, D.W. Toohey, W.H. Brune, and J.G. Anderson, J. Geophys. Res. 89, 9581 (1984).

54. A.P. Ongstad and J.W. Birks, J. Chem. Phys. 81, 3922 (1984).

55. A.P. Ongstad and J.W. Birks, J. Chem. Phys. 85, 3359 (1986).

56. J.J. Margitan, J. Phys. Chem. 88, 3639 (1984).

57. C. Park, J. Phys. Chem. 80, 565 (1976).

58. R.L. Jaffee, Chem. Phys. 40, 185 (1979).

59. J.L. Gole, J. Phys. Chem. 84, 1333 (1980).

60. Chemical Kinetics and Photochemical Data for Use in Stratospheric Modeling, JPL Publication 87-41, (NASA, Jet Propulsion Laboratory, 1987).

61. A.G. Hearn, Proc. Phys. Soc. 78, 932 (1961).

62. L.T. Molina and M.J. Molina, J. Geophys. Res. 91, 14501 (1986).

63. K. Mauersberger, J. Barnes, D. Hanson and J. Morton, Geophys. Res. Lett. 13, 671 (1986).

64. M. Mandelman and R.W. Nicholls, J. Quant. Spectrosc. Radiat. Transfer 17, 483 (1977).

65. P.H. Wine, A.R. Ravishankara, D.L. Philen, D.D. Davis, and R.T. Watson, Chem. Phys. Lett. 50, 101 (1977).

66. G.D. Hayman, J.M. Davies, and R.A. Cox, Geophys. Res. Lett. 13, 1347 (1986).

67. J.W. Vanderzanden and J.W. Birks, Chem. Phys. Lett. 88, 109 (1982).

68. K.Y. Choo and M.T. Leu, J. Phys. Chem. 89, 4832 (1985).

69. Chemical Kinetics and Photochemical Data for Use in Stratospheric Modeling, JPL Publication 92-20 (NASA, Jet Propulsion Laboratory, 1992).

70. L.F. Keyser, J. Phys. Chem. 92, 1193 (1988).

71. S.P. Sander, R.P. Friedl, and Y.L. Yung, Science 245, 1095 (1989).

72. M. Trolier, R.L. Mauldin III, and A.R. Ravishankara, J. Phys. Chem. 94, 4896 (1990).

73. D. Davis and W. Braun, Applied Optics 7, 2071 (1968).

74. F.C. Fehsenfeld, K.M. Evenson, and H.P Broida, Rev. Sci. Instr.36, 294 (1965).

75. J. U. White, J. Opt. Soc. Am. 32, 285 (1942).

BIOGRAPHICAL SKETCH

Mr. Nicovich was born on a frosty morn in February of 1950 in Hattiesburg, Mississippi. He graduated in 1968 from Hattiesburg High School. In 1972 Mr. Nicovich received a B.A. degree in Chemistry from Millsaps College, Jackson, Mississippi. Not knowing any better, he entered the University of Florida in 1972 as a graduate student in the Chemistry Department. Under the guidance of Prof. M. L. Muga, he obtained a Master's degree in 1978. That same year, he began working as chemical technician for the Gulf Coast Research Laboratory in Ocean Springs, Mississippi. He joined the staff of what is now the Georgia Tech Research Institute in early 1980. Later that year, he once again enrolled in the graduate program at the University of Florida as an off-campus student. A portion of his final course work has been completed in the School of Chemistry at Georgia Tech. Mr. Nicovich has coauthored approximately 30 refereed publications and has presented numerous papers at professional meetings.

Mr. Nicovich is married to Rebecca Cirlot Nicovich. They have two children, Rusty and Angie, born in 1982 and 1985, respectively. The family maintains a modest, middle-class lifestyle in Gwinnett County, Georgia.

I certify that I have read this study and that in my opinion it conforms to acceptable standards of scholarly presentation and is fully adequate, in scope and quality, as a dissertation for the degree of Doctor of Philosophy.

Robert H Hanrahan

Robert H. Hanrahan, Chairman
Professor of Chemistry

I certify that I have read this study and that in my opinion it conforms to acceptable standards of scholarly presentation and is fully adequate, in scope and quality, as a dissertation for the degree of Doctor of Philosophy.

A. R. Ravishankara, Cochairman
Adjunct Professor of Chemistry
University of Colorado

I certify that I have read this study and that in my opinion it conforms to acceptable standards of scholarly presentation and is fully adequate, in scope and quality, as a dissertation for the degree of Doctor of Philosophy.

M Luis Muga

M. Luis Muga
Professor of Chemistry

I certify that I have read this study and that in my opinion it conforms to acceptable standards of scholarly presentation and is fully adequate, in scope and quality, as a dissertation for the degree of Doctor of Philosophy.

Phillip M Achey

Phillip M. Achey
Professor of Microbiology and
Cell Science

This dissertation was submitted to the Graduate Faculty of the Department of Chemistry in the College of Liberal Arts and Sciences and to the Graduate School and was accepted as partial fulfillment of the requirements for the degree of Doctor of Philisophy.

May 1993

Dean, Graduate School

UNIVERSITY OF FLORIDA
3 1262 08556 8490